NPS

Author(s)	Holgren, Marvin A.; Comfort, Clayton L.
Title	Comparison of experimental stresses and deflections with those predicted by a strain energy method for an F8U-3 wing loaded in torsion
Publisher	Monterey, California: U.S. Naval Postgraduate School
Issue Date	1963
URL	http://hdl.handle.net/10945/11800

COMPARISON OF EXPERIMENTAL STRESSES AND
DEFLECTIONS WITH THOSE PREDICTED BY A
STRAIN ENERGY METHOD FOR AN F8U-3
WING LOADED IN TORSION

MARVIN A. HOLGREN
and
CLAYTON L. COMFORT

COMPARISON OF EXPERIMENTAL STRESSES AND
DEFLECTIONS WITH THOSE PREDICTED BY
A STRAIN ENERGY METHOD FOR AN F8U-3 WING
LOADED IN TORSION

****

Marvin A. Holgren and Clayton L. Comfort

COMPARISON OF EXPERIMENTAL STRESSES AND

DEFLECTIONS WITH THOSE PREDICTED BY

A STRAIN ENERGY METHOD FOR AN F8U-3 WING

LOADED IN TORSION

by

Marvin A. Holgren

Lieutenant Commander, United States Navy

and

Clayton L. Comfort

Captain, United States Marine Corps

COMPARISON OF EXPERIMENTAL STRESSES AND

DEFLECTIONS WITH THOSE PREDICTED BY

A STRAIN ENERGY METHOD FOR AN F8U-3 WING

LOADED IN TORSION

by

Marvin A. Holgren and Clayton L. Comfort

This work is accepted as fulfilling

the thesis requirements for the degree of

MASTER OF SCIENCE

IN

AERONAUTICAL ENGINEERING

from the

United States Naval Postgraduate School

ABSTRACT

The stress level in the milled skin at the root of
a tapered, multicell swept wing is predicted by means of
a matrix-force method. The solution is achieved by
minimizing the internal strain energy, and the results
compared with experimental tests. A single loading,
consisting of a nose-up couple, is applied to each tip rib.
The loading is transferred from the tip rib to an idealized
structure by means of simple torsion theory. The idealized
structure represents the inboard one-half of each semi-span.

Results indicate that an accurate solution of the
stress distribution in the actual wing can be achieved
provided that the root boundary conditions are preserved.
An extension of the analysis is suggested in order to
more closely define the maximum accuracy inherent in the
particular matrix-force method of solution.

TABLE OF CONTENTS

LIST OF ILLUSTRATIONS

TABLE OF SYMBOLS

$[A]$	Matrix of coefficients of non-redundant loads
$[A^{-1}]$	Inverse of $[A]$ matrix
a_r	Coefficient of redundant load
a_{nr}	Coefficient of non-redundant load
$\{AT\}$	Matrix of Resultant Loads
AFTIB	Aft intermediate beam
$[B]$	Matrix of coefficients of redundant and and applied loads
$[C]$	Matrix of deflection influence coefficients
$[CHECK]$	Unit diagonal matrix
CIB	Center intermediate beam
$[CJ]$	Matrix product of $[A^{-1}]$ and $[B]$
E	Modulus of Elasticity
$[F]$	Flexibility Matrix
FB	Front beam
FIB	Front intermediate beam
FWD I B	Forward intermediate beam
F_n	Panel edge force in line of intermediate rib
F_p	Panel edge force normal to intermediate rib
f_n	Panel edge stress in line of intermediate rib
f_p	Panel edge stress normal to intermediate rib
f_s	Shear stress obtained from Equation (1)
$[G]$	$[CJ]$ matrix augmented by trivial relations
G	Shear modulus

GF	Strain Gage factor
$[H]$	Strain energy matrix
L	Spanwise length, inches
P	Axial force in bars, pounds
$\{P\}$	Column matrix of applied loads
q	Shear flow, pound/inch
R	Resistance, ohms
RB	Rear beam
RIB	Rear intermediate beam
$[S]$	Stress coefficient matrix
S	Linear distance along perimeter of cut section, inches
T	Torque, inch-pounds
t	Thickness, inches
U	Internal strain energy
V	Constant d.c. voltage source
V_o	Wheatstone Bridge output voltage
w	Panel edge length, inches
x_w	x-axis coordinate of wing, inches
y_w	y-axis coordinate of wing, inches
ϵ	Strain, micro-inches per inch
O	Angle of twist
μ	Poisson's ratio
σ	Normal stress
τ	Shear stress

ϕ_p	Angle of principal axis measured from either y-axis of aircraft, or first gage of rosette.
Λ_{cib}	Sweep angle of CIB
Λ_p	Average sweep angle of panel
[ ]	Square or rectangular matrix
⌊ ⌋	Row matrix
{ }	Column matrix

INTRODUCTION

Highly swept wings of low thickness to chord ratios were first built with conventional stringer sheet methods. This introduced the problem of how to successfully predict and then to relieve the severe concentration of stress along the rear spar and aft root section skin.

The stress concentration was reduced somewhat by shifting to multi-cell construction. Multi-cell construction as used herein describes wings having closely spaced spanwise spars or webs, and relatively few streamwise ribs.

Wing analysis by customary beam bending and torsion methods was unable to accurately account for the root area stress levels unless modification factors were used. This was due primarily to the neglect of bending-torsion inter-action. However, as flight speeds increased and aspect ratios decreased, the inability of beam theory to properly define chordwise deformations caused even greater concern since thermo-aeroelastic problems replaced static stressing in order of importance.

In order to properly account for bending-torsion inter-action, chordwise curvatures, shear deflections, the increasing use of large cut-outs, and very heavy milled skin, several alternative methods of analysis have been developed. Without considering the older relaxation techniques and their iterative solutions, each depends

upon the use of a digital computer for solution. Each attempts to achieve a mathematical model which exhibits a properly deformed shape having absolute displacements comparable to the actual case.

The most prevalent of these methods treat the structure as an assemblage of elastic components, which allows matrix formulation of the solution in terms of the various energy theorems. Argyris (Ref. 1) has shown that these energy theorems derive from the two fundamental principles of virtual displacements and virtual forces, both of which originated in the work of Maxwell, Mohr, and Engesser. Since both principles are independent of elastic laws or the structural material, their application to non-linear problems or to structures where initial thermal strains exist is quite easy.

The "matrix-force" method leads to an analysis in terms of forces as the unknowns, while the "matrix-displacement" method leads to an analysis in terms of displacements. Either method provides for exact satisfaction of equilibrium and compatibility in a structure made up of discrete elements. Simplification of structural modifications during the preliminary design stage is an additional advantage which accrues from the use of discrete elements.

Each method is again categorized as to whether "lumped-parameter" or "finite element" idealization of plane panels is used. "Lumped-parameter" idealization as used herein allows distinct properties of the structure, such as direct stress, shear, bending and torsion, to be separated or concentrated at discrete locations. The web or panel may be attached to the adjacent flanges at corners, mid-points of the panel, or continuously. "Finite-element" idealization prescribes plane panels of either triangular or rectangular shape, to be attached at corners or nodes of the structure. In either idealization, panel warping must be avoided, even by slightly revising the geometry of the structure, in order to achieve a rigorous solution.

Although a complete solution, giving both forces and displacements, may be obtained from either the matrix-force or matrix-displacement method, it has been shown in Ref. 2 that if only forces are of interest, the matrix-force method is the most efficient. Conversely, if only deflections are of interest, the matrix-deflection method is the most efficient.

The degree of redundancy in the force method is less than for the displacement method. However, the stiffnesses of the elements, as used by the displacement approach, are easier to obtain than are the flexibilities of elements

required by the force approach. The force method has the additional disadvantage of neglecting Poisson's effect for that portion of the axial-load carrying skin which is lumped with the beam flanges.

Argyris (Ref. 3) has shown that while the force method is nearly always more suitable for fuselage analysis, the displacement method may often be more convenient for the analysis of complex wings, since in the displacement method structural "node points" specify the matrix size. This generally results in smaller matrices than would be required to obtain similar accuracy by the force method.

Current literature abounds with instances where the two methods, each formulated several ways, have been applied to laboratory specimens. This allows some study of parameter effects, but allows no true indication of the method applicability to an actual wing which may possess extreme and sometimes abrupt variations in skin thickness, discontinuous spars, massive ribs, skin and web cut-outs, and taper.

It is the object of this report to compare predicted stress and strain levels near the root of an actual wing (which possesses all of the aforementioned analytical obstacles) with the stresses and strains obtained experimentally. The specimen to be analyzed was obtained from a Mach 2.5 all-weather fighter project which was canceled

by the U. S. Navy before the structural test program was completed. The matrix-force method of analysis is used, and consists of a "lumped-parameter" structural idealization as proposed by Wehle and Lansing (Ref. 4). The matrix formulation of the solution is similar to the scheme proposed by Lang and Bisplinghoff (Ref. 5) and organized in considerable detail in Ref. 6. This formulation allows efficient use of the digital computer and at the same time allows intermediate results to be printed out for study. This characteristic makes changes to the structural ideal-ization relatively simple to incorporate, and causes the effect of such a change to be readily apparent. Thus from the outset it was recognized that a follow-on analysis, using the same digital computer program, would allow investigation of the boundary conditions, and indicate the merit of the idealization with only limited additional effort.

This work was conducted at the U. S. Naval Postgraduate School, Monterey, California, during the 1962-1963 school year. The authors are deeply indebted to Professor C. H. Kahr, who conceived the need for such an investigation. Professor Kahr, together with Associate Professor U. Haupt, rendered invaluable assistance and encouragement throughout the project. The authors express their gratitude to Aeronautical Laboratory Supervisor R. E. McConnell and

assistants R. A. Besel and R. O. Cunningham, whose
cooperative efforts were so essential in the procurement,
fabrication and installation of all experimental apparatus.
Appreciation is also expressed to Chance Vought Aircraft,
Inc., for their cooperation in furnishing essential data.

II   THEORETICAL ANALYSIS

1.   General

The structure chosen for the analysis was the wing
center section of an F8U-3, as shown in Fig. 1 below. This
section consists of seven spars and one post beam per semi-
span, upper and lower milled skins, two massive pivot ribs
closely spaced about the aircraft center line, two inter-
mediate ribs, and two heavy wing fold ribs located at the
extremities of the center section.
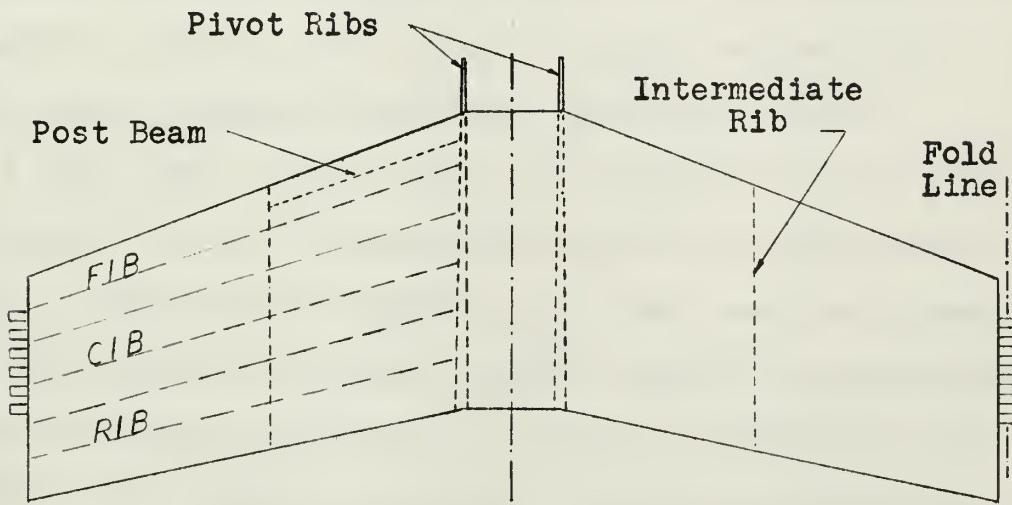
Fig. 1
Sketch of F8U-3 Wing Center Section

The first requirement for the analysis was to study
the pictures and drawings of the dis-assembled wing in
order to establish a basis for simplifying assumptions.
These simplifications would be necessary to enable
representation of the structure by a mathematical model

consisting only of axial-load carrying bars and plane, shear carrying, constant thickness panels.

The first simplification was introduced by considering the pivot rib to be the root location. The pivot rib was thus assumed to be infinitely stiff and free of chordwise bending. This step was taken to simplify the mathematical model, reducing by 16 the number of components to be analyzed. This would undoubtedly reduce the accuracy of the solution. However, the effect should be predictable, and once the reduced solution is achieved, incorporation of the center section (pivot rib to aircraft center line) would require comparatively minor additional effort.

A post beam, shown in Fig. 1, extended from the pivot rib ("root") to the intermediate rib in the actual wing. Since no shear web was involved, the post beam was removed from the idealized structure and its flange area distributed to the surrounding structure. The posts themselves were ignored. The remaining structure was then represented by axially loaded bars and flat shear panels of constant thickness, as shown in Fig. 2.

It was then necessary to determine the cross-sectional areas of the bars and the thickness of the shear panels. This was done for the bars at the cross-sections located at stations $y_W = 25.095$ and $y_W = 81.98$, Fig. 3. A bar end area included the existing flange area, and the total skin

Fig. 2
Perspective of
Idealized Model

$Y_w = 25.095$

$Y_w = 81.98$

$X_w = 57.42$

9
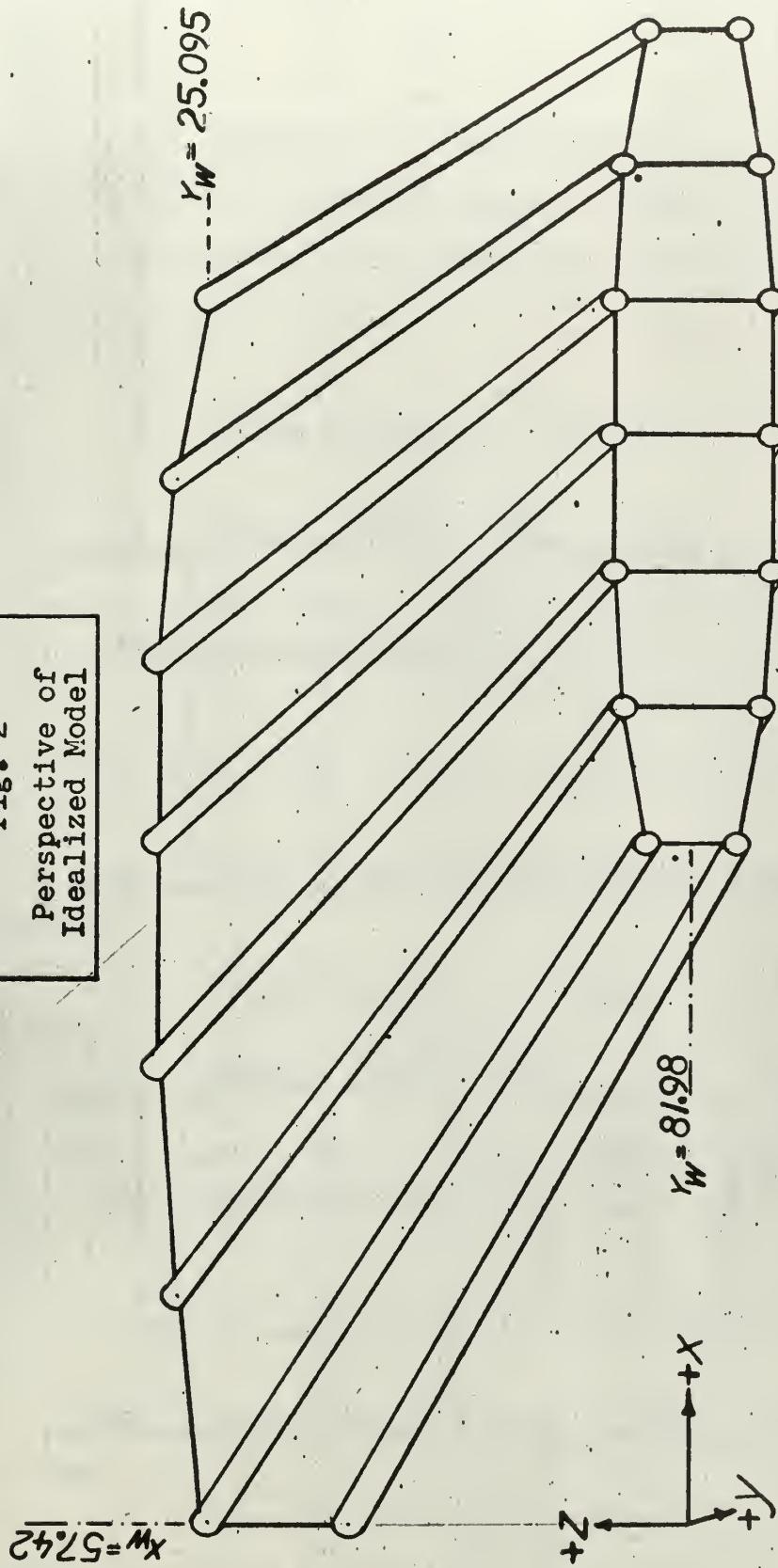
Fig. 3

GEOMETRY OF STREAMWISE CUTS

AT $y_w = 25.095$ AND $y_w = 81.98$

Wing Station $y_w = 25.095$

Wing Station $y_w = 81.98$

10
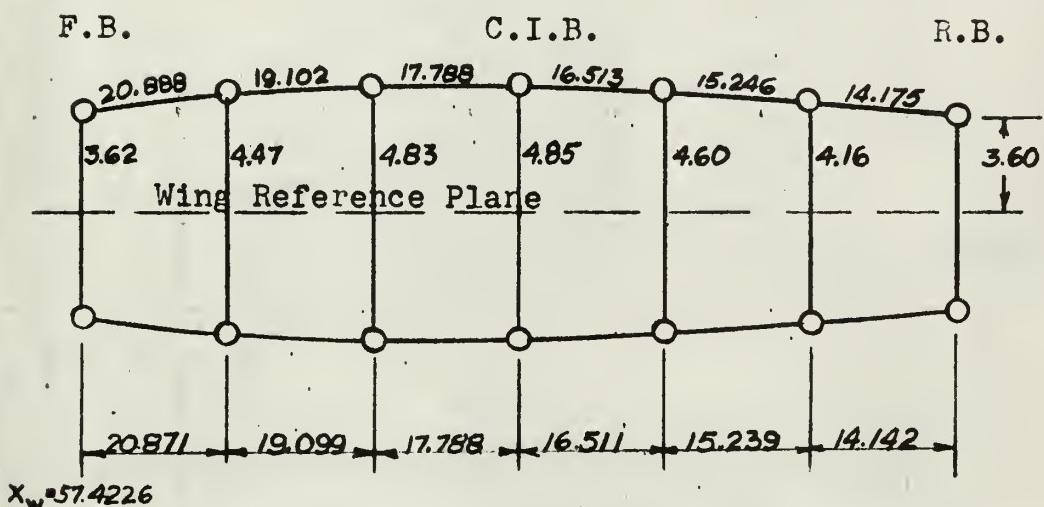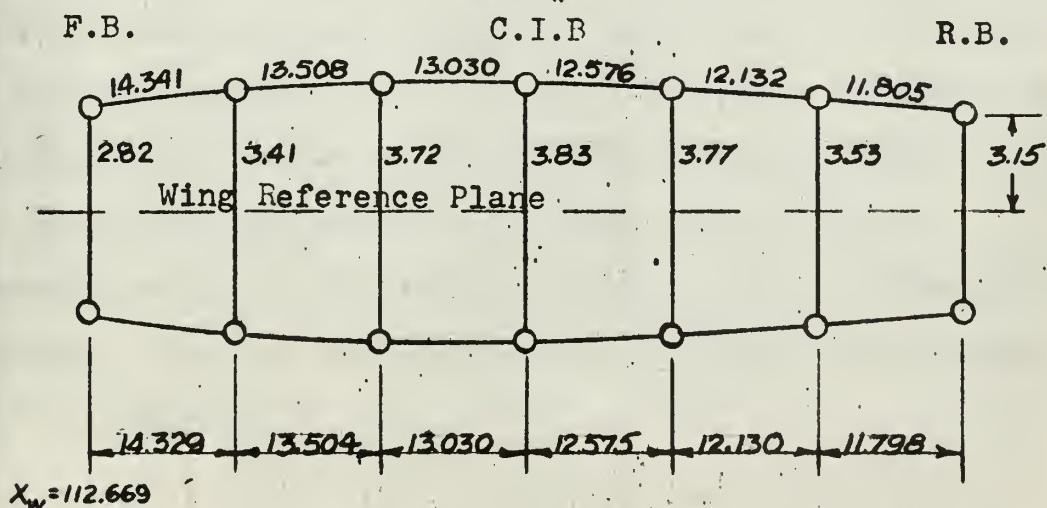
area perpendicular to the bar, taken from the center of
the panel just ahead to the center of the panel just behind,
as shown in Fig. 4. Spar web areas were not included.
The concentration of axial load carrying skin at the flange
locations has the effect of removing lateral contraction
of the covers from much of the analysis ($\mu = 0$).
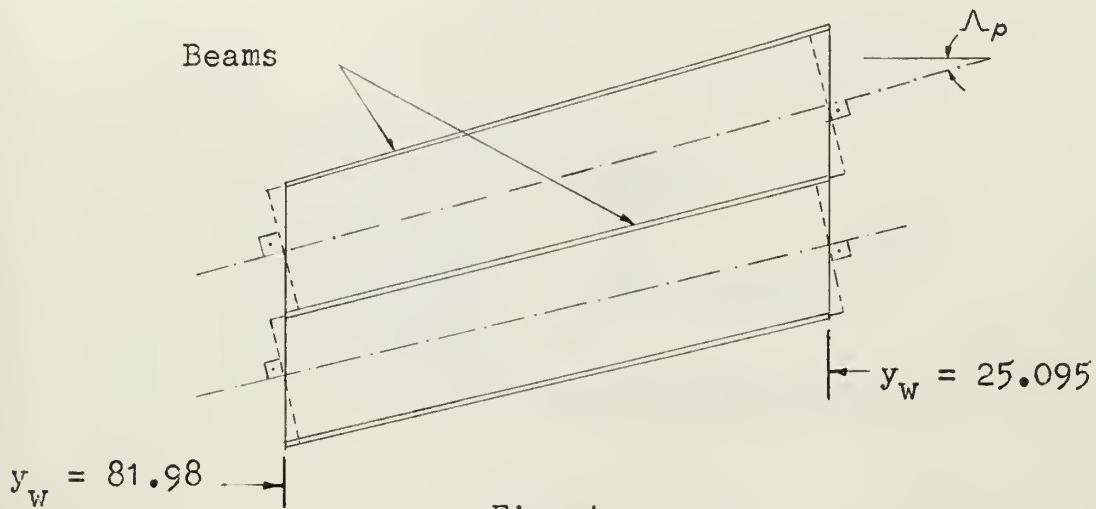
Fig. 4

Distribution of Cover Skin to Beam Flanges

Difficulty was experienced in determining the "average"
skin thickness of each of the 14 cover panels due to the
span-wise variation of thickness. Chordwise variation in
thickness was easier to account for since the aspect ratio
of the individual panels was on the order of four.
Representation of the multiply tapered skin by panels of
average thickness will undoubtedly penalize the accuracy
of the analysis.

11

The un-tapered bars of the intermediate rib were
formed by adding to the existing chordwise flanges. The
added area consisted of a skin area equal to the local
thickness times a plate width (equal to the panel width)
distributed evenly on either side of the rib, as shown
in Fig. 5.
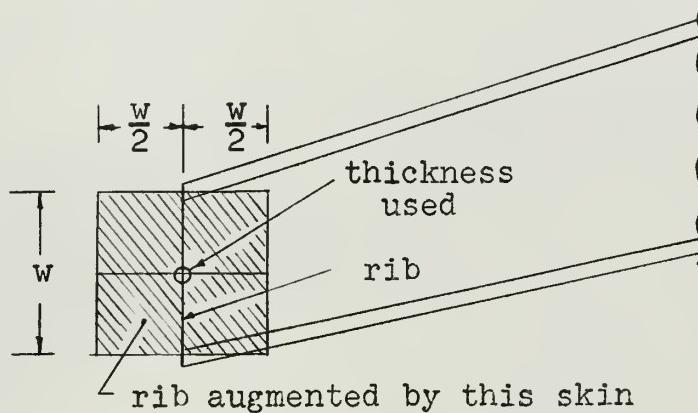
Fig. 5

Distribution of Cover Skin Area to Rib Bar Area

The dimensions of the resulting elements of the
idealized wing are listed in Table I.

2.   Loading Method

After establishing the idealized model, it was
necessary to establish a means of load application. It
must transfer a load identical to the tip-applied load on
the actual wing to the idealized model at the intermediate
rib. As shown in Fig. 6, a nose-up (the wing is mounted
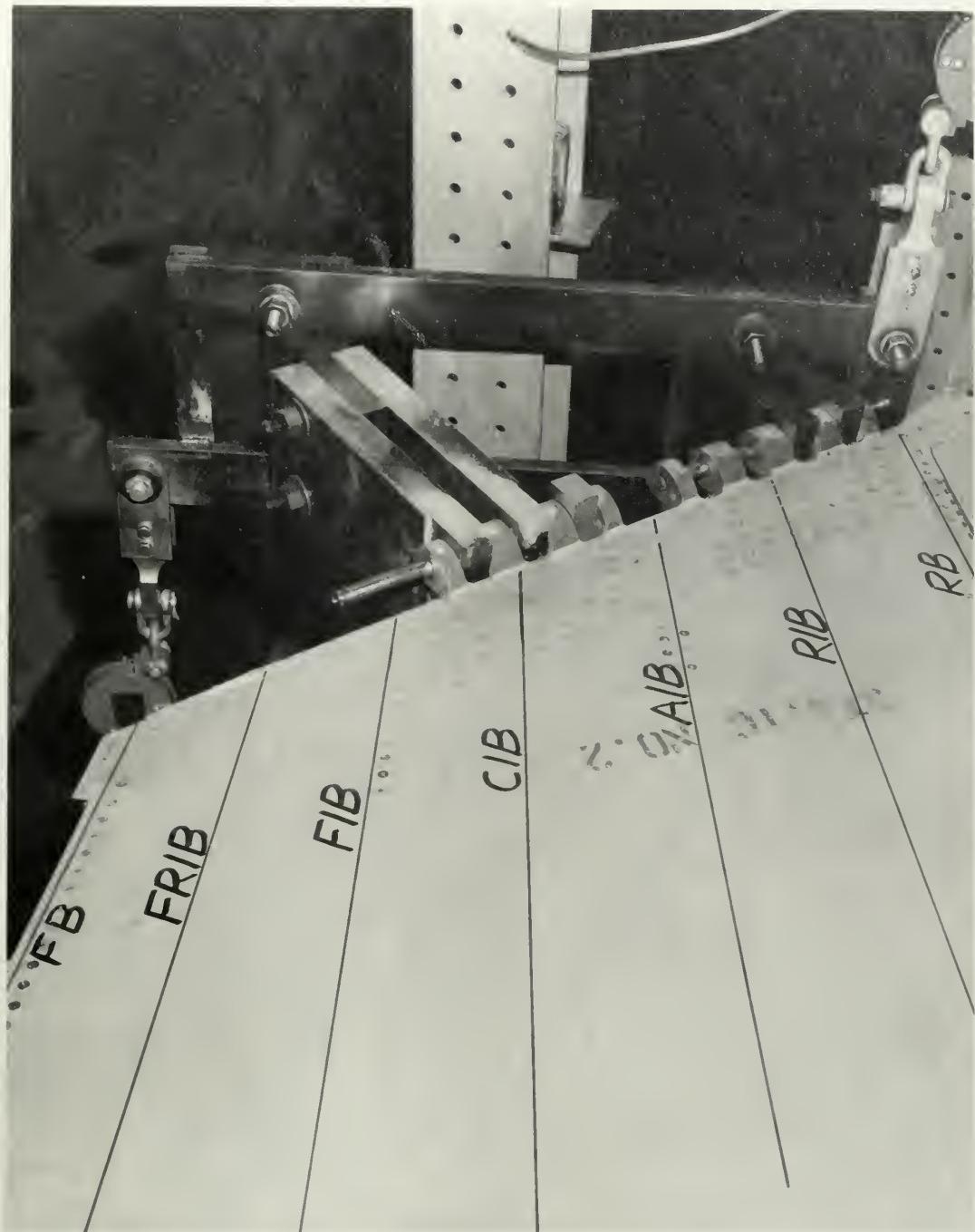
Fig. 6

Application of Couple to Wing Tip

Fig. 7

Distribution of Loads to
Idealized Wing

$P_{27} = \frac{1}{2}\Delta P_1$

$P_{13} = F_{n_1} + \Delta q_{n_1}$

14
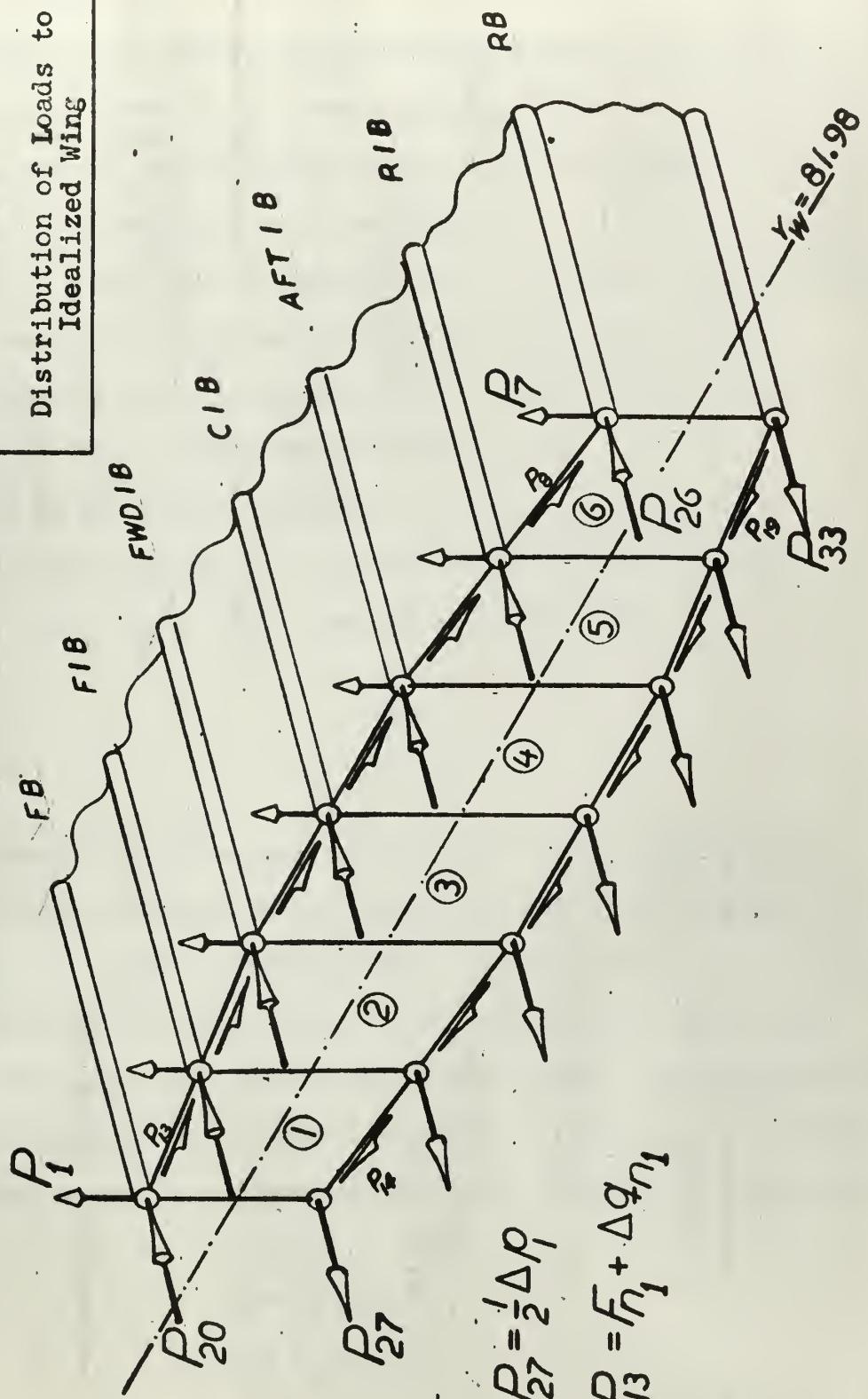
inverted) couple perpendicular to the C.I.B. was applied to each wing tip.

Considering only the instrumented wing, this couple must be converted to 12 cover shears, seven vertical web shears, and 14 axial flange loads on a streamwise cross-section (intermediate rib) at station $y_W = 81.98$, as shown in Fig. 7. This was accomplished by assuming simple torsion theory would be satisfactory inboard from the tip to approximately the intermediate rib. This assumption was based upon tests reported in Ref. 7.

The shear flows induced at two cross-sections perpendicular to the C.I.B., and located at stations $y_W = 74.3$ and $y_W = 98.7$, were determined from

$$T = \sum 2 A q \tag{1}$$

The calculations and results are shown in Appendix A. A linear interpolation, using the planform dimensions from Fig. 8, gave the shear flow for each cell, as oriented perpendicular to the C.I.B. These individual cell shear flows were then resolved in stresses along, and perpendicular to, the streamwise intermediate rib at station $y_W = 81.98$. From Mohr's circle of stresses, shown in Fig. 9, there is:

$$\theta = (90 - 2\Lambda)$$
$$f_n = f_s \sin \theta$$
$$f_p = f_s \cos \theta$$

15

FIG. 8
CENTER SECTION OF F8U-3 PORT WING
(Main Structural Elements)
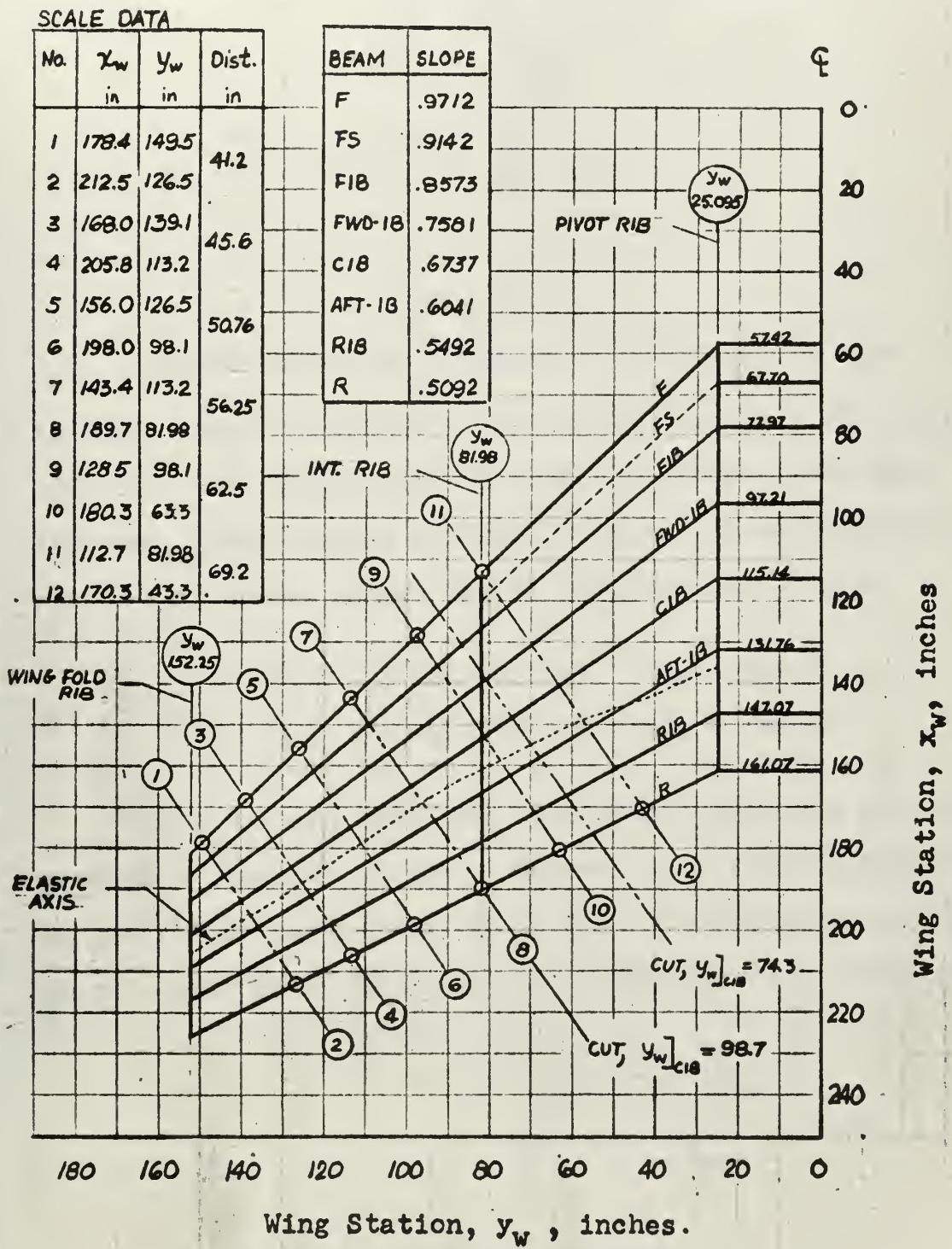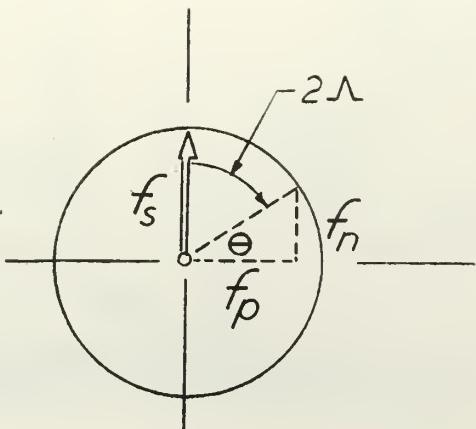
Fig. 9

Mohr's Circle of Stresses at Intermediate Rib

Applying these stresses to the panel edge along the stream-
wise rib, and taking average panel thickness t **and edge**
distance w; the forces F_n and F_p due to streamwise shear
stress and stress normal to the rib, f_s and f_p, are:

$$F_n = f_n \; w \; t = f_w \; \sin \theta \; wt \;\; = q_s \; w \; \sin \theta$$
$$F_p = f_p \; w \; t = f_s \; \cos \theta \; wt \;\; = q_s \; w \; \cos \theta$$

It can be seen that the streamwise component may be
carried by the rib flanges. However, the force component
perpendicular to the rib, F_p in Fig. 10, cannot be carried
by the shear panel and must be separated into a streamwise
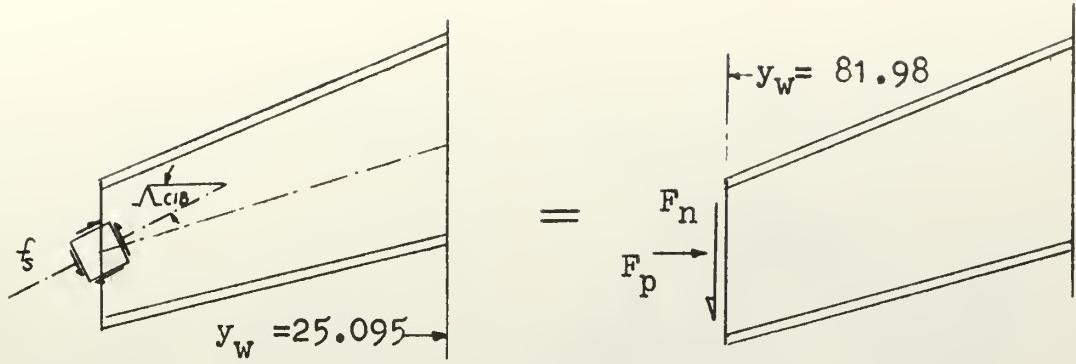
Fig. 10
Component of Shear Force
Perpendicular to Intermediate Rib

component, $\triangle q_n$, which is additive to the force F_n, and
a component $\triangle p$ taken axially by the adjacent flanges, as
shown in Fig. 11.
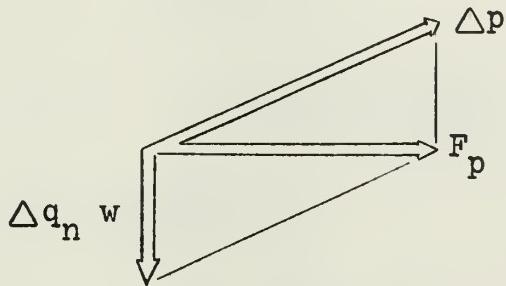
Fig. 11
Vectorial Relation Between $\triangle q_n$ and $\triangle p$

One-half of the $\triangle p$ component was assigned to each adjacent
flange. The various load components and the resulting
applied loads on the idealized model are given in Table II.
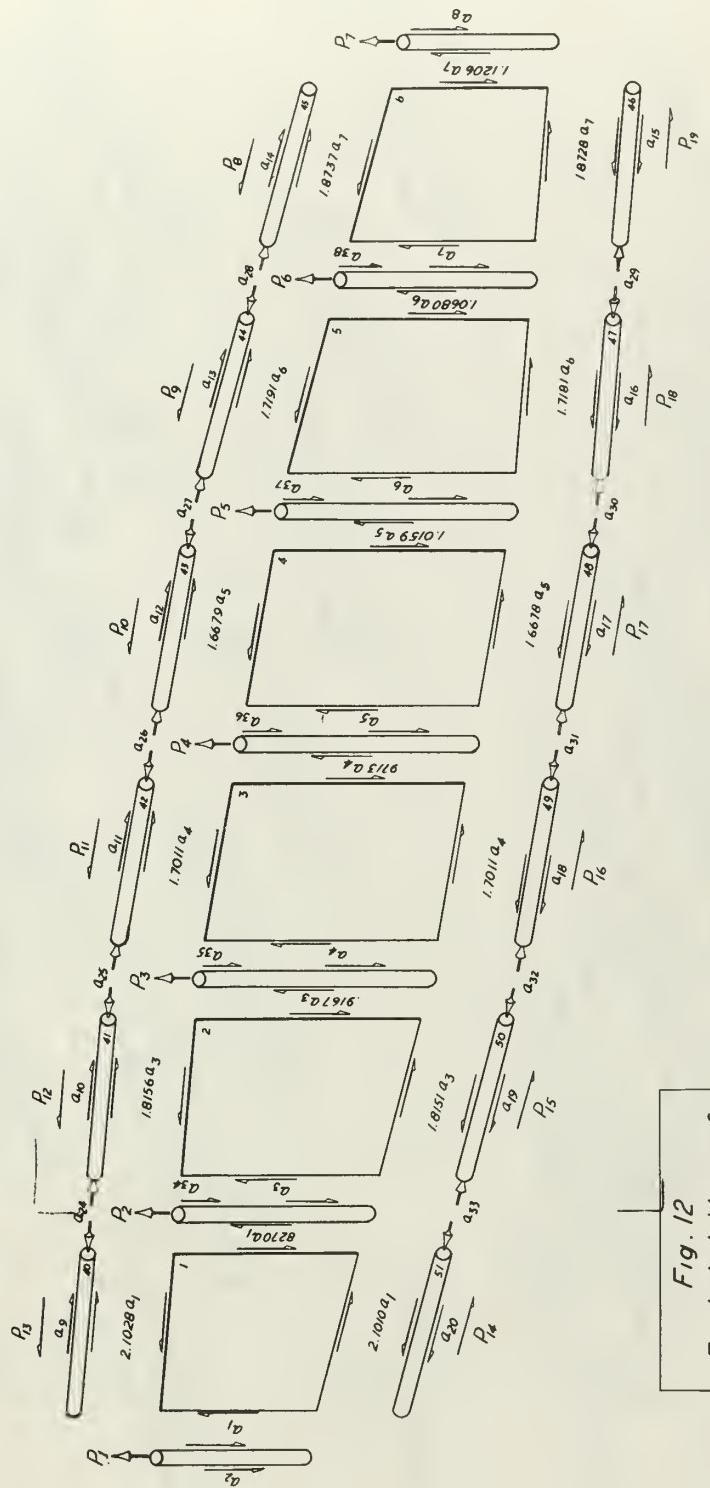
Fig. 12
Exploded View of
End Rib
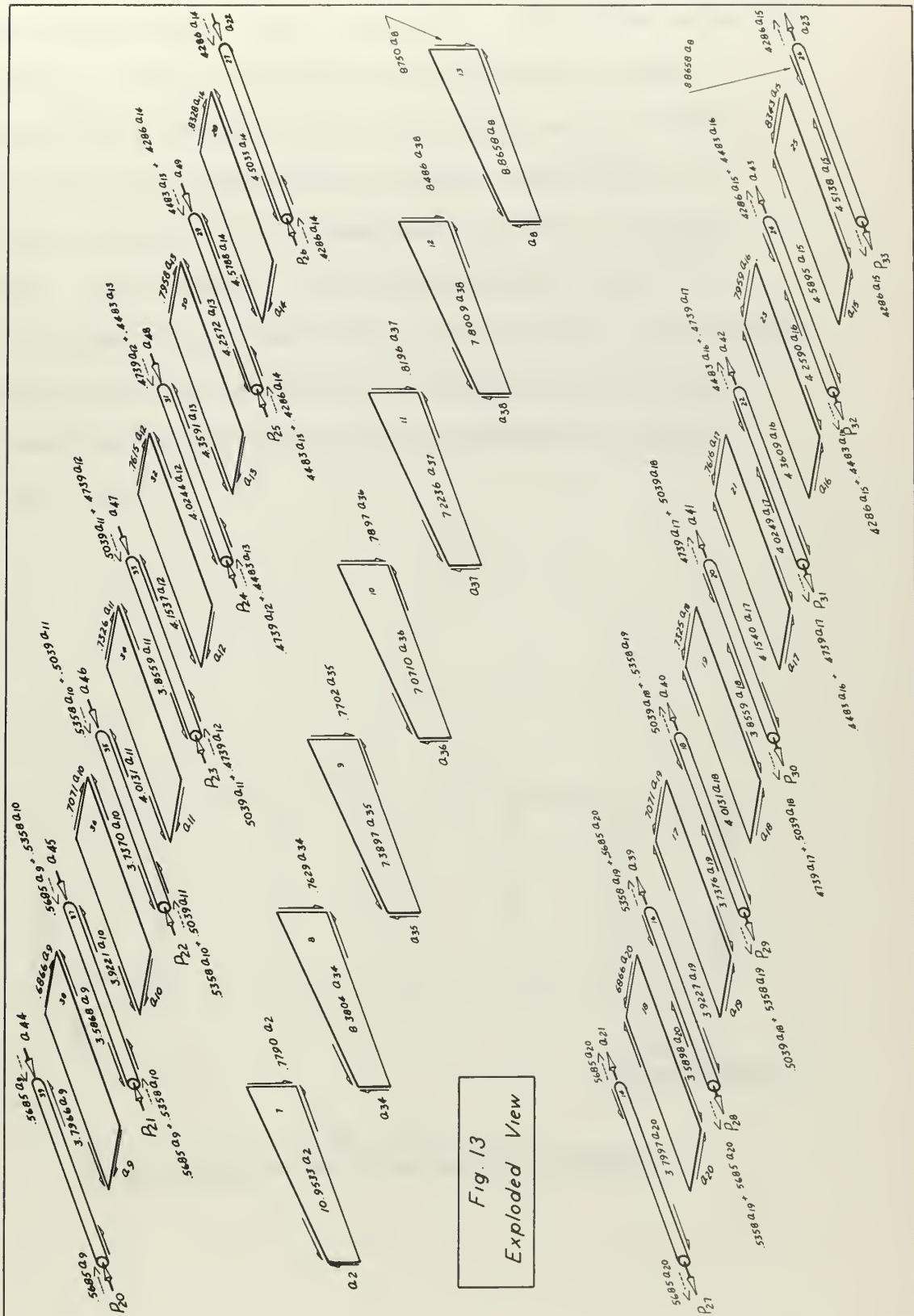
Fig. 13
Exploded View

20

3. Element Loads

Loads were assigned to the individual structural components as shown in Figs. 12 and 13. Only the redundants and sufficient loads to define the individual member flexibilities and general state of stress were included.

The statically determinate system was defined by making cuts inboard of the intermediate rib at station $y_W = 81.98$. By "cutting" the five interior beam webs and all flanges except the lower front and two rear flanges, a minimum determinate and stable structure was obtained. A cross-section of the determinate structure is shown in Fig. 14.
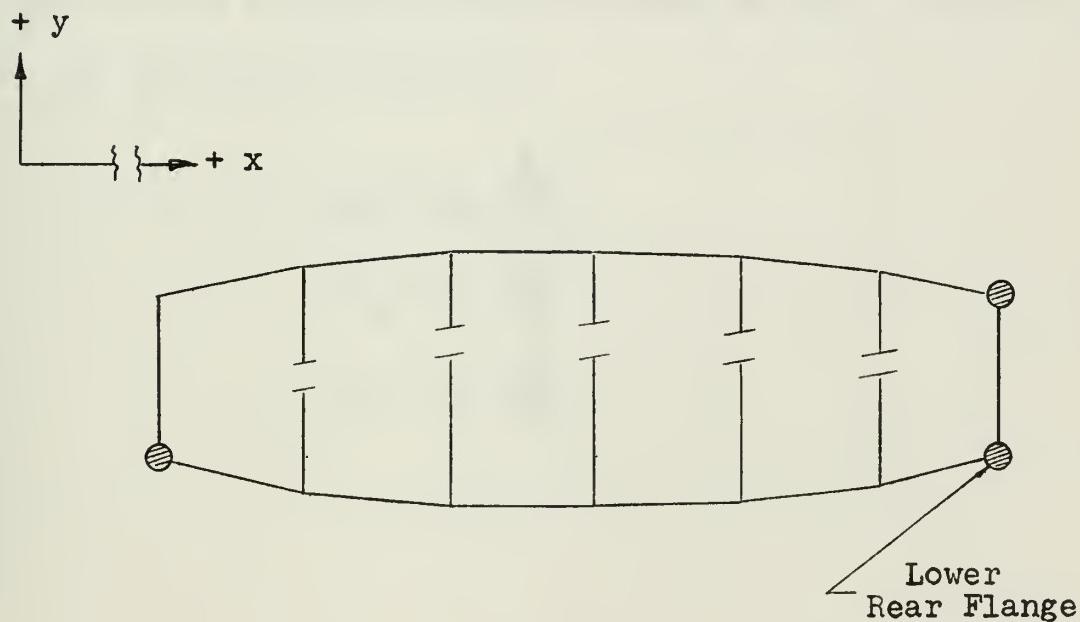
Fig. 14
Cross-section of Determinate System

Since the intermediate "tip" rib at station $y_w = 81.98$ was considered to be determinate, there were 16 redundant and 33 determinate loads. The load numbering system shown in Fig. 13 was established in order to facilitate organization of the analysis method, and to assist in conditioning a matrix for later inversion. Applied loads are therefore numbered P_1 through P_{33}, and the determinate reactions are numbered a_1 through a_{33}. The redundant loads were then assigned numbers a_{34} through a_{49}.

Shear panel edge loads were proportioned by first assigning a unit shear force to the outer edges of all cover panels and beam webs. Unit shear loads were assigned to the forward edge of the rib webs. By representing a typical panel as shown in Fig. 15, where a_i is the unit load, there is:

$$a_b = a_i \frac{\ell_b}{w_c}$$

$$a_c = a_i \frac{w_i}{w_c}$$

$$a_d = a_i \frac{\ell_b}{w_c}$$
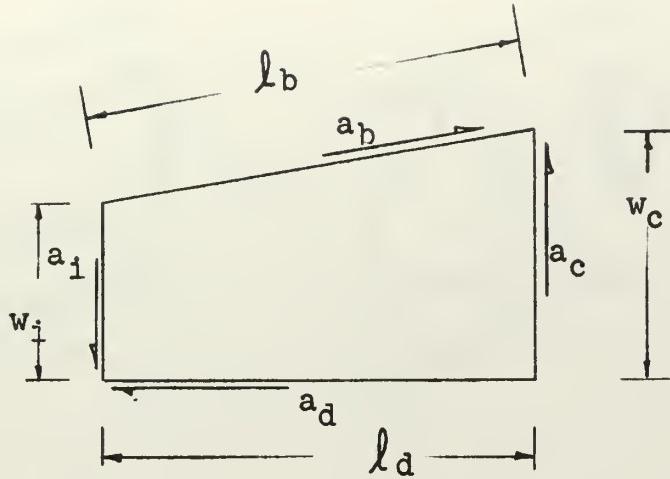
Fig. 15

Proportioning of Panel Edge Loads

The geometry of the panels and the ratios necessary for determining the loads are shown in Table III.

4. Bending Torsion Interaction

Interaction between bending stresses and cover shears was accounted for by the method reported in Ref. 4. Swept panels were assumed to have parallel edges, as shown in Fig. 16. A rectangular panel was then formed with a constant shear flow equal to the average of the end shear flows, as given in Fig. 13.
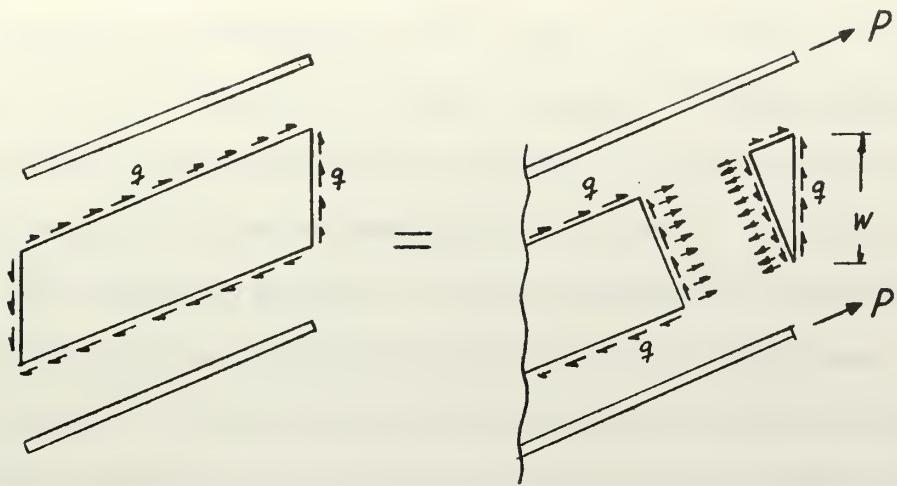
Fig. 16

Allowance For Interaction of Bending Stresses and Cover Shears

The triangular segment remaining was placed in equilibrium by reacting one-half its spanwise component at each spar cap by the load P, where

$$P = q \, w \, \sin \Lambda p$$

Interior spar caps receive a contribution from panels on either side. These loads are shown by dashed arrows in Fig. 13.

5. Equilibrium Equations

Since the redundant loads were to be obtained by minimizing the internal strain energy, 33 independent equilibrium equations were required to establish the load distribution in the determinate structure. Because there were more than 33 members in the structure, some choice was available in writing the equilibrium equations. It was decided to avoid where possible the writing of equations for those members or combinations of members where it was likely a small load would be applied or resisted.

The first six equations were obtained by expressing the equilibrium of the entire model in relation to the axis system chosen:

$$1.) \quad \sum F_x = 0$$
$$2.) \quad \sum F_y = 0$$
$$3.) \quad \sum F_f = 0$$
$$4.) \quad \sum M_{xx} = 0$$
$$5.) \quad \sum M_{yy} = 0$$
$$6.) \quad \sum M_{zz} = 0$$

Using the right-hand rule, each applied load and its "external" reaction may contribute incremental moments according to

$$\triangle M_{xx} = (F_z)_i Y_i - (F_y)_i Z_i$$
$$\triangle M_{yy} = (F_z)_i X_i - (F_x)_i Z_i$$
$$\triangle M_{zz} = (F_y)_i X_i - (F_x)_i y_i$$

Cover shears at either end were assumed to act at the forward or top edge of the panel or beam web.

The delta moments are then summed and set equal to zero.

The next eleven equations were obtained from axial equilibrium of the 11 redundant beam flanges, elements 16, 18, 20, 22, 24, 29, 31, 33, 35, 37, and 39.

Ten more equations were obtained from the rib at station $y_W = 81.98$ by considering the equilibrium of inter-beam segments between the R.B. and R.I.B., R.I.B.-A.I.B., A.I.B.-C.I.B., C.I.B.-FWD.I.B., and FWD.I.B.-F.I.B. For a rib segment, looking inboard from the tip, the moments about the y-axis (lower forward corner of the segment) and forces in the x-direction were set equal to zero, giving two equations per segment.

Following Ref. 5, the vertical shear loads in the beam webs, applied at station $y_W = 81.98$ by loads P_1 through P_7, were assumed to act through seven imaginary posts of unit cross-section, as shown in Fig. 12. The final six equations were obtained by setting all but the F.I.B. post in equilibrium.

This gave a total of 33 equilibrium equations. Each equation was arranged internally so that only the non-redundant (a_1 through a_{33}) loads appeared on the left side of the equation. The applied loads (P_1 through P_{33}) and redundants ($a_{34} - a_{49}$) appeared on the right side.

6. Matrix Formulation

Following the matrix formulation given by References 12 and 13, all at the equilibrium equations can be expressed by

$$[A]_{33 \times 33} \{a_{nr}\}_{33 \times 1} = [B]_{33 \times 49} \left\{ \begin{matrix} \cdot P \cdot \\ \cdots \\ a_r \end{matrix} \right\}_{49 \times 1} \tag{1}$$

Solving equation (1) for the non-redundant loads a_{nr} requires the inversion of the matrix of coefficients, $[A]$. Therefore the row order of the 33 equilibrium equations was arranged to favorably condition the $[A]$ matrix by either placing the large terms on the main diagonal or symmetrically placing groups of terms about the main diagonal. This in turn fixed the arrangement of the $[B]$ matrix. The $[A]$ and the $[B]$ matrices are shown in Tables IV and V.

Since there are 16 redundants, 16 additional equations must be obtained by minimizing the strain energy of the system.

From Refs. 4 and 5, the internal strain energy of the structure may be written as

$$U = \frac{1}{2E} \lfloor a_1 \cdots a_n \rfloor [F] \{a_1 \cdots a_n\} \tag{2}$$

where elements of the symmetric $[F]$ matrix are the sums of
the various member flexibilities. These flexibilities were
obtained as shown in Appendix B. The $[F]$ matrix was
designated $[UC]$ for the digital computer program, and
together with the $[A]$ and $[B]$ matrices, formed the basic
structural input to the digital computer program shown in
Appendix C.

Referring again to equations (1) and (2) it is necessary
to express the strain energy in terms of the external forces
and redundant loads.

Equation (1) was re-arranged by taking the inverse of
matrix $[A]$, and post multiplying the inverse $[A^{-1}]$ by
matrix $[B]$, giving the equation

$$\{a_{nr}\}_{33 \times 1} = [A^{-1}]_{33 \times 33} [B]_{33 \times 49} \left\{ {P \atop a_r} \right\} = [CJ]_{33 \times 49} \left\{ {P \atop a_r} \right\} \quad (3)$$

The column matrix $\{a_{nr}\}$ and the $[CJ]$ matrix were
increased to 49x1 and 49x49 dimensions respectively, by
simply adding the trivial equations

$$\begin{aligned}
a_{34} &= a_{34} \\
a_{35} &= a_{35} \\
&\cdot \\
a_{49} &= a_{49}
\end{aligned} \quad (4)$$

The augmented matrix $[CJ]$ was then redesignated the
$[G]$ matrix.

The transpose of matrix $[G]$ was then taken, allowing the strain energy matrix $[H]$ to be formed:

$$[H]_{49 \times 49} = [G']_{49 \times 49} [F]_{49 \times 49} [G]_{49 \times 49} \qquad (5)$$

By substituting equation (5) into equation (2), the internal strain energy may now be written as

$$U = \frac{1}{2E} \lfloor P_1 \cdots P_{33} \, a_{34} \cdots a_{39} \rfloor_{1 \times 49} [H] \{ P_1 \cdots P_{33} \, a_{34} \cdots a_{49} \} \qquad (6)$$

The strain energy is then minimized by differentiating equation (6) and setting the result equal to zero, according to

$$\frac{\partial U}{\partial a_r} = 0 \qquad (7)$$

Since $[H]$ is a symmetrical matrix, it may be shown that the operations of equation (7), as performed upon the expanded form of equation (6), may be expressed simply by

$$\{ a_r \}_{16 \times 1} = - [H_{22}^{-1}]_{16 \times 16} [H_{21}]_{16 \times 33} \{ P \}_{33 \times 1} \qquad (8)$$

The sub-matrices $[H_{22}]$ and $[H_{21}]$ come from the partitioning of $[H]$ according to:

.

$$[H]_{49 \times 49} = \begin{bmatrix} H_{11} _{pxp} & \vdots & H_{12} _{pxr} \\ - - - & \vdots & - - - \\ H_{21} _{rxp} & \vdots & H_{22} _{rxr} \end{bmatrix}_{49 \times 49} \qquad \begin{matrix} p = \text{applied load} = 33 \\ \\ r = \text{redundant} = 16 \end{matrix} \qquad (9)$$

By defining the product of $\left[H_{22}{}^{-1} \right]$ X $\left[H_{21} \right]$ as:

$$[EN]_{16 \times 33} = -\left[H_{22}{}^{-1} \right]_{16 \times 16} \left[H_{21} \right]_{16 \times 33} \qquad (10)$$

the answers to the redundant loads, as given in the computer program of Appendix C, are:

$$\{a_r\}_{16 \times 1} = [EN]_{16 \times 33} \{P\}_{33 \times 1} \qquad (8b)$$

The total loading system is then determined from

$$\{a\}_{49 \times 1} = [S]_{49 \times 33} \{P\}_{33 \times 1} \qquad (9)$$

where the matrix $[S]$ is constructed from $[EN]$ and $[G]$ by

$$[S] = [G]_{49 \times 49} \begin{bmatrix} [I]_{33 \times 33} \\ - - - - - \\ [EN]_{16 \times 33} \end{bmatrix}_{49 \times 33} \qquad (10)$$

Finally the internal strain energy is written in terms of the applied loads and the flexibility influence coefficients $[C]$ as:

$$U = \tfrac{1}{2} \left\lfloor P_1 \; \ldots . P_{33} \right\rfloor \left[C \right]_{33 \times 33} \left\lfloor P_1 \; \ldots . \; P_{33} \right\rfloor \qquad (11)$$

By substituting equation (8b) into equation (6), the matrix of flexibility influence coefficients is given by

$$\left[C \right] \;=\; \frac{1}{E} \left(\left[H_{11} \right] \;-\; \left[H_{12} \right] \left[EN \right] \right) \qquad (12)$$

7. Computer Programming

The solution of equations (1) through (12) was adapted by a FORTRAN program to the CDC 1604 computer. The variable names and abbreviations, flow charts, programs and sub-routines are given in Appendix C.

Considerable effort was required to establish the desired program within the basic computer storage capacity. Any future additions to the main program would require either use of machine language or an input-output program on peripheral equipment.

Print-outs throughout the program were made in order to establish a means for continuing accuracy checks. Although a complete hand solution of one set of data is possible in many computer programs where merely repetitious iterations are done, here only equilibrium of elements and

31

standard machine inversion checks could be made.

The first machine check was performed by writing a short auxiliary program named CHECK. This confirmed the accuracy of the inversion of the matrix $[A]$ as accomplished by the single-precision Gauss 3 subroutine. The matrix $[CHECK]$ was formed from

$$\begin{bmatrix} CHECK \end{bmatrix}_{33 \times 33} = \begin{bmatrix} A \end{bmatrix}_{33 \times 33} \begin{bmatrix} A^{-1} \end{bmatrix}_{33 \times 33} \overset{?}{=} \begin{bmatrix} 1 & & & & & \\ & 1 & & & & \\ & & \cdots & & & \\ & & & \cdot\cdot & & \\ & & & & \cdot\cdot & \\ & & & & & 1 \\ & & & & & & 1 \end{bmatrix}_{33 \times 33} \tag{13}$$

and is shown in Appendix C.

The second check was made by comparing the member loads of the statically determinate structure with values from the $[CJ]$ matrix shown in Table VI. For example consider the statically determinate structure shown in Fig. 17.
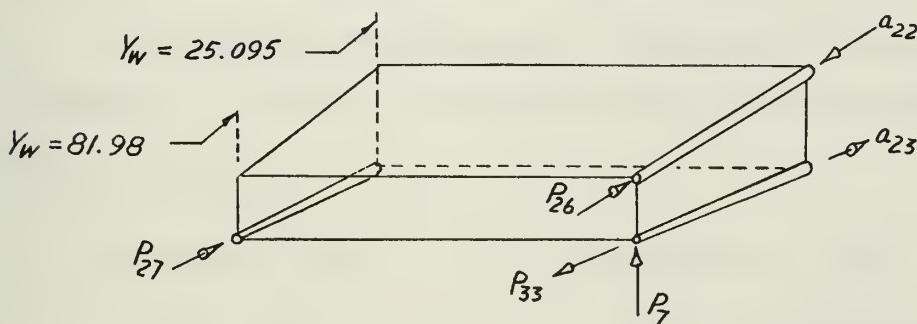
Fig. 17

Loaded Determinate Structure For $[CJ]$ Check

From statics a value of a_{22} may be obtained for a unit load P_7. This should compare with the value $CJ_{22,7}$ in the expression

$$\left\{a_{nr}\right\}_{33 \times 1} = \left[CJ\right]_{33 \times 49} \left\{\frac{P}{a_r}\right\}_{49 \times 1} \tag{14}$$

where all terms in the column load matrix are zero except P_7.

Setting the y-component of a_{22} equal to $(a_{22})_y$, by statics:

$$(a_{22})_y = P_7 \times \frac{(81.98 - 25.095)}{7.20} = 7.900694 \ P_7$$

$$a_{22} = \frac{7.900694 \ P_7}{.89114} = 8.86583 \ P_7$$

From equation (14), and the matrix $\left[CJ\right]$

$$a_{22} = P_1 \ (8.8660330) + \ldots + P_7 \ (8.8660330)$$

which checks well to the fourth decimal.

By similar reasoning, the three non-redundant flanges, elements 14, 26 and 27, should react directly the loads P_{27}, P_{26}, P_{33}.

Applied loads	Reaction by $\left[CJ\right]$ matrix
$P_{27} = 1.0$	$a_{21} = 1.0000558$
$P_{26} = 1.0$	$a_{22} = 1.0000268$
$P_{33} = 1.0$	$a_{23} = 1.0000238$

Again considering a unit load at P_7, the total shear load should be carried by the rear beam web, a_8. From the $[CJ]$ matrix, a unit load at P_7 gives

$$a_8 = 1.0103419$$

Consequently, the cover panel shear loads should be zero. From the $[CJ]$ matrix,

a_9 = .0000646	a_{15} = .0000437
a_{10} = .0000591	a_{16} = .0000471
a_{11} = .0000550	a_{17} = .0000511
a_{12} = .0000510	a_{18} = .0000550
a_{13} = .0000471	a_{19} = .0000591
a_{14} = .0000438	a_{20} = .0000645

The next check was to determine the state of equilibrium of each flange and post. For example, the front post of the intermediate rib, station $y_w = 81.98$, Fig. 12, gives

$$1.0000000 - .5981273 - .4018727 = .0000000$$

for a unit load at P_1. For the seventh post, the result from a unit load at P_7 is also zero. A maximum deviation from true equilibrium of 7.9 percent existed at the second

34

post from the front. It should be noted that no equilibrium equation was written for this post.

Referring to Fig. 13, a unit redundant load was applied in turn to each redundant flange. The greatest deviation from equilibrium was in element 39, where

$$\text{Error}_{[CJ]} = -0.0000043 \text{ lb}$$

Table VII contains the results of the CJ matrix equilibrium checks, which completes the check of the basic equations and computer operations on them, as well as the validity of the matrix inversion sub-routine.

A print-out statement was used to determine that proper partitioning of the $[H]$ matrix occured. Since computer storage space was not available, hand calculations were performed to confirm the proper inversion of $[H_{22}]$.

An interim calculation according to equation (8b) gave the redundant load matrix $\{AR\}$. One of these values was computed by hand as a random check and found to be correct. All 16 values were then checked with the final 16 loads of the $\{AT\}$ matrix obtained from equation (9).

This completed the computer program checks. The program was then run twice and answers compared in order to detect any computer core errors. There were none.

The flexibility influence coefficient, stress influence coefficient, and load matrices, $[C]$, $[S]$, and $\{AT\}$, are listed in Tables VIII, IX, and X.

8. Theoretical Results

Compared with ordinary beam theory solutions, the accurate determination of stresses in an idealized structure by a matrix force method requires considerable engineering judgment. It has been pointed out by Warren (Ref. 9) that errors of one-hundred percent may occur in interpreting the results of such a solution. Therefore the original formulation assumptions were used in determining the results of this analysis.

The investigation was narrowed to determining the average panel stress at station $y_W = 34.5$ from the loads of the $\{A^r\}$ matrix. For each panel, the maximum normal stress, the angle of the principal axis, and the maximum shearing stress were determined. From the components shown in Fig. 18, and noting that the direction of shear flow reflects the minus sign indicated by load a_9 in the $\{AT\}$ matrix,
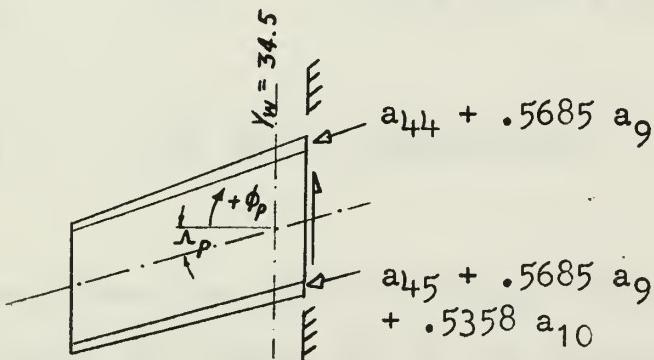
Fig. 18

Theoretical Root Panel Stresses

36

the axial load components of the skin were determined. Using the solution formulation data of Table I, the bar loads (excepting a_{10}) were re-apportioned by area ratios to the panels from which the skin came. For panel 38, shown in Fig. 18,

$$\frac{.974}{1.50} a_{44} + \frac{1.03}{3.04} a_{45} + 1.137 a_9 = \text{axial load}_{38}$$

$$.6493(5461) + .3388(8682) + 1.137(-3785) = 2184$$

or, axial panel load = 2184 lb compression. This compressive force, when divided by the panel and cross-section (taken perpendicular to the panel sweep angle, Λ_p), gives

$$\sigma_{\Lambda_p} = \frac{2184}{tw} = \frac{2184}{.145 \times 20.89 \times .73865}$$

$$\sigma_{\Lambda_p} = 978 \text{ psi (compression)}$$

The shearing stress was found by taking the average shearing force, given for either end of the panel by the $\{AT\}$ matrix, and dividing it by the same tw used in determining the axial stress. The shearing stress and axial stress thus found were resolved by Mohr's circle to a

37

maximum principal stress, σ_{max}, a maximum shearing stress, τ_{max}, and the angle of the principal axis, ϕ_p. These stresses and angles, as listed in Table XI, refer to the mid-plane of the skin, since average values are used for their determination. These values are shown graphically in Fig. 25.

The vertical deflections of the intermediate rib (station $y_w = 81.98$) end points were calculated from the deflection influence coefficient matrix $[C]$ by applying the theoretical vertical loads P_1 through P_7. At the forward end of the rib(load point for P_1) the deflection was + .0601 in. At load point seven, the deflection was -.0647 in. These values are plotted in Fig. 26.

1. Introduction

In order to determine the actual stresses and compare them with those predicted by theory, an experimental investigation has been carried out on the full scale F8U-3 wing acquired from Chance Vought Aircraft, Incorporated. The experimental set-up was also designed to provide the Aeronautical Structures Laboratory of the U. S. Naval Postgraduate School with a permanent specimen of modern wing construction mounted such that a variety of test-to-theory correlation experiments could be academically demonstrated.

The F8U-3 wing was structurally complete in every detail and was representative of current doubly tapered multi-cell swept wing configurations. It was divided into three major sections, the center section which extended to the wing fold rib at wing station $y_w = 152.25$ and an outer panel on either side. For this experiment the two outer panels were removed along with the leading edges and those portions of the trailing edges outside of the main structural box that were not integrally connected with its single piece skin. Hereafter the term wing will refer to the main structural elements of the center section which consisted of seven spars, hereinafter called beams, and two streamwise ribs. The section was a typical thick

milled skin construction and the skins were tapered along the span as well as in the chordwise direction.

Structural behavior was investigated with the wing subjected to two pure torque loads applied perpendicular to the elastic axis at the wing fold rib. The elastic axis is defined by the curve connecting the shear centers of all sections of the wing. Its position was taken from manufacturer's data as shown in Fig. 8. The torque loads were applied to each wing fold rib by hydraulic cylinders actuated from a common pressure manifold. The load magnitudes were measured by dynamometers connected in series with each cylinder and the torque was then easily computed knowing the fixed lever arm. Nominal torque values of 294000 in. lb and 336000 in. lb were used. These were well within the elastic range but still of sufficient magnitude to give adequate strain levels throughout the structure for repeatably accurate measurements.

Some electrical strain gages were already installed by Chance Vought Aircraft, Incorporated, at various locations, but for the purposes of this and future investigations additional SR-4 strain gage rosettes of the AR-7-2 and A-7 type were installed in particular areas. Those of immediate interest were located in the skins, beam webs and beam caps around a section perpendicular to the center

intermediate beam at wing station $y_W = 98.7$. From the wing fold to this point the elastic axis remains nearly parallel to the center intermediate beam which was used as the reference axis of the wing. Other rosettes were located around a streamwise section near the root at wing station $y_W = 34.5$. Here rosettes were placed on both sides of the very thick skin to check for differential bending effects. It was expected that the stresses that are unpredictable by simple beam theory in this area would show closer agreement with the predictions of the matrix force method of analysis. Strain gage data was programmed into a digital computer to obtain principal stresses and directions at all rosette locations.

Deflections were measured by means of scales hung from the structure along the front and rear beams and read by a transit. Jig support deflections were also measured in this manner.

2. Equipment

The variable incidence swept wing was of a conventional multi-cell construction with a quarter-chord sweep back of 42 degrees. The main structural elements are shown in Fig. 8. Fig. 19 is a photograph of the wing with the upper skin removed. Attachment was made to the fuselage at approximately wing station $y_W = 25$ by two pivot lugs located approximately 5.3 inches aft of the main box rear beam,

two bumpers located at the main box front beam and two incidence actuators located approximately 17.8 inches forward of the main box front beam. The wing fold at wing station $y_w = 152.25$ was accomplished by fittings with multiple upper and lower lugs. The upper and lower surfaces were single piece thick skins tapered along the span and chord. The front beam had numerous supporting lugs integrally machined into the beam giving it a very discontinuous variation of thickness. The structure primarily consisted of 7079-T6 thick skins and forgings with 7075-T6 sheet metal beams.

The wing was mounted inverted on a rigid support jig and fastened to it at four points, the two fuselage pivot lugs and the two points on the main box front beam directly opposite the bumper points. Plywood pads were used under the jig to distribute the loads to the laboratory floor. A photograph of the mounted wing is shown in Fig. 20.

The torque loads were applied through a fitting connected to the wing fold lugs as shown in Fig. 6. The fitting assembly was designed to provide a loading plane perpendicular to the plane of the wing and the elastic axis. It consisted primarily of mild steel parts designed to develop the ultimate strength of the wing fold lugs. A limiting torque of 420000 in. lb was selected which was well below the design ultimate at this station but still high

enough to ensure adequate strain levels in the wing. A 42
inch lever arm was used to permit attainment of the 420000
in. lb of torque with loads of only 10000 lb. This enabled
the use of available 10000 lb dynamometers which were
graduated in 100 lb increments. Instruments of larger
capacity had 250 lb increments.

Only the port wing was instrumented but the torque was
applied to each wing fold station for balance and to
minimize warping of the structure and support jig. Each
of the four loads were applied through a series linkage of
attachment fittings, clevises, hydraulic cylinder and
dynamometer as shown in Fig. 21. The four hydraulic
cylinders were high pressure wing fold actuators and were
simultaneously subjected to pressure from a common manifold
to insure load equalization. Except for the dynamometers
each linkage was designed for 30000 lb and was pre-tested
to 15000 lb before installation.

Load magnitude was determined and monitored by two
separate means. On the instrumented wing two 10000 lb
Dillon Dynamometers were used to monitor equality of
individual loads. They were graduated in 100 lb increments
but could be accurately read to 10 lb. The final load
magnitudes were determined by hydraulic manifold pressure
related to pressure-load calibration curves for the
cylinders as found in Appendix D. The hydraulic gage was

mounted at the data taking station and provided an excellent means of setting the load and monitoring the consistancy of its magnitude throughout the run. It was a 1500 psi gage graduated in 10 psi increments and could be accurately read to 5 psi.

The dynamometers and the hydraulic system were calibrated on a 300,000 lb Riehle Tensile Testing Machine (Appendix D). The Reihle machine had exhibited a maximum calibration error of only 0.35 percent over the entire 300,000 lb range, but showed no error in the range of 7000 lb to 9000 lb, which was of concern in this case. Therefore the calibration curves represent variation from absolute values.

The up-load linkages were anchored to a three column supporting structure shown in Fig. 21. The base of this structure was arranged to accommodate attachment of the down-load linkage thereby minimizing strength requirements of the base elements. Considering future uses of this structure the base was located approximately in the plane of the load fitting such that single point loads could be applied anywhere along its reach and be readily anchored with a minimum of effort.

Hydraulic pressure was supplied by an electrically driven Vickers V-line Piston Type Pump shown in Fig. 22. It was rated at 5000 psi, 1800 rpm and 1.72 cu in. per

revolution. By means of a pressure compensator in
conjunction with a volume limit hand control and relief
valve, pressures could be held within 5 psi of any desired
setting for long period of time and with very few adjust-
ments. This feature enabled accurate repetition of the
same loads which was essential in the data taking process.

All strains were measured with SR-4 strain gage
rosettes manufactured by Baldwin-Lima-Hamilton Corporation.
In Appendix E is a list of the 485 gages, their gage factors,
resistances and coordinate locations in the wing. The types
of gages installed by Chance Vought Aircraft were deduced
from resistance tests and inspection. They were all of
the AX-5 or AR-1 type. The gages installed for this
experiment and for future multi-purpose investigations were
either of the AR-7-2 or A-7 type. The gages of particular
interest to this investigation are depicted in Fig. 23.
Selected root skin rosettes are backed-up on both sides of
the skin. Although additional back-up rosettes were
desired throughout the inboard panels, they could not be
installed because of time, laboratory priority and monetary
considerations. Note that all of the gages have a gage
factor very close to 2.0 and resistances of 120 ohms. This
enabled the use of a single temperature compensating gage
and factilitated reading all gages without adjusting any
of the other instruments.

Selectivity in reading any combination of gages was made possible by routing all gage leads to a junction panel as shown in Fig. 24. Any number of gages could then be connected into either switching and balancing units or automatic scanning devices as future needs dictate. All electrical connections were soldered to minimize contact resistance except for the banana plug connections between the junction panel and the switching and balancing unit.

A 20 channel Baldwin-Lima-Hamilton Switching and Balancing Unit was used. It was connected to an external Wheatstone bridge circuit powered by a Hewlett Packard Power Supply (Model 721A). A constant 6 volts was used throughout the tests. The bridge output was amplified, then fed into a voltage-to-frequency converter and displayed as strain in units of micro-inches per inch by an electronic counter. Calibration of this equipment proceeded each run and the method is described in Appendix F.

The electronic counter was a Model 521DR manufactured by Hewlett Packard Corporation. The voltage-to-frequency converter was a Model DY-2210 manufactured by Dymec Incorporated and the amplifier was a Kintel Model 111BF. By using the electronic counter, readings could be taken faster and more accurately than with the common strain indicators. Strain indicators can normally be read to about 5 micro-inches per inch, whereas the electronic counter

indicates strains to one micro-inch per inch.

Wing deflections were measured by means of scales hung at intervals along the front and rear beams and read by a transit manufactured by Keuffel and Esser Company. The scales were graduated in .02 inch increments but could be read to .005 inch. The locations of the scales are shown in Fig. 8. Note that a single scale could be paired with one of two others such that either a streamwise chord or a section perpendicular to the center intermediate beam would be defined. For instance, scale numbers 8 and 7 define the test section perpendicular to center intermediate beam at wing station y_w = 98.7 and number 8 and 11 terminate the streamwise rib at wing station y_w = 81.98. This was believed to be of use in future investigations.

3. Experimental Procedures

The experimental procedures consisted of two tests, in each case a different magnitude of torque being applied at the wing fold rib. In the first test a nominal 294000 in. lb was applied and 336000 in. lb in the second test. These values were initially attained by dynamometer indications of 7000 lb and 8000 lb respectively, which will be the names of the two tests hereafter. The purpose of the 7000 lb test was to establish reliability of the entire 485 strain gages and to check for linearity of strain readings in the structure. The 8000 lb test was accomplished

47

to correlate the theoretical results. Therefore in the 8000 lb test attention was focused on approximately 150 gages of particular interest.

The procedure in conducting the tests was straight forward, but because of the large number of strain measurements the tests took considerable length of time. Only 20 gages could be read during any one run because only one switching and balancing unit was employed. Additional units were tried but the added wiring and connections, resistance peculiarities inherent in each unit and prolonged time required to adjust initial zeroes, produced an unacceptable drift in the zero rechecks. On the other hand load repeatability was very accurate and therefore a single unit was used and the number of runs increased. The sequence of operation for each run was as follows:

1. The electronic counter was calibrated before each series of runs and rechecked after completion.

2. The switching and balancing unit leads were plugged into 20 gage terminals at the junction panel.

3. All strain gages and dynamometers were zeroed.

4. The hydraulic loads were applied and adjusted by reference to previously known values of hydraulic pressure and strain gage readings from the same check gage used in each test run.

5. The dynamometers were read and compared with each

other to insure that equal couple loads were being applied to each wing.

    6.   The strains were read and recorded twice.

    7.   The loads were removed.

    8.   All zero values of strain were re-checked and recorded.

Extreme care was employed to achieve load and strain repeatability. The electronic counter was calibrated before each run and checked afterwards. A maximum departure from linearity over a range of 1000 micro-inches per inch was only 5 micro-inches per inch. The average departure . was closer to 2 micro inches per inch. This effect on maximum strain levels encountered (approximately 200 micro-inches per inch) was therefore quite negligible.

In addition particular care was exercised to minimize the strain gage zero drift. For instance, the variable temperature effects of sunlight and outside electrical interference with the sensitive instrumentation were virtually eliminated by conducting all tests at night. At least one hour warm-up time was given all instruments to insure steady state conditions. All initial zeroes were re-checked three times before loading. All permanent electrical connections were soldered to minimize contact resistance and, as a double precaution, a test was repeated

if any electrical leads had been disturbed or if the voltage supply varied any time during the run. By reading only 20 gages per run the time per run was minimized, thereby reducing the critical time the system would be exposed to outside effects. Two strain readings at load were taken also as a double check. With such care, average zero rechecks within 1.5 micro-inch per inch were continually demonstrated.

Two strain gages were selected to act as cross-checks on the repeatability of the loads, results and test conditions. Gages 32 and 53 were monitored in each test run. The magnitudes of strain on each run were then compared to the original values. In over 40 runs the average departure from mean values of the check gages was only 1.39 micro-inch per inch. The mean value for gage 53 in the 8000 lb test was 178.6 giving an error of only 0.78 percent. Since the hydraulic pressure reading required to produce this strain level was always the same the load repeatability was also within an accuracy of one percent.

Accuracy of measuring the absolute load magnitude was then dependent only on the accuracy of the dynamometers and hydraulic pressure gage. During the weeks of testing, difficulty was encountered in re-setting the dynamometers to the same zero. Also there was noticable differences

in readings under load conditions which verified suspicions of unreliable zero settings. On the other hand the hydraulic pressure gage readings checked consistantly with strain gage 32 and 53 readings and therefore the pressure gage was felt to be more reliable in establishing magnitudes of applied loads.

Deflection measurements were made for only the 8000 lb test condition. Since this loading condition and consequently the deflections were repeated over 20 times it was deemed necessary to only sample the deflections periodically throughout the test series. Although more deflection measurements were taken to ensure repeatability in the series only three complete sets of data were recorded.

4.   Experimental Results

From the recorded strain data the only calculations required were those involved in determining the principal stresses, maximum shear stress and principal axes at each rosette location. These calculations for all rosettes in the 7000 lb test and those particular rosettes of interest in the 8000 lb test were performed on a Control Data Corporation 1604 Digital Computer. The results along with the FORTRAN program and the measured strains are found in Appendix G.

The data for the 7000 lb test was pertinent to this experiment only to show linearity of strain readings. A sampling of net strain readings from various locations for both loading conditions is shown in Table XII. Satisfactory linearity is demonstrated by noting that the average difference between measured strains for the 8000 lb test and those extrapolated from the 7000 lb test is 2.3 micro-inches per inch regardless of the magnitude of the measurement. The discrepancy is obviously quite small but it would be still further diminished if the accuracy of the applied loads were considered. Therefore it can be concluded that linearity of strain readings was indeed achieved.

Another result of the 7000 lb test was the discovery of 9 faulty rosettes. However none of the faulty rosettes hampered the results of this experiment. The faulty gages are indicated in Appendix E.

Calibration of the hydraulic system after the completion of the tests revealed that instead of 8000 lb, actually 8400 lb loads were being delivered to the linkages. Considering a gage reading accuracy of 5 psi and the slope of the calibration curve as 10.84 lb load per psi hydraulic pressure, the accuracy of the applied loads would be plus or minus 50 lb or 0.6 percent. The difference in desired and achieved magnitudes is not of real importance however

since linearity of strains enables interpolation to the desired values.

Since a degree of uncertainty always exists concerning the extent to which a pure torque loading is realized, an equilibrium check was made at the instrumented section perpendicular to the GIB at $y_W = 98.7$. At this section all rosettes were oriented such that the diagonal gages were at a 45 degree angle to the section, which facilitated shear flow calculations. Therefore theoretically calculated shear flows could be readily checked with experimental results since the theoretical calculations were all ready completed in the determination of the loading for the idealized structure as shown in Appendix A.

The experimental shear flows were calculated by considering only the strains in the diagonal gages. This essentially eliminated the effects of any normal stresses caused by unknown bending loads and the results would better represent the shear flow induced by only the effectively applied torque. From the experimental data for the 8000 lb load, shear flows were calculated using the relation,

$$q = \frac{E\ t\ \epsilon_2}{1 + \mu} \qquad (15)$$

These results are listed in Table XIII and are labled on
the schematic diagram in Fig. 25. The values of shear
flow in the top and bottom skin of the same cell compared
closely. The average value of each cell was used as also
shown in Table XIII and Fig. 25 and compared to the
theoretical values. The theoretical shear flows for
T = 336000 in. lb were 3.85 percent higher than the experi-
mental values. The total torque resisted was then computed
as the sum of the (2Aq) for each cell. This value was
323,785. in. lb which is 8.2 percent lower than the
352,800 in. lb possible with an 8400 lb force acting on a
42 inch lever arm, and 3.6 percent lower than that used in
the analysis.

Neglecting the accuracy of the experimental loads and
shear flow determination this means that 720 lb of the
applied load of 8400 lb was not effective in producing pure
torque. In this regard, during the tests there had been
visible evidence of streamwise twisting of the wing fold
rib and a measured spanwise tilt of the entire wing. There
was also an element of uncertainty regarding the exact
angle of the elastic axis since it was scaled from a
reproduced drawing. Coupled with understandable inaccuracies
of maintaining a constant loading plane, perfectly parallel
lines of force and a perfectly rigid loading jig, the amount
of the bending load component is within reason. Although

no calculations were made to determine the magnitude of the bending component its existance can be qualitatively confirmed by observing the magnitudes of the strain readings for the perpendicular gages at the section being analyzed, namely rosette numbers 131, 46, 49, 52, 55, 58, etc.

Using a torque value of 323,785. in. lb the theoretical shear flows were obtained by interpolating between values computed for the 294000 and 336000 in. lb condition. They are also shown in Table XIII and Fig. 25. As would be expected the comparison with experimental values is very good. The average error in the theoretical shear flows is only 1.95 percent. Considering the loss of effective applied torque the torsional equilibrium check was believed to be quite close.

The computer program described in Appendix G solves the well known rectangular rosette equations for σ_{max}, σ_{min}, τ_{max} and ϕ_p. The input to the program was the value of strain for each gage in the rosette. The lowest numbered gage was consistantly called ϵ_1, the diagonal and perpendicular gages were the next higher numbered gages respectively. The principal axis was then computed with respect to the ϵ_1 axis. To compare these results with theoretical values the orientation of the principal axes were adjusted to the y_W axis of the wing by simple arithmetic.

55

The root area rosettes used to compare with results of the theoretical root analysis were numbers 13, 19, 28, 367, 279 and 161 on the inside surfaces and back-up rosettes numbers 481, 478, 472, 466, 457, and 484 on the exterior surfaces. Differential bending was readily apparent in all of the root panels as seen in Table XIV by noting the differences of strain in matching gages on opposing surfaces. The effect is less in panel number 21 which lies near the elastic axis. The average of the two gage readings was taken as representative of the strain at mid-thickness of the skin. The values of σ_{max}, τ_{max} and ϕ_p were then hand calculated using the equations in Appendix G and are listed in Tables XI and XIV and plotted in Fig. 26.

The deflection measurements were of concern primarily in establishing test conditions. In this regard the average values of the total deflections are plotted in Fig. 26. It is clearly shown that the support jig rocks forward and the entire structure tilts right-wing-down. It was also noted during the test that the amount increased slightly with each cycle which indicated plastic yielding of the plywood pads under the support jig. Obviously any tilt would adversly affect the lines of action of the applied loads since the load linkages were positioned to accommodate only one loading plane. This would account for some of the discrepancy in achieving pure torque loads. It would be

wise to consider adjusting the load fittings and linkages
such that a more symmetric loading could be realized in
future tests. Furthermore it would be advantageous to
replace the plywood pads with a more suitable material.

IV COMPARISON OF RESULTS

Extreme care was taken to ascertain strain and load

...itudes and insure repeatability of loads to minimize

any experimental error in the determination of the compar-

itively low stress levels found in the critical root area.

All of these errors were kept well below one percent and

logically do not appreciably influence any comparison with

theory.

The only experimental error that would noticeably

affect the final results would be the understandable

discrepancy in developing pure torque loading on which

the theoretical analysis was based. The equilibrium check

at the section perpendicular to $C.I.B.$ at $y_W = 98.7$ indicated

that the torque developed was 3.6 percent lower than that

used in the analysis and nine percent lower than actually

applied at the tip. This meant that about 8.6 percent of

the applied load introduced unwanted bending effects that

were not accounted for in the analysis. The cause of the

torque discrepancy is correctly attributed mainly to the

method of loading and tilting of the support jig. Other

than reducing the accuracy of the experimental results

to a comparatively minor degree the effect of the small

bending loads would not measureably influence the

comparison with theory in such a complex structure. These

factors become even less important in establishing the

general validity of this analytical method to an actual complicated wing when one is reminded that the literature mentions 100 percent disagreements in comparing results of other methods applied to simplified thin-skinned laboratory specimen.

Experimental and theoretical results for the root area are listed in Table XI. Three observations may be made immediately. The sense of maximum normal stress, the orientation of the principal axis, and magnitude of stresses at the critical rear panel area agree rather well. Maximum shear stresses differ by only 25 percent, and although one of the maximum normal stresses differs by 40 percent the other is only seven percent. On the other hand, the theoretical stresses obtained at the leading edge are much too high. This is shown graphically in Fig. 27. Since the equilibrium checks made during formulation of the problem indicated excellent equilibrium existed, and agreement of theoretical and experimental results at the rear of the wing is good, the leading edge divergence was likely to be the result of an initial assumption.

Attention was immediately directed to the root boundary conditions. It was assumed that the pivot rib (considered to be the root of the idealized model) was infinitely stiff and completely resisted chordwise deformation. This is still felt to be a reasonably accurate assumption. However,

re-examination of the drawings of the pivot rib indicates
that the rib width varies by descreasing from rear to front
substantially. Moreover, the skin thickness varies the
same way. It would therefore appear that significant twist
about the streamwise axis occurs towards the front of the
pivot rib. This has the effect of removing the root
restraint imposed upon the theoretical analysis, and allows
stress relief to occur towards the leading edge in the actual
case.

The sizeable differences in back-up gage readings
would further stimulate interest into investigating the
plate bending and twisting effects of individual panels
about their respective axes. Unfortunately, insufficient
back-up gages were installed to establish any definite
conclusions, but examination of the stresses at the
available back-up locations and the stresses measured by
neighboring rosettes on only one side of the skin evokes
considerable concern in this area. Panels 25 and 30
would be particularly well suited for such an investigation
in the future.

It is therefore believed that the analysis method
can achieve accurate results for this wing. The boundary
condition in question could be removed entirely from the
analysis by moving the theoretical root to the aircraft
center line. This would introduce only 16 new unknowns

to the analysis, all within the additional rib required at station $y_w = 25.095$. The addition of 16 unknowns would in turn require conversion of the computer program to machine language in order to accommodate the increased storage requirements. This could be accomplished by use of the Fortran MAP program available at the U. S. Naval Postgraduate School Computer Facility.

There were no load attachment points on the specimen corresponding to the analytical load attachment points. This could have enabled direct experimental verification of a greater portion of the flexibility influence coefficient matrix $[C]$ (Table VIII). However two node points can be compared here. The measured net vertical deflections at scale numbers 8 and 11 (Fig. 26) are compared to deflections caused by the analytically calculated vertical loads P_1 through P_7. At scale number 8 the theoretical value differs from the measured value by only 16.8 percent and at scale number 11 the difference is only 14.8 percent. The better agreement between theoretical and measured deflections was expected(Ref. 9).

Improved accuracy in the solution could undoubtedly be obtained by reducing the size of the structural grid. This would at the least double the number of unknowns. With the additional element flexibilities required, computer programming should be extended to do more of the

labor. As has been pointed out by Rattinger and Gallagher (Ref. 2), up to three man-years may be required for completely programming a solution using a displacement method. It is felt that the force method of this report could be extended to twice the current size with about one man-month additional effort, if project familiarity were equal to that of the writers.

V CONCLUSIONS AND RECOMMENDATIONS

1. Conclusions

It can therefore be concluded that a valid comparison was achieved between experimental and theoretical stresses as predicted by the matrix force method of analysis, using a structural idealization proposed by Wehle and Lansing. Further, this analytical method gave remarkably reasonable results in the critical rear root area of the highly complex structure.

The failure of the method to agree with actual stress conditions in the forward root area is attributed primarily to the simplifying assumption that the pivot rib was infinitely rigid.

2. Recommendations

It is recommended that all cover skin rosettes, especially those between the intermediate and pivot rib, be backed-up. This would greatly enhance the experimental potentiality of the laboratory by providing means to investigate the plate phenomena of bending and twisting of individual panels about their respective axes.

In addition greater academic value could be realized from the analytical results if means were provided for applying single point loads at the intersections of the intermediate rib and the beams. This would permit further interesting academic demonstrations by utilizing the matrix

of flexibility influence coefficients produced in this analysis.

It is further recommended, to improve the accuracy of the analytical predictions along the entire root area, that the root boundary condition assumed in this analysis be eliminated by moving the theoretical root to the wing center line rib. This would not require substantial increase in analytical complexity and would greatly enhance the agreement between theory and actual measurement.

It is finally recommended that the experimental method of loading be improved to enable better development of pure torque. In this regard an exterior rib, clamped around the section perpendicular to the center intermediate rib at wing station $y_W = 143$, would eliminate the streamwise twist of the wing fold rib. Regardless of the method of loading, the plywood pads under the wing support jig should be replaced with a more suitable material.

REFERENCES

1. Argyris, J. H., and S. Kelsey: Energy Theorems And Structural Analysis, Butterworths, London, 1960.

2. Rattinger, I., and Richard H. Gallagher: Supersonic Aeroelastic Effects On Stability And Control. Wright Air Development Division Technical Report WADC 58-95, April, 1960.

3. On The Analysis Of Complex Elastic Structures, Argyris, J. H. Applied Mechanics Reviews, July, 1958.

4. A Method For Reducing The Analysis Of Complex Redundant Structures To A Routine Procedure, Wehle, L. B. Jr., and Warner Lansing, Journal Of The Aeronautical Sciences, October, 1952.

5. Some Results Of Sweptback Wing Structural Studies, Lang, A. L., and R. L. Bisplinghoff. Journal Of The Aeronautical Sciences, November, 1951.

6. Smith, F. C.: Stress and Deflection Analysis of Aircraft Structures Using Strain Energy Theory in Conjunction With Electronic Digital Computers. Chance Vought Aircraft, Inc., Report 10917, November, 1957.

7. Islinger, J. S.: Stress Analysis And Stress Measurements For A Swept-back Wing Having Ribs Parallel To The Airstream. McDonnell Aircraft Corporation Report 1127, April, 1949.

8. Bisplinghoff, R. L., Ashley, H., and R. L. Halfman: Aeroelasticity, Addison-Wesley, Cambridge, 1955.

9. Warren, D. S., Castle, R. A., and R. C. Gloria: An Evaluation Of The State-of-the-Art Of Thermo-Mechanical Analysis of Structures, Wright Air Development Division Technical Report WADD TR 61-152, January, 1962.

10. The Quadrilateral Shear Panel, Garvey, S. J. Aircraft Engineering, May, 1951.

11. Bruhn, E. F., and A. F. Schmitt: Analysis and Design of Aircraft Structures, Vol. 1, Analysis For Stress And Strain, Art A6.13, Tri-State Offset Co., Cincinnati, Ohio, 1958.

BEAM	LENGTH	DIRECTION COSINES			AVERAGE WEB THICKNESS	STATION Yw = 25.095						STATION Yw = 81.98					
		x	y	z		UPPER SKIN EFF. AREA	UPPER FLANGE EFF. AREA	EQUIV. UPPER FLANGE	LOWER SKIN EFF. AREA	LOWER FLANGE EFF. AREA	EQUIV LOWER FLANGE	UPPER SKIN EFF. AREA	UPPER FLANGE EFF. AREA	EQUIV UPPER FLANGE	LOWER SKIN EFF. AREA	LOWER FLANGE EFF. AREA	EQUIV. LOWER FLANGE
	79.302	.69666	.71732	.01009	.162	.974	.364	1.50*	.824	.304	1.30*	1.13	.364	1.50*	1.00	.304	1.30*
	74.921	.65009	.75927	.01415	.032	2.84	.203	3.04	2.39	.134	2.52	2.48	.203	2.68	2.14	.134	2.27
	71.385	.60391	.79688	.01555	.040	4.80	.370	5.17	3.72	.134	3.85	3.06	.370	3.43	2.69	.134	2.82
	68.589	.55916	.82936	.01487	.063	6.51	.370	6.88	4.95	.134	5.08	3.50	.370	3.87	3.18	.134	3.31
	66.457	.51788	.85597	.01249	.063	7.64	.370	8.01	6.08	.134	6.21	3.50	.370	3.87	3.17	.134	3.30
	64.904	.48235	.87645	.00971	.090	7.99	.370	8.36	6.69	.134	6.82	3.47	.370	3.84	3.15	.134	3.28
	63.834	.45373	.89114	.00705	.200	3.92	.206	4.13	3.41	.206	3.62	1.74	.206	1.95	1.58	.206	1.79

*includes post beam
**untapered

	END RIB Yw = 81.98		
BAR**	EFF. WEB AREA	EFF. COVER SKIN AREA	EFF. BAR AREA
40	.28	3.02	3.30
41	.28	4.06	4.34
42	.28	4.32	4.60
43	.28	4.72	5.00
44	.28	4.54	4.82
45	.28	4.42	4.70
46	.28	3.84	4.12
47	.28	3.88	4.16
48	.28	3.78	4.06
49	.28	3.94	4.22
50	.28	4.06	4.34
51	.28	2.58	2.86

PANEL (from L.E.)	AVG. SKIN THICKNESS		END WIDTH Yw = 25.095	Yw = 81.98	AVERAGE SWEEP ANGLE
1	.175	.152	20.88	14.34	42° 23'
2	.250	.211	19.10	13.51	38° 53'
3	.370	.300	17.79	13.03	35° 34'
4	.420	.350	16.51	12.58	32° 33'
5	.477	.400	15.24	12.13	29° 57'
6	.490	.420	14.16	11.81	27° 53'

TABLE I
Geometry Of
Idealized Model

66

TABLE II

COMPONENTS FOR APPLIED LOADS

Cell	q_s Shear Flow Station 81.98	$q_{n_i} =$ $q_s \sin \theta$ *	$F_p =$ $q_s w \cos \theta$ *	$\Delta p =$ $F_p / \cos \Lambda$	$\Delta q_n =$ $\frac{1}{w}(\Delta p \, \sin \Lambda_p)$
1	265.74	99.84	3581.83	4781.46	3223.13
2	302.03	113.76	3790.74	4869.70	3056.91
3	398.78	149.82	4815.86	5920.33	3443.56
4	457.81	171.99	5335.69	6330.00	3405.79
5	472.81	177.43	5310.11	6128.50	3059.59
6	442.47	166.23	4840.75	5476.53	2561.21

* $\theta = (90 - 2\Lambda)$

(See Appendix C for resultant $\{P\}$ matrix)

TABLE III

THE EDGE SHEAR FORCES ON THE PANELS
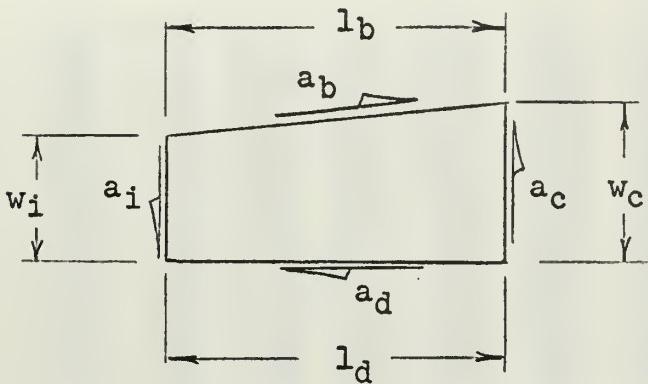
Piece No.	w_i in.	w_c in.	l_b in.	l_d in.	$a_b/a_i =$ l_b/w_c	$a_c/a_i =$ w_i/w_c	$a_d/a_i =$ l_d/w_c
1	5.64	6.82	14.340883	14.328741	2.102769	.826979	2.100988
2	6.82	7.44	13.507743	13.504185	1.815557	.916666	1.815079
3	7.44	7.66	13.030764	13.030300	1.701144	.971279	1.701084
4	7.66	7.54	12.575610	12.575467	1.667853	1.015915	1.667834
5	7.54	7.06	12.137011	12.129637	1.719123	1.067989	1.718079
6	7.06	6.30	11.804608	11.798490	1.873747	1.120635	1.872776
7	5.64	7.24	79.3021	79.3021	10.953328	.779006	10.95333
8	6.82	8.94	74.9206	74.9206	8.380380	.762864	8.38038
9	7.44	9.66	71.3846	71.3846	7.389710	.770186	7.38971
10	7.66	9.70	68.5890	68.5890	7.071030	.789691	7.07103
11	7.54	9.20	66.4567	66.4567	7.223554	.819565	7.22355
12	7.06	8.32	64.9038	64.9038	7.800938	.848558	7.80094
13	6.30	7.20	63.8339	63.8339	8.865819	.875000	8.86582
15	14.328741	20.870584	79.3021	74.9206	3.799707	.686557	3.58977
17	13.504185	19.099132	74.9206	71.3846	3.922723	.707058	3.73758
19	13.030300	17.787945	71.3846	68.5890	4.013088	.732535	3.85593
21	12.575467	16.511403	68.5890	66.4567	4.154038	.761623	4.02490
23	12.129637	15.239329	66.4567	64.9038	4.360868	.795943	4.25897
25	11.798490	14.141857	64.9038	63.8339	4.589482	.834295	4.51383
28	11.804608	14.174828	64.9038	63.8339	4.578807	.832787	4.50333
30	12.132011	15.245680	66.4567	64.9038	4.359051	.795767	4.25719
32	12.575610	16.513296	68.5890	66.4567	4.153562	.761544	4.02444
34	13.030764	17.787956	71.3846	68.5890	4.013086	.732561	3.85592
36	13.507743	19.102224	74.9206	71.3846	3.922088	.707129	3.73698
38	14.340883	20.887886	79.3021	74.9206	3.796559	.686564	3.58680

TABLE IV
Matrix [A]

	1	2	3	4	5	6	7	8	9	10	11
	1.000000	1.000000	.000000	.000000	.000000	.000000	.000000	.000000	.000000	.000000	.000000
	.000000	-10.953330	.000000	.000000	.000000	.000000	.000000	.000000	-3.796560	.000000	.000000
	.000000	.000000	.916670	-1.000000	.000000	.000000	.000000	.000000	.000000	.000000	.000000
	.000000	.000000	.000000	.971280	-1.000000	.000000	.000000	.000000	.000000	.000000	.000000
	.000000	.000000	.000000	.000000	1.015920	-1.000000	.000000	.000000	.000000	.000000	.000000
	.000000	.000000	.000000	.000000	.000000	1.067990	-1.000000	.000000	.000000	.000000	.000000
	.000000	.000000	.000000	.000000	.000000	.000000	1.126400	-1.000000	.000000	.000000	.000000
	.000000	.000000	.000000	.000000	.000000	.000000	.000000	90.654010	2.483300	2.882220	3.505340
	.000000	.000000	.000000	.000000	.000000	.000000	.000000	.000000	3.586800	-3.922090	.000000
10	.000000	.000000	.000000	.000000	.000000	.000000	.000000	.000000	.000000	3.735880	-4.013090
	.000000	.000000	.000000	.000000	.000000	.000000	.000000	.000000	.000000	.000000	3.855920
	.000000	.000000	.000000	.000000	.000000	.000000	.000000	.000000	.000000	.000000	.000000
	.000000	.000000	.000000	.000000	.000000	.000000	13.221800	.000000	.000000	.000000	.000000
	.000000	.000000	.000000	.000000	.000000	.000000	.000000	.000000	.000000	.000000	.000000
	.000000	.000000	.000000	.000000	.000000	.000000	.000000	.000000	.000000	.000000	.000000
	.000000	.000000	.000000	.000000	.000000	.000000	.000000	.000000	.000000	.000000	.000000
	.000000	.000000	.000000	.000000	.000000	.000000	.000000	.000000	.000000	.000000	.000000
	.000000	.000000	.000000	.000000	.000000	.000000	.000000	.000000	.000000	.000000	.000000
	.000000	.000000	.000000	.000000	.000000	.000000	.000000	.000000	-.686000	-.707020	-.732560
20	.000000	.000000	.000000	.000000	.000000	.000000	.000000	.000000	.000000	.000000	.000000
	.000000	.000000	.000000	.000000	.000000	.000000	.000000	.000000	.000000	.000000	.000000
	.000000	.000000	12.378830	.000000	.000000	.000000	.000000	.000000	.000000	6.818210	.000000
	.000000	.000000	.000000	12.656070	.000000	.000000	.000000	.000000	.000000	.000000	7.439730
	.000000	.000000	.000000	.000000	12.775670	.000000	.000000	.000000	.000000	.000000	.000000
	.000000	.000000	.000000	.000000	.000000	12.954330	.000000	.000000	.000000	.000000	.000000
	.000000	.000000	.000000	.000000	.000000	.000000	.000000	.000000	.000000	.000000	.000000
	.000000	.779010	.000000	.000000	.000000	.000000	.000000	.875000	-.027940	-.013330	-.008200
30	.000000	.000000	.000000	.000000	.000000	.000000	.000000	.000000	.000000	.000000	.000000
	.000000	.000000	.000000	.000000	.000000	.000000	.000000	.000000	.000000	1.000000	.000000
	.000000	.000000	.000000	.000000	.000000	.000000	.000000	.000000	.000000	.000000	1.000000

	12	13	14	15	16	17	18	19	20	21	22
	.000000	.000000	.000000	.000000	.000000	.000000	.000000	.000000	.000000	.000000	.000000
	.000000	.000000	.000000	.000000	.000000	.000000	.000000	.000000	.000000	.000000	.000000
	.000000	.000000	.000000	.000000	.000000	.000000	.000000	.000000	.000000	.000000	.000000
	.000000	.000000	.000000	.000000	.000000	.000000	.000000	.000000	.000000	.000000	.000000
	.000000	.000000	.000000	.000000	.000000	.000000	.000000	.000000	.000000	.000000	.000000
	4.358960	5.364670	6.401253	6.407510	5.365850	4.359400	3.505210	2.881940	2.483260	2.522130	2.311010
	-4.153560	.000000	.000000	.000000	.000000	.000000	.000000	.000000	.000000	.000000	.000000
	4.024440	-4.359050	.000000	.000000	.000000	.000000	.000000	.000000	.000000	.000000	.000000
	.000000	4.257190	-4.578810	.000000	.000000	.000000	.000000	.000000	.000000	.000000	.000000
10	.000000	.000000	7.056300	.000000	.000000	.000000	.000000	.000000	.000000	.000000	.000000
	.000000	.000000	.000000	4.589480	-4.258970	.000000	.000000	.000000	.000000	.000000	.000000
	.000000	.000000	.000000	.000000	4.360870	-4.024900	.000000	.000000	.000000	.000000	.000000
	.000000	.000000	.000000	.000000	.000000	4.154040	-3.855930	.000000	.000000	.000000	.000000
	.000000	.000000	.000000	.000000	.000000	.000000	4.013090	-3.737580	.000000	.000000	.000000
	.000000	.000000	.000000	.000000	.000000	.000000	.000000	3.922720	-3.589770	.000000	.000000
	-.761460	-.795440	-.830850	.832350	.795610	.761540	.732540	.706940	-.685980	.696720	-.453720
	.000000	.000000	.000000	.000000	.000000	.000000	.000000	.000000	.000000	.717280	-.891120
	.000000	.000000	.000000	.000000	.000000	.000000	.000000	.000000	.000000	2.596550	3.208030
	.000000	.000000	.000000	.000000	.000000	.000000	.000000	.000000	.000000	.000000	-92.364900
20	.000000	.000000	.000000	.000000	.000000	.000000	.000000	.000000	.000000	.000000	.000000
	.000000	.000000	.000000	.000000	.000000	.000000	.000000	.000000	.000000	.000000	.000000
	7.659920	.000000	.000000	.000000	.000000	.000000	.000000	.000000	.000000	.000000	.000000
	.000000	7.538520	.000000	.000000	.000000	.000000	.000000	.000000	.000000	.000000	.000000
	.000000	.000000	1.000000	-1.000000	.000000	.000000	.000000	.000000	.000000	.000000	.000000
	.011530	.022970	.032900	.032960	.022970	.011530	-.000820	-.013330	-.027940	.010090	.006540
30	.000000	1.000000	.000000	.000000	-1.000000	.000000	.000000	.000000	.000000	.000000	.000000
	1.000000	.000000	.000000	.000000	.000000	-1.000000	.000000	.000000	.000000	.000000	.000000
	.000000	.000000	.000000	.000000	.000000	.000000	-1.000000	.000000	.000000	.000000	.000000
	.000000	.000000	.000000	.000000	.000000	.000000	.000000	-1.000000	.000000	.000000	.000000

	23	24	25	26	27	28	29	30	31	32	33
	.000000	.000000	.000000	.000000	.000000	.000000	.000000	.000000	.000000	.000000	.000000
	.000000	.000000	.000000	.000000	.000000	.000000	.000000	.000000	.000000	.000000	.000000
	.000000	.000000	.014513	.000000	.000000	.000000	.000000	.000000	.000000	-.014510	.000000
	.000000	.000000	.000000	.013210	.000000	.000000	.000000	.000000	-.013210	.000000	.000000
	.000000	.000000	.000000	.000000	.015020	.000000	-.015020	.000000	.000000	.000000	.000000
	.000000	.000000	.000000	.000000	.000000	.012420	-.012420	.000000	.000000	.000000	.000000
	2.311010	.000000	.000000	.000000	.000000	.000000	.000000	.000000	.000000	.000000	.000000
	.000000	.000000	.000000	.000000	.000000	.000000	.000000	.000000	.000000	.000000	.000000
	.000000	.000000	.000000	.000000	.000000	.000000	.000000	.000000	.000000	.000000	.000000
10	.000000	.000000	.000000	.000000	.000000	.000000	.000000	.000000	.000000	.000000	.000000
	.000000	.000000	.000000	.000000	.000000	.000000	.000000	.000000	.000000	.000000	.000000
	.000000	.000000	.000000	.000000	.000000	7.058610	.000000	.000000	.000000	.000000	.000000
	.000000	.000000	.000000	.000000	.000000	.000000	.000000	.000000	.000000	.000000	.000000
	.000000	.000000	.000000	.000000	.000000	.000000	.000000	.000000	.000000	.000000	.000000
	.000000	.000000	.000000	.000000	.000000	.000000	.000000	.000000	.000000	.000000	.000000
	.000000	.000000	.000000	.000000	.000000	.000000	.000000	.000000	.000000	.000000	.000000
	.000000	.000000	.000000	.000000	.000000	.000000	.000000	.000000	.000000	.000000	.000000
	.000000	.000000	.000000	.000000	.000000	.000000	.000000	.000000	.000000	.000000	.000000
	.000000	.000000	.000000	.000000	.000000	.000000	.000000	.000000	.000000	.000000	.000000
20	-.453720	.000000	.000000	.000000	.000000	.000000	.000000	.000000	.000000	.000000	.000000
	.891120	.000000	.000000	.000000	.000000	.000000	.000000	.000000	.000000	.000000	.000000
	3.208030	.000000	.000000	.000000	.000000	.000000	.000000	.000000	.000000	.000000	.000000
	92.364900	.000000	.000000	.000000	.000000	.000000	.000000	.000000	.000000	.000000	.000000
	.000000	6.814260	-6.818210	.000000	.000000	.000000	.000000	.000000	.000000	.000000	.000000
	.000000	.000000	7.438020	-7.439730	.000000	.000000	.000000	.000000	.000000	.000000	.000000
	.000000	.000000	.000000	7.659690	-7.659920	.000000	.000000	.000000	.000000	.000000	.000000
	.000000	.000000	.000000	.000000	7.539910	-7.538520	.000000	.000000	.000000	.000000	.000000
	.006540	.000000	.000000	.000000	.000000	1.000320	1.000320	.000000	.000000	.000000	.000000
30	.000000	.000000	.000000	.000000	1.000190	-1.000000	-1.000000	-1.000190	.000000	.000000	.000000
	.000000	.000000	.000000	.999970	-1.000000	.000000	.000000	.000000	.999970	.000000	.000000
	.000000	.000000	.999770	-1.000000	.000000	.000000	.000000	.000000	.000000	.999770	.000000
	.000000	.999420	-1.000000	.000000	.000000	.000000	.000000	.000000	.000000	-1.000000	.999420

TABLE V
Matrix [B]
Input Form

1 1	1.0	1 34	0.0	2 20	1.0	2 44	-1.0
3 3	-1.0	335	1.0	4 4	-1.0	436	1.0
5 5	-1.0	537	1.0	6 6	-1.0	638	1.0
7 7	-1.0	8 1	55.2466	8 2	69.5754	8 3	83.0796
8 4	96.1099	8 5	108.6853	8 6	120.8150	8 7	132.6135
8 8	7.4179	8 9	5.9191	810	4.2884	811	3.0187
812	1.8124	813	0.5448	814	0.5448	815	1.8124
816	3.0187	817	4.2884	818	5.9191	819	7.4172
820	2.5220	821	3.2013	822	3.5384	823	3.5707
824	3.3099	825	2.8758	826	2.3642	827	2.5220
828	3.2013	829	3.5384	830	3.5707	831	3.3099
832	2.8758	833	2.3642	834	-15.9213	835	-30.7843
836	-45.6107	837	-60.8687	838	-75.9532	839	-3.2013
840	-3.5384	841	-3.5707	842	-3.3099	843	-2.8758
844	-2.5220	845	-3.2013	846	-3.5384	847	-3.5707
848	-3.3099	849	-2.8758	921	1.0	934	8.3804
945	-1.0	1022	1.0	1035	7.3897	1046	-1.0
1123	1.0	1136	7.0710	1147	-1.0	1224	1.0
1237	7.2236	1248	-1.0	1325	1.0	1338	7.8009
1349	-1.0	14 7	0.0	14 8	7.0563	1532	-1.0
1538	-7.8009	1543	1.0	1631	-1.0	1637	-7.2236
1642	1.0	1730	-1.0	1736	-7.0710	1741	1.0
1829	-1.0	1835	-7.3897	1840	1.0	1928	-1.0
1934	-8.3804	1939	1.0	20 8	-0.99948	20 9	-0.99980
2010	-0.99999	2011	-0.99996	2012	-0.99974	2013	-0.99915
2014	0.99915	2015	0.99974	2016	0.99996	2017	0.99999
2018	0.99980	2019	0.99948	2020	-0.69666	2021	-0.65009
2022	-0.60391	2023	-0.55916	2024	-0.51788	2025	-0.48235
2026	-0.45373	2027	0.69666	2028	0.65009	2029	0.60391
2030	0.55916	2031	0.51788	2032	0.48235	2033	0.45373
2039	-0.65009	2040	-0.60391	2041	-0.55916	2042	-0.51788
2043	-0.48235	2044	0.69666	2045	0.65009	2046	0.60391
2047	0.55916	2048	0.51788	2049	0.48235	2120	-0.71732
2121	-0.75927	2122	-0.79688	2123	-0.82936	2124	-0.85597
2125	-0.87645	2126	-0.89114	2127	0.71732	2128	0.75927
2129	0.79688	2130	0.82936	2131	0.85597	2132	0.87645
2133	0.89114	2139	-0.75927	2140	-0.79688	2141	-0.82936
2142	-0.85597	2143	-0.87645	2144	0.71732	2145	0.75927
2146	0.79688	2147	0.82936	2148	0.85597	2149	0.87645
22 1	56.885	22 2	56.885	22 3	56.885	22 4	56.885
22 5	56.885	22 6	56.885	22 7	56.885	22 8	1.83113
22 9	1.12519	2210	0.27134	2211	-0.48011	2212	-1.30551
2213	-2.34025	2214	-2.34025	2215	-1.30551	2216	-0.48011
2217	0.27134	2218	1.12519	2219	1.83113	2220	2.59681
2221	3.39403	2222	3.84895	2223	4.02233	2224	3.93750
2225	3.64622	2226	3.20813	2227	2.59681	2228	3.39403
2229	3.84895	2230	4.02233	2231	3.93750	2232	3.64622
2233	3.20813	2239	-3.39403	2240	-3.84895	2241	-4.02233
2242	-3.93750	2243	-3.64622	2244	-2.59681	2245	-3.39403
2246	-3.84895	2247	-4.02233	2248	-3.93750	2249	-3.64622
23 8	56.8554	23 9	56.8736	2310	56.8844	2311	56.8827
2312	56.8702	2313	56.8367	2314	-56.8367	2315	-56.8702
2316	-56.8827	2317	-56.8844	2318	-56.8736	2319	-56.8554
2320	0.0	2321	-15.8462	2322	-31.8510	2323	-47.9019
2324	-63.5718	2325	-78.4498	2326	-92.3667	2327	0.0
2328	15.8462	2329	31.8510	2330	47.9019	2331	63.5718
2332	78.4498	2333	92.3667	2339	-15.8462	2340	-31.8510
2341	-47.9019	2342	-63.5718	2343	-78.4498	2344	0.0
2345	15.8462	2346	31.8510	2347	47.9019	2348	63.5718
2349	78.4498	2412	6.8182	2511	7.4397	2610	7.6599
27 9	7.5385	28 8	1.0	29 1	1.0	29 2	1.0
29 3	1.0	29 4	1.0	29 5	1.0	29 6	1.0
29 7	1.0	29 8	0.03219	29 9	0.01978	2910	0.00477
2911	-0.00844	2912	-0.02295	2913	-0.04114	2914	-0.04114
2915	-0.02295	2916	-0.00844	2917	0.00477	2918	0.01978
2919	0.03219	2920	0.01009	2921	0.01415	2922	0.01555
2923	0.01487	2924	0.01249	2925	0.00971	2926	0.00705
2927	0.01009	2928	0.01415	2929	0.01555	2930	0.01487
2931	0.01249	2932	0.00971	2933	0.00705	2934	-0.76286
2935	-0.77019	2936	-0.78969	2937	-0.81957	2938	-0.84856
2939	-0.01415	2940	-0.01555	2941	-0.01487	2942	-0.01249
2943	-0.00971	2944	-0.01009	2945	-0.01415	2946	-0.01555
2947	-0.01487	2948	-0.01249	2949	-0.00971	30 9	1.0
3018	-1.0	3110	1.0	3117	-1.0	3211	1.0
3216	-1.0	3312	1.0	3315	-1.0		

Table VI
Matrix $[CJ]_{33 \times 49}$

Seven Columns Per Page

1	2	3	4	5	6	7
.598127	-.327439	-.257290	-.189602	-.124277	-.061267	.000022
.401873	.327439	.257290	.189602	.124277	.061267	-.000022
.665961	.809153	-.146801	-.104302	-.063274	-.023723	.014746
.596015	.693787	.785932	-.154726	-.097443	-.042211	.011512
.566441	.640150	.709618	.776648	-.142992	-.065500	.009876
.562138	.621649	.677734	.731852	.784081	-.101880	.009044
.592316	.649593	.703573	.755659	.805927	.854414	.009229
.663773	.727960	.788452	.846822	.903154	.957490	1.010342
-1.159430	-.944685	-.742298	-.547013	-.358546	-.176759	.000065
-1.060313	-.863926	-.678841	-.500250	-.327895	-.161648	.000059
-.987361	-.804486	-.632135	-.465832	-.305335	-.150527	.000055
-.916608	-.746837	-.586837	-.432451	-.283455	-.139740	.000051
-.846247	-.689508	-.541790	-.399255	-.261696	-.129013	.000047
-.786806	-.641077	-.503734	-.371211	-.243315	-.119951	.000044
-.785232	-.639794	-.502726	-.370469	-.242828	-.119711	.000044
-.846168	-.689444	-.541740	-.399218	-.261672	-.129001	.000047
-.916801	-.746994	-.586960	-.432542	-.283515	-.139769	.000051
-.987680	-.804746	-.632339	-.465983	-.305434	-.150575	.000055
-1.060486	-.864067	-.678951	-.500332	-.327948	-.161675	.000059
-1.158845	-.944209	-.741924	-.546738	-.358366	-.176670	.000065
-.000000	-.000000	-.000000	-.000000	-.000000	-.000000	-.000000
8.866033	8.866033	8.866033	8.866033	8.866033	8.866033	8.866033
8.866033	8.866033	8.866033	8.866033	8.866033	8.866033	8.866033
-.646568	-2.257934	-1.794824	-1.347952	-.916713	-.500668	-.095979
-.497418	-1.651491	-2.739149	-2.036788	-1.358953	-.705097	-.069092
-.470755	-1.275365	-2.033670	-2.765364	-1.829741	-.927268	-.049437
-.442605	-.954483	-1.436902	-1.902393	-2.351632	-1.176225	-.032913
-.322946	-.575915	-.814326	-1.044370	-1.266384	-1.480528	-.017330
.324519	.577197	.815333	1.045112	1.266870	1.480768	.017330
.444256	.955828	1.437959	1.903172	2.352143	1.176477	.032913
.472214	1.276553	2.034603	2.766052	1.830192	.927491	.049437
.498556	1.652419	2.739878	2.037325	1.359306	.705271	.069092
.647534	2.258722	1.795443	1.348408	.917012	.500815	.095979

$$[CJ] - 2$$

8	9	10	11	12	13	14
.036899	.037669	.039542	.042045	.045770	.051703	.010636
-.036899	-.037669	-.039542	-.042045	-.045770	-.051703	-.010636
.034379	.034678	.035642	.037019	.039139	.024387	-.022867
.035882	.036412	.037889	.039932	.028518	.015871	-.026460
.040567	.041390	.043551	.033290	.022985	.011318	-.028936
.049881	.051159	.039397	.029728	.019886	.008558	-.031406
.062674	.052079	.039989	.030006	.019789	.007952	-.034162
.070235	.058362	.044813	.033626	.022176	.008912	-.038283
.106457	.108677	.114080	.121303	.132049	.149167	.030687
.097356	.099387	.104328	.110933	.120760	.136415	.028063
.090658	.092549	.097150	.103301	.112452	.127030	.026132
.084161	.085917	.090188	.095898	.104393	.117927	.024260
.077701	.079321	.083265	.088537	.096380	.108874	.022398
.072243	.073750	.077416	.082318	.089610	.101227	.020824
-.064340	-.062880	-.059247	-.054351	-.047043	-.035369	.157176
-.069333	-.067760	-.063845	-.058569	-.050694	-.038114	.169374
-.075121	-.073416	-.069174	-.063458	-.054926	-.041295	.183512
-.080928	-.079092	-.074522	-.068364	-.059172	-.044488	.197700
-.086894	-.084922	-.080015	-.073403	-.063534	-.047767	.212273
-.094953	-.092798	-.087436	-.080211	-.069427	-.052198	.231961
-.764737	-.764982	-.765127	-.765104	-.764936	-.764486	.764486
.287108	.177081	.044001	-.073119	-.201765	-.363040	-.366458
.902660	.792830	.659867	.542729	.413947	.252310	-.981807
.183427	.189783	.203545	.221340	.247334	-.711696	.131170
.343094	.352019	.372465	.399356	-.560988	-.530593	.117642
.494713	.506429	.533983	-.429501	-.399895	-.376442	.098736
.646520	.661364	-.303205	-.278067	-.257154	-.239627	.074731
.810056	-.171278	-.152296	-.138496	-.126648	-.116090	.043173
.053084	.034691	.015677	.001871	-.009961	-.020463	.093135
.069450	.054833	.019530	-.005610	-.026476	-.043860	.208500
.061992	.050451	.022996	-.013545	-.043068	-.066280	.343761
.042114	.033310	.012932	-.013978	-.053739	-.083788	.496563
.017647	.011353	-.002375	-.020182	-.046239	-.087331	.667707

15	16	17	18	19	20	21
.004679	.000945	-.001560	-.003425	-.004185	.0546C4	.043469
-.004679	-.000945	.001560	.003425	.004185	-.054604	-.043469
-.008142	-.010273	-.011651	-.012606	.054153	.060804	.057410
-.013838	-.002433	-.004478	-.005946	.036489	.054417	.053040
-.017294	-.006997	.003262	.001109	.027107	.051717	.051458
-.020102	-.010269	-.000601	.011169	.021526	.051323	.051813
-.022350	-.012143	-.002161	.009937	.020543	.054078	.054891
-.025047	-.013608	-.002422	.011136	.023021	.060603	.061513
.013498	.002727	-.004500	-.009881	-.012073	-.105861	.125411
.012344	.002493	-.004115	-.009036	-.011041	-.096811	-.140276
.011495	.002322	-.003832	-.008414	-.010282	-.090150	-.130625
.010671	.002155	-.003558	-.007811	-.009545	-.083690	-.121264
.009852	.001990	-.003284	-.007212	-.008812	-.077266	-.111956
.009160	.001850	-.003054	-.006705	-.008193	-.071839	-.104092
.145616	.138351	.133461	.129791	.128262	-.071677	-.065837
.156916	.149087	.143818	.139863	.138216	-.077240	-.070946
.170014	.161532	.155823	.151538	.149753	-.083687	-.076868
.183159	.174021	.167870	.163254	.161331	-.090157	-.082811
.196660	.186848	.180244	.175287	.173223	-.096803	-.088916
.214900	.204178	.196961	.191545	.189289	-.105781	-.097162
.764936	.765104	.765127	.764982	.764737	-1.000056	-.845400
-.205185	-.076540	.040580	.173661	.283688	.809454	.956900
-.820898	-.692387	-.575286	-.442088	-.331864	.809454	.785339
.090120	.064085	.046284	.032545	-.233361	-.059017	.136139
.087630	.047890	.020988	.000602	-.145950	-.045401	.100015
.075564	.046062	.009533	-.017927	-.094124	-.042970	.059596
.057389	.036545	.011416	-.023888	-.058456	-.040403	.024154
.032708	.020896	.007100	-.011911	-.030289	-.029481	.001239
.103704	.115561	.129370	.148364	.166700	.029643	.037004
.226033	.246955	.272103	-.692449	.341841	.040591	.055083
.367216	.396829	-.566650	-.539078	.536820	.043161	.064041
.526955	-.433390	-.406492	-.386028	.760399	.045587	.071475
-.291337	-.265347	-.247545	-.233764	1.032539	.059212	.086841

22	23	24	25	26	27	28
.033989	.024259	.016002	.007931	.000001	.000001	-.002875
-.033989	-.024259	-.016002	-.007931	-.000001	-.000001	.002875
.048118	.038192	.025181	.012564	.000833	-.000002	.006221
.046621	.036420	.023823	.011803	.000650	-.000001	.007239
.046558	.038353	.024920	.012277	.000558	-.000000	.007936
.047802	.040717	.028631	.014035	.000511	.000000	.008626
.051005	.043961	.031721	.016898	.000521	.000000	.009387
.057158	.049264	.035548	.018936	.000584	.000000	.010519
.098059	.069989	.046168	.022880	.000004	.000004	-.008294
.089677	.064006	.042221	.020924	.000004	.000003	-.007585
-.165678	.059602	.039316	.019485	.000003	.000003	-.007063
-.153806	-.185426	.036499	.018089	.000003	.000003	-.006557
-.141999	-.171192	-.195711	.016700	.000003	.000003	-.006054
-.132025	-.159168	-.181964	-.202870	.000003	.000002	-.005628
-.055302	-.043870	-.029019	-.014187	.000003	-.000016	-.043634
-.059593	-.047274	-.031271	-.015288	.000003	-.000017	-.047020
-.064568	-.051220	-.033881	-.016564	.000004	-.000018	-.050945
-.069560	-.055180	-.036501	-.017845	.000004	-.000020	-.054883
-.074687	-.059248	-.039192	-.019160	.000004	-.000021	-.058929
-.081614	-.064743	-.042827	-.020937	.000004	-.000023	.214175
-.682561	-.511949	-.338279	-.166714	-.000004	1.000056	.845400
1.048542	1.093407	1.094728	1.060437	1.000027	.000018	.101080
.703703	.574792	.406460	.211091	.000007	.000018	.272641
.081876	.044594	.023150	.008466	-.005421	-.000010	-.036391
.258866	.177913	.111075	.052196	-.003902	-.000010	-.032660
.172438	.299429	.190891	.091747	-.002792	-.000008	-.027402
.096280	.177961	.268948	.130310	-.001859	-.000006	-.020722
.036442	.076770	.122486	.171152	-.000979	-.000003	-.011957
.040256	.038491	.030409	.017471	.000979	-.000015	-.026037
.062795	.061173	.048327	.026295	.001859	-.000032	-.058223
.075881	.073921	.056011	.030209	.002793	-.000050	-.095934
.085651	.080715	.060050	.032451	.003903	-.000071	-.138535
.098382	.090858	.066614	.036122	.005422	-.000096	-.186278

29	30	31	32	33	34	35
-.003653	-.003225	-.002154	-.001012	.000001	.667642	.481468
.003653	.003225	.002154	.001012	-.000001	-.667642	-.481468
.007048	.006581	.004304	.002289	.000833	-.275926	.554455
.009888	.008097	.005116	.002595	.000650	-.188647	-.368351
.011660	.011414	.007127	.003516	.000558	-.142422	-.279407
.013178	.013967	.010959	.005332	.000511	-.115168	-.227115
.014524	.015765	.013093	.007721	.000521	-.110933	-.219338
.016277	.017663	.014673	.008653	.000584	-.124316	-.245798
-.010538	-.009303	-.006215	-.002921	.000004	1.926192	1.389068
-.009637	-.008512	-.005684	-.002671	.000004	-.375191	1.270320
-.008974	-.007925	-.005293	-.002487	.000004	-.349377	-.658480
-.008331	-.007353	-.004914	-.002309	.000003	-.324341	-.611294
-.007692	-.006793	-.004536	-.002132	.000003	-.299444	-.564370
-.007151	-.006315	-.004218	-.001982	.000003	-.278411	-.524728
-.083555	-.121239	-.156745	-.190202	.000003	-.277603	-.523376
-.090040	-.130643	-.168909	.029836	.000003	-.299146	-.563992
-.097555	-.141554	.065446	.032326	.000003	-.324117	-.611070
-.105098	.106843	.070505	.034826	.000003	-.349175	-.658313
.154708	.114719	.075702	.037393	.000004	-.374914	1.270295
.169057	.125359	.082724	.040861	.000004	1.924836	1.388115
.682561	.511949	.338279	.1667.14	.000004	.000000	.000000
.151244	.160424	.132661	.076154	.000004	.000000	.000000
.496083	.679040	.820928	.925501	1.000024	.000000	.000000
-.057173	-.061430	-.047151	-.026497	-.005421	3.093957	1.977363
-.053981	-.057958	-.044993	-.024997	-.003903	2.216014	4.253180
-.046122	-.052093	-.041572	-.023065	-.002792	1.545211	2.967102
-.035005	-.040419	-.034598	-.019508	-.001859	.983284	1.889707
-.020057	-.023213	-.020309	-.012482	-.000979	.486114	.935407
-.056322	-.091663	-.132169	-.175678	.000979	-.485306	-.934056
-.123693	-.198273	-.282192	-.136654	.001859	-.982178	-1.887978
-.201806	-.320804	-.204866	-.098466	.002792	-1.543881	-2.965149
-.290150	-.200233	-.125686	-.059240	.003902	-2.214480	-4.251059
-.122717	-.073609	-.042194	-.017702	.005420	-3.092144	-1.975265

36	37	38	39	40	41	42
.338325	.224309	.115240	.002875	.003653	.003226	.002154
-.338325	-.224309	-.115240	-.002875	-.003653	-.003226	-.002154
.420912	.276236	.139517	-.006221	-.007048	-.006581	-.004304
.469520	.306469	.154475	-.007239	-.009888	-.008097	-.005116
-.424733	.374470	.188657	-.007936	-.011660	-.011414	-.007127
-.345168	-.498116	.252915	-.008626	-.013178	-.013967	-.010959
-.333312	-.482222	-.662407	-.009387	-.014524	-.015766	-.013093
-.373523	-.540398	-.742320	-.010519	-.016277	-.017668	-.014673
.976090	.647145	.332476	.008294	.010538	.009308	.006215
.892646	.591822	.304054	.007585	.009637	.008512	.005684
.831230	.551104	.283134	.007063	.008974	.007926	.005293
-.930730	.511612	.262845	.006557	.008331	.007358	.004914
-.859285	-1.184810	.242668	.006054	.007692	.006793	.004536
-.798928	-1.101588	-1.478073	.005623	.007151	.006316	.004218
-.797021	-1.099057	-1.474699	.043634	.083555	.121239	.156745
-.858872	-1.184347	.242500	.047020	.090040	.130648	.168909
-.930564	.511519	.262742	.050945	.097555	.141554	-.065446
.831290	.551066	.283055	.054883	.105098	-.106843	-.070505
.892568	.591687	.303920	.058929	-.154708	-.114719	-.075702
.975353	.646566	.332108	-.214175	-.169057	-.125359	-.082724
.000000	.000000	.000000	-.845400	-.682561	-.511949	-.338279
.000000	.000000	.000000	-.101080	-.151244	-.160424	-.132661
.000000	.000000	.000000	-.272641	-.496083	-.679040	-.820928
1.228755	.743506	.360409	.036391	.057173	.061430	.047151
2.884878	1.836419	.917554	.032660	.053981	.057958	.044993
4.514167	2.908448	1.463261	.027402	.046122	.052098	.041572
2.874906	4.044536	2.040715	.020722	.035005	.040418	.034598
1.423008	2.004500	2.718373	.011957	.020057	.023218	.020309
-1.421101	-2.001970	-2.715000	.026037	.056322	.091668	.132169
-2.872586	-4.041543	-2.037511	.058223	.123693	.198278	.282192
-4.511682	-2.905548	-1.460161	.095934	.201806	.320804	.204866
-2.882332	-1.833556	-.914532	.138535	.290150	.200233	.125686
-1.226285	-.740776	-.357518	.186278	.122717	.073609	.042194

43	44	45	46	47	48	49
.001012	-.054604	-.043469	-.033989	-.024259	-.016002	-.007931
-.001012	.054604	.043469	.033989	.024259	.016002	.007931
-.002289	-.060804	-.057410	-.048118	-.038192	-.025181	-.012564
-.002595	-.054417	-.053040	-.046621	-.036420	-.023823	-.011803
-.003516	-.051717	-.051458	-.046558	-.038353	-.024920	-.012277
-.005332	-.051323	-.051813	-.047802	-.040717	-.028631	-.014035
-.007721	-.054078	-.054891	-.051005	-.043961	-.031721	-.016898
-.008653	-.060603	-.061513	-.057158	-.049264	-.035548	-.018936
.002921	.105861	-.125411	-.098059	-.069989	-.046168	-.022880
.002671	.096811	.140276	-.089677	-.064006	-.042221	-.020924
.002487	.090150	.130625	.165678	-.059602	-.039316	-.019485
.002309	.083690	.121264	.153806	.185426	-.036499	-.018089
.002132	.077266	.111956	.141999	.171192	.195711	-.016700
.001982	.071839	.104092	.132025	.159168	.181964	.202870
.190202	.071677	.065837	.055302	.043870	.029019	.014187
-.029836	.077240	.070946	.059593	.047274	.031271	.015288
-.032326	.083687	.076868	.064568	.051220	.033881	.016564
-.034826	.090157	.082811	.069560	.055180	.036501	.017845
-.037393	.096803	.088916	.074687	.059248	.039192	.019160
-.040861	.105781	.097162	.081614	.064743	.042827	.020937
-.166714	1.000056	.845400	.682561	.511949	.338279	.166714
-.076154	-.809454	-.956900	-1.048542	-1.093407	-1.094728	-1.060437
-.925501	-.809454	-.785339	-.703703	-.574792	-.406460	-.211091
.026497	.059017	-.136139	-.081876	-.044594	-.023150	-.008466
.024997	.045401	-.100015	-.258866	-.177913	-.111075	-.052196
.023065	.042970	-.059596	-.172438	-.299429	-.190891	-.091747
.019508	.040403	-.024154	-.096280	-.177961	-.268948	-.130310
.012482	.029481	-.001239	-.036442	-.076770	-.122486	-.171152
.175678	-.029643	-.037004.	-.040256	-.038491	-.030409	-.017471
.136654	-.040591	-.055083	-.062795	-.061173	-.048327	-.026295
.098466	-.043161	-.064041	-.075881	-.073921	-.056011	-.030209
.059240	-.045587	-.071475	-.085651	-.080715	-.060050	-.032451
.017702	-.059212	-.086841	-.098382	-.090858	-.066614	-.036122

TABLE VII

CHECK OF CJ EQUILIBRIUM

Element	Equation	Error
16	$3.58977(a_{20})$ $-$ $3.922723(a_{19})$ $+$ a_{39}	$-.00000006$
18	$3.73758(a_{19})$ $-$ $4.013088(a_{18})$ $+$ a_{40}	$+.00000018$
20	$3.85593(a_{18})$ $-$ $4.154038(a_{17})$ $+$ a_{41}	$+.00000028$
22	$4.02490(a_{17})$ $-$ $4.360868(a_{16})$ $+$ a_{42}	$+.00000033$
24	$4.25897(a_{16})$ $-$ $4.589482(a_{15})$ $+$ a_{43}	$-.00000077$
29	$4.578887(a_{14})$ $-$ $4.25719(a_{13})$ $-$ a_{49}	$+.00000053$
31	$4.359051(a_{13})$ $-$ $4.02444(a_{12})$ $-$ a_{48}	$+.00000082$
33	$4.153562(a_{12})$ $-$ $3.85592(a_{11})$ $-$ a_{47}	$+.00000047$
35	$4.013086(a_{11})$ $-$ $3.73698(a_{10})$ $-$ a_{46}	$-.00000068$
37	$3.922088(a_{10})$ $-$ $3.58680(a_9)$ $-$ a_{45}	$-.00000026$
39	$3.796559(a_9)$ $+$ $10.95333(a_2)$ $-$ a_{44}	$-.00000430$
2nd post	$.826979(-.3274394) + 1.0 - .8091530 - 0$	$-.0799385$
3rd post	$.916666(-.1468006) + 1.0 - .7859316 - 0$	$+.0795013$
4th post	$.971279(-.1547262) + 1 - .7766476 - 0$	$+.0730701$
5th post	$1.015915(-.142922) + 1 - .7840807 - 0$	$+.0707227$
6th post	$1.067989(-.1018803) + 1 - .8544135 - 0$	$+.0367795$
7th post	$1.120635(-.0092286) + 1 -1.0103419 - 0$	$+ 0.00000$

TABLE VIII
ANALYTICAL DEFLECTION INFLUENCE COEFFICIENTS

F8U-3 WING CENTER SECTION BETWEEN Y-25.095 AND Y-81.98
DEFLECTIONS ARE FOR 10,000 lb LOAD

LOAD APPLICATION POINTS ⟶

DEFLECTIONS, AT POINTS ⟶

	1	2	3	4	5	6	7	8	9	10	11	12	13	14	15	16	17	18	19	20	21	22	23	24	25	26	27	28	29	30	31	32	33
1	.290210	.205593	.139027	.090481	.054904	.032948	.012978	-.004129	-.003530	-.007835	-.011203	-.013608	-.021099	-.023399	-.017918	-.015395	-.009618	-.009430	-.015964	.010311	.004098	.002480	.002441	.001358	.001085	-.000477	.012779	.005437	.003843	.003032	.001823	.001325	-.000156
2	.205993	.200345	.151532	.111540	.081526	.059270	.041992	-.003097	-.004202	-.008034	-.009031	-.009700	-.010964	-.011590	-.010512	-.009794	-.008937	-.004836	.001124	.008285	.005203	.004001	.004246	.003413	.003093	.001902	.010282	.008852	.003711	.005229	.004184	.003132	.002493
3	.239027	.151532	.150936	.329271	.105717	.097937	.075021	-.000008	-.001013	-.003287	-.003011	-.003699	-.004352	-.003935	-.003179	-.003449	-.002901	-.001526	.002211	.009120	.005249	.005408	.005373	.003050	.005165	.004027	.007037	.009940	.007183	.007008	.009276	.004216	.003923
4	.090481	.111540	.129271	.146241	.130959	.119249	.112484	.002144	.001044	.000249	.000489	.000210	-.000910	.000142	.001851	.002099	.001379	.004194	.011243	.004543	.004908	.006033	.006895	.009964	.001423	.007799	.005913	.006346	.001189	.008770	.009467	.004914	.009199
5	.054906	.081528	.105711	.130959	.139108	.153837	.158910	.003981	.004960	.004343	.005660	.002337	.001197	.003376	.004957	.004088	.004870	.008497	.014535	.003031	.004434	.008256	.007393	.008046	.010078	.011397	.004510	.006014	.007654	.009734	.010979	.012011	.013339
6	.032829	.039270	.081957	.119269	.155837	.197042	.209943	.011204	.009823	.002828	.003921	.004134	.002359	.003397	.007065	.008920	.010921	.012926	.015012	.002082	.004013	.009400	.009029	.010570	.013160	.019089	.003448	.003551	.001898	.010919	.012033	.013143	.018436
7	.013978	.041967	.075021	.112284	.136910	.209943	.279743	.018274	.014622	.010857	.007914	.005469	.003564	.006994	.008440	.011491	.014715	.018008	.013389	.001299	.003816	.006853	.004910	.012044	.016016	.021440	.002940	.005250	.000023	.011270	.014493	.019141	.024976
8	-.004379	-.005097	-.000800	.002144	.005981	.011204	.018274	.012193	.010352	.009134	.000284	.004739	.007429	-.006479	-.006592	-.009345	-.004310	-.006429	-.006120	.005132	.003033	.002104	.002848	.002582	.001317	-.001318	-.003401	-.002933	-.002492	-.001844	-.000187	.001143	.004329
9	-.005530	-.004202	-.001913	.001044	.004960	.009821	.014622	.010552	.010304	.009449	.008525	.002983	.008720	-.006607	-.006541	-.009496	-.004491	-.006303	-.009719	.003173	.003073	.003120	.002868	.004406	.000965	-.001443	-.003544	-.002994	-.002394	-.001933	-.000816	.000941	.004039
10	-.007833	-.008054	-.003287	.000249	.004385	.007828	.010851	.009134	.009449	.009993	.009253	.009954	.009332	-.006993	-.006740	-.009212	-.004427	-.006510	-.001013	.005298	.003215	.003213	.002793	.007017	.000669	-.001549	-.003642	-.003133	-.002114	-.001986	-.000982	.000144	.003541
11	-.011203	-.008051	-.003911	.000489	.003660	.005921	.007914	.008297	.008225	.009253	.010178	.009913	.009972	-.007175	-.001109	-.009941	-.006119	-.004520	-.007503	.003335	.003410	.003302	.002390	.001805	.000479	-.001679	-.004419	-.003384	-.002171	-.001961	-.000613	.000564	.003134
12	-.015600	-.009700	-.003698	.000210	.002537	.004154	.003489	.007734	.001383	.008934	.009913	.011419	.011510	-.007322	-.007467	-.007115	-.006795	-.006557	-.001409	.001833	.003898	.003113	.002391	.001654	.000345	-.001789	-.004914	-.003329	-.002702	-.001934	-.001028	.000417	.002837
13	-.021099	-.010969	-.004552	-.000910	.001197	.002516	.003584	.007438	.001720	.008392	.009622	.011550	.014004	-.007103	-.007495	-.007147	-.006812	-.006581	-.002109	.004110	.003020	.003071	.002309	.001579	.000054	-.001991	-.005337	-.003909	-.002804	-.001973	-.001044	.000311	.002644
14	-.023539	-.011390	-.003935	.000762	.003574	.005397	.004994	-.004419	-.009901	-.009843	-.007125	-.001534	-.007705	.015005	.012510	.010595	.004025	.004430	.015809	-.003284	-.003309	-.002822	-.001977	-.000946	.000400	.002939	.003997	.003719	.003249	.002393	.001972	.000119	-.001491
15	-.017916	-.010312	-.003179	.001851	.004937	.007065	.008940	-.009292	-.008541	-.006740	-.007108	-.007407	-.007493	.012370	.012410	.010996	.009289	.008517	.012644	-.004900	-.003449	-.002923	-.001848	-.000911	.000580	.003113	.003749	.003903	.003333	.002493	.001989	.000490	-.001334
16	-.013361	-.008744	-.003449	.002049	.006080	.009929	.011443	-.004345	-.008499	-.008712	-.006943	-.007115	-.007147	.010595	.010699	.010900	.009929	.009089	.010909	-.004513	-.003502	-.002430	-.001891	-.000910	.000709	.003382	.003494	.003553	.003499	.002867	.004140	.000912	-.001200
17	-.009816	-.009957	-.002901	.001374	.006670	.010921	.014713	-.009570	-.009497	-.006622	-.004719	-.004793	-.004917	.009025	.009209	.009929	.010661	.010195	.008174	-.001588	-.003100	-.002303	-.001923	-.000848	.000071	.003775	.003274	.004327	.004401	.003123	.002439	.001099	-.001034
18	-.004950	-.004954	-.001926	.002184	.006901	.012928	.012904	-.004425	-.008103	-.008516	-.006520	-.006557	-.004561	.008256	.000517	.009086	.010149	.011428	.004053	-.001509	-.002934	-.002484	-.001900	-.000811	.001061	.004469	.003172	.003102	.003495	.002211	.002850	.001463	-.000048
19	-.013666	.001574	.008211	.011290	.012535	.015074	.015589	-.008520	-.006719	-.007013	-.002303	-.007405	-.007109	.013008	.014444	.010409	.008914	.000453	.012211	-.004903	-.002497	-.002120	-.001361	-.000459	.000974	.003909	.004509	.004348	.003881	.003230	.002400	.001191	-.000944
20	.010311	.008465	.009120	.004543	.003031	.002062	.001299	.003133	.002173	.003298	.002535	.003951	.004110	-.003282	-.004800	-.004315	-.003888	-.001594	-.004803	.011687	.002348	.001125	.001237	.000789	.000129	-.000917	-.003634	-.001944	-.001334	-.000913	-.000538	.000002	.001053
21	.004060	.003205	.005269	.004906	.004494	.004073	.005018	.003033	.003073	.003213	.003470	.003698	.005688	-.003309	-.003440	-.003302	-.003108	-.002934	-.002391	.002146	.010938	.002024	.001389	.000924	.000354	-.000831	-.001929	-.001844	-.001318	-.000754	-.000534	.000237	.001122
22	.002468	.004081	.005400	.006035	.009216	.006400	.004415	.003104	.002120	.003213	.003302	.003173	.005011	-.002422	-.002423	-.042930	-.002393	-.002484	-.002120	.001123	.002024	.007999	.001799	.001182	.000214	-.000204	-.001310	-.001203	-.001191	-.000719	-.000250	.000333	.001293
23	.002941	.004874	.005573	.009445	.007393	.006039	.006810	.002499	.002089	.002253	.002340	.002591	.002309	-.001077	-.001869	-.001881	-.001925	-.001900	-.001591	.001251	.001509	.001788	.006219	.001517	.000969	.000161	-.000053	-.000729	-.000729	-.000991	-.000231	.000319	.000927
24	.001550	.002415	.005090	.008944	.000890	.010320	.012092	.002502	.002408	.004051	.001003	.001954	.001514	-.000444	-.000911	-.000610	-.000849	-.000821	-.000459	.000789	.000921	.003102	.001377	.008157	.001118	.001239	-.000477	-.000321	-.000253	-.000201	-.000175	.000192	.000513
25	.001083	.003043	.005185	.001423	.014078	.013160	.016010	.001217	.004465	.000449	.000479	.000345	.000254	.000480	.000388	.000709	.000811	.001091	.000974	.000129	.000334	.000612	.000969	.001710	.006900	.003200	.000133	.000284	.000463	.000374	.000219	-.000153	-.000320
26	-.000477	.001902	.004977	.007799	.011597	.014009	.021440	-.001514	-.001443	-.001968	-.001675	-.001109	-.001031	.004936	.003113	.003382	.002773	.004499	.001384	-.000917	-.000621	-.000204	.000161	.001459	.003200	.014201	.001133	.001147	.001199	.001470	.000966	-.000413	-.002121
27	.012779	.010282	.007851	.003935	.004510	.003448	.002940	-.003401	-.005546	-.003642	-.004279	-.004014	-.005327	.003967	.003746	.003484	.003214	.005112	.004586	-.003832	-.001929	-.001310	-.000855	-.000477	.000155	.001133	.019900	.002743	.001910	.001403	.000923	.000499	-.000053
28	.005437	.009822	.009940	.008540	.009014	.005551	.001230	-.002053	-.002967	-.003153	-.001594	-.003329	-.001904	.005119	.003805	.003393	.003347	.003102	.004390	-.001944	-.001994	-.001203	-.000129	-.000311	.000280	.001147	.002745	.012729	.002291	.001400	.001104	.000510	-.000509
29	.003843	.003111	.007103	.001799	.001094	.001894	.000823	-.002492	-.002594	-.002114	-.002172	-.002782	-.000804	.003220	.003333	.003499	.001401	.003245	.003891	-.001334	-.001218	-.001191	-.000749	-.000253	.000365	.001108	.001910	.002201	.009942	.002084	.001420	.000823	-.000141
30	.003052	.003229	.007008	.006710	.009714	.010419	.011210	-.004444	-.001935	-.001946	-.001941	-.001934	-.001915	.002593	.002493	.002097	.003125	.003211	.002250	-.000913	-.000154	-.000719	-.000491	-.000201	.000374	.001010	.001405	.001400	.002094	.001974	.001937	.001205	.000525
31	.001823	.004154	.009674	.004801	.010919	.012055	.014995	-.000107	-.000818	-.000952	-.000975	-.001028	-.001014	.001077	.001909	.002140	.000459	.002030	.002490	-.000530	-.000354	-.000250	-.000231	-.000113	.000419	.000999	.000923	.001104	.001420	.001937	.001434	.004133	.001662
32	.001325	.001151	.002216	.000914	.012077	.015743	.019161	.001143	.000991	.000744	.000394	.000417	.000511	.000316	.000690	.000031	.001099	.001495	.001101	.000002	.000231	.000351	.000319	.000142	-.000133	-.000495	.000269	.000510	.000823	.001103	.002133	.007844	.003647
33	-.000196	.002453	.005435	.009199	.013336	.018656	.024976	.004329	.004038	.003541	.003134	.002937	.004944	-.001497	-.001150	-.001200	-.001024	-.000848	-.000944	.001055	.001122	.001293	.000947	.000375	-.000370	-.000127	-.000033	-.000509	-.000141	.000523	.001494	.003491	.013571

TABLE IX
STRESS COEFFICIENT MATRIX [S]

	1	2	3	4	5	6	7	8	9	10	11	12	13	14	15	16	17	18	19	20	21	22	23	24	25	26	27	28	29	30	31	32	33
1	-.980139	-.190829	-.104804	-.048405	-.012276	.012470	.032178	.006165	.007231	.004944	.014022	.021932	.030914	.033522	.024142	.016778	.015272	.009947	.024111	.030761	.000403	.000903	.000303	.001469	.002139	.003751	.035378	.000204	.000111	.000822	.001594	.002549	.002504
2	.319281	.190879	.104904	.048403	.012216	-.012476	-.032179	-.006163	-.001233	-.009996	-.014022	-.021952	-.030916	-.035522	-.024162	-.018778	-.015474	-.009941	-.024111	-.030781	-.000403	-.000903	-.000303	-.001469	-.002139	-.003731	-.035319	-.004204	-.000317	-.000822	-.001599	-.002369	-.003904
3	.494311	.493447	-.118318	-.095142	-.050804	-.029215	-.016992	.042135	.004782	.010001	.018210	.027084	.019058	.022433	.033504	.014340	.013574	.000062	.018108	.024234	.023123	.003429	.003312	.002155	.001097	.000422	.031966	.021743	.004532	.003597	.005118	.001268	.000939
4	.272091	.429509	.391063	-.243429	-.142416	-.079903	-.030385	.011224	.015244	.023148	.052404	.025031	.015785	.023347	.022150	.040212	.025856	.020014	.034104	.016497	.022962	.020043	.000907	.000901	-.000705	.000106	.021611	.028450	.024421	.000916	.000551	-.000125	-.000104
5	.100991	.211156	.330120	.424304	-.351089	-.222470	-.127937	.070135	.026548	.053952	.028319	.020948	.014580	.022013	.028036	.056460	.042745	.033953	.051318	.001971	.013928	.020806	.016450	-.003918	-.007034	-.006654	.011577	.020413	.026140	.021162	-.004598	-.006000	-.010044
6	.011099	.003417	.161685	.250477	.461457	-.427102	-.270664	.020596	.034559	.028107	.021421	.015735	.011952	.011610	.021607	.027510	.055116	.044515	.033201	.002826	.009327	.014001	.017181	.010178	-.013501	-.020109	.005115	.012484	.018262	.020790	.012848	-.015577	-.023429
7	-.040261	-.000536	.040286	.067063	.146335	.250263	-.521205	.050504	.027559	.019026	.013511	.010316	.000995	.011904	.013522	.016774	.023057	.052654	.011219	-.000249	.004052	.006470	.010355	.009001	-.001116	-.038649	.000527	.003600	.009443	.012148	.011672	-.000913	-.045449
8	-.045230	-.000648	.045146	.097567	.163967	.258064	.415354	.040066	.050660	.021321	.013206	.011540	.010076	.013340	.014950	.018796	.025858	.036512	.019564	-.000502	.004525	.007414	.011604	.010925	-.001310	-.043305	.000591	.004215	.010502	.013413	.013080	-.001090	-.048490
9	-.625605	-.350357	-.164526	-.073170	-.003315	.043452	.001705	.058441	.041164	.046240	.060023	.079161	.101104	.037140	.020115	.007611	-.001242	-.006519	.024111	-.197509	.021008	.015616	.010900	.009496	.005770	.000611	.046122	-.014899	-.009830	-.005285	.000163	.006351	.017002
10	-.526914	-.577254	-.196018	-.075540	.001792	.055659	.099771	.014901	.078310	.087039	.101253	.116255	.123835	-.010232	-.022942	-.029500	-.054914	-.038211	-.024550	-.032341	-.166622	.029710	.024797	.017600	.007406	-.009212	-.008092	.002425	-.024919	-.017214	-.002100	.006110	.026502
11	-.491600	-.362630	-.261260	-.087406	.027564	.110135	.100614	.127180	.131514	.141550	.152201	.152732	.154140	-.062390	-.064672	-.043805	-.066763	-.069411	-.014823	.004996	-.019136	-.171514	.055570	.055916	.016246	-.012035	-.049945	-.023241	-.015695	-.050412	-.013986	.008439	.042941
12	-.424072	-.349015	-.260031	-.166457	-.009180	.121440	.221992	.171506	.174568	.118345	.169953	.162604	.162665	-.090585	-.094424	-.092112	-.081080	-.063416	-.104100	.023174	.018593	-.027129	-.151228	.065151	.031279	-.014033	-.060554	-.043018	-.022104	-.010214	-.022157	.005629	.031203
13	-.322005	-.251011	-.195562	-.126039	-.014729	.102550	.162744	.195030	.108565	.111794	.155118	.141039	.146962	-.087291	-.091620	-.090458	-.063040	-.015469	-.095095	.040544	.036406	.021361	-.024227	-.159129	.071244	.021049	-.065060	-.047107	-.033454	-.012154	.002514	-.002253	.022581
14	-.229629	-.150404	-.101195	-.039748	.053764	.199426	.482289	.156069	.133503	.111635	.097602	.091557	.092465	-.039015	-.042900	-.041056	-.033533	-.019065	-.041551	.025472	.025676	.024721	.012730	-.015140	-.100179	.110305	-.059139	-.027024	-.019012	-.004826	.008360	.013159	-.034121
15	-.236030	-.166541	-.140579	-.046042	.041720	.183652	.440055	-.005705	-.015566	-.051022	-.031201	-.030907	-.035920	.070701	.007522	.093304	.106152	.131150	.064119	-.054321	-.022316	-.015304	-.007114	.006320	.011315	-.026949	.010134	.021405	.020004	.011349	-.013741	-.100084	.103445
16	-.353353	-.261019	-.203953	-.133717	-.021554	.181066	.356575	-.059407	-.082661	-.069652	-.015249	-.076259	-.012103	.135145	.133610	.140966	.151244	.173962	.174852	-.054606	-.058063	-.026509	-.011506	.002315	-.001550	.020155	.029254	.023409	.013142	-.027812	-.139851	.099647	.023934
17	-.452621	-.356005	-.264222	-.190605	-.011172	.121566	.229490	-.011505	-.070299	-.010517	-.014042	-.077047	-.075205	.147564	.146120	.153125	.142117	.158944	.152932	-.056927	-.056313	-.019915	-.006128	-.016001	.063084	.031444	.020758	.004903	-.035530	-.154192	.060902	.051914	-.001442
18	-.418916	-.572593	-.214005	-.085517	.020968	.105067	.175861	-.037900	-.051545	-.055267	-.052494	-.053415	-.051146	.140599	.139328	.139111	.128412	.117880	.188515	-.040097	-.010047	-.009253	-.025051	-.011505	.066979	.033121	-.005414	-.044554	-.175945	.050122	.033027	.017508	-.008999
19	-.518486	-.361215	-.105415	-.063617	.014155	.062263	.112799	-.054627	-.032495	-.031421	-.028423	-.020200	-.015171	.120440	.113500	.099244	.084602	.075211	.113380	-.007229	.002605	-.019461	-.014993	-.065702	.003994	.022556	-.057533	-.107191	.036191	.024214	.010100	.009443	-.045116
20	-.621311	-.355300	-.179100	-.066061	.005406	.051528	.068595	-.009115	-.008524	-.004217	.002508	.015676	.051944	.106117	.068030	.065656	.032006	.043940	.100153	.041877	-.012511	-.004994	-.005104	.000073	.005062	.015902	-.190509	.019264	.013602	.011444	.010491	.001441	.002928
21	1.131016	.742323	.490624	.276250	.140187	.052228	-.012351	-.104129	-.110211	-.124231	-.146159	-.100641	-.210048	.013758	.031593	.043412	.051845	.057595	.021711	-.171786	-.031259	-.059279	-.022999	-.016093	-.001329	.019857	-.111407	.010810	.040092	.054401	.018525	.000584	-.031901
22	.432452	.551264	.142277	.958197	1.262215	1.453267	3.653965	-.319015	-.200684	-.296940	-.291531	-.091559	-.312059	.321394	.346693	.373679	.405130	.441616	.315918	-.116815	-.003710	-.045077	.027551	.159552	.440391	.131011	.171701	.164724	.163600	.132094	.071214	-.067096	-.284730
23	.465010	.505519	.161857	1.004636	1.256019	1.313214	1.718044	.408419	.319116	.243540	.516431	.290204	.261718	-.259090	-.241145	-.231985	-.225700	-.242011	-.001119	.143720	.131812	.135163	.117281	.059689	-.061695	-.240991	-.080404	-.055524	-.012011	.055235	.180476	.446402	.110912
24	.541153	-.966608	-.362322	-.267039	-.024136	.176229	.385015	.099282	.099642	.108404	.125168	.155956	-.001547	.122025	.090146	.064510	.049940	.044251	-.151295	-.139125	.015215	.001111	-.004229	.001215	.010358	.024939	.101776	-.084934	-.024742	-.023644	-.009775	.011284	.045265
25	.894111	-.084260	-1.062123	-.517039	-.124570	.180540	.455114	.310001	.166176	.212921	.259429	-.018101	-.047608	.151840	.127980	.019461	.042054	.022466	.014115	-.146161	-.131049	.047051	.026504	.024014	.019030	.010362	.154604	.027071	-.041448	-.053614	-.011808	.019842	.072156
26	.665034	.203847	-.526078	-1.016621	-.239946	.160257	.522150	.324235	.344074	.393197	-.533083	-.463238	-.466712	.128550	.119059	.065944	.022619	-.011506	.085163	-.114126	-.151110	-.090974	.085691	.060457	.014692	.004860	.143446	.053122	-.015244	-.063318	-.024444	.037065	.114560
27	.600575	.267010	-.055972	-.430654	-.954084	-.089348	.597332	.579400	.395516	-.366432	-.311550	-.085675	-.278750	.074664	.072416	.052072	.012796	-.042269	.048904	-.060254	-.025948	-.027199	-.027420	.119164	.034444	-.034372	.094299	.042111	.003630	-.051095	-.090035	.017905	.154009
28	.305156	.159450	.026299	-.126340	-.127050	-.650714	.495095	.715040	-.184506	-.141226	-.182069	-.110850	-.109400	.017661	.017039	.069601	-.009667	-.041210	.006973	-.022960	-.035421	-.021251	-.032131	-.002515	.102350	-.037801	.030139	.016523	.001370	-.015930	-.020421	-.011315	.119161
29	-.312165	-.167311	-.034202	.116256	.315010	.016965	-.510525	.062511	.031607	.004625	-.011050	-.019573	-.019165	.111057	.112459	.124695	.151306	.192017	.119116	-.034614	-.015744	-.002448	.012225	.024751	.069109	-.101541	.019116	.031080	.031105	.014500	.006012	-.002474	.022244
30	-.426321	-.284940	.039022	.412866	.975222	.010656	-.615652	.055123	.032531	-.015344	-.030261	-.068050	-.070613	.216426	.205104	.312919	.310458	-.534420	.102110	-.064121	-.050470	-.003057	.030157	.044592	-.015784	-.115722	.051149	.008754	.082272	.042207	-.112105	-.057584	.001622
31	-.690536	-.288715	.305737	.996704	.210492	-.178951	-.590653	.011798	.005509	-.026490	-.077545	-.110910	-.119511	.460916	.477121	.526942	-.154482	-.339041	.221840	-.122156	-.046279	.009129	.052145	.026071	-.023829	-.098430	.097220	.125011	.090543	-.019492	-.059054	-.041012	-.011552
32	-.906795	.049345	1.096236	.499071	.105111	-.200926	-.415506	-.021043	-.025616	-.042591	-.014492	-.121690	-.145050	.940770	.872384	-.265602	-.245221	-.125495	.114214	-.140661	-.021272	.034523	.020943	.009022	-.016053	-.065208	.150541	.127793	-.043228	-.029416	-.024227	-.024151	-.026317
33	-.545929	.961719	.557036	.291669	.027077	-.183556	-.193864	-.051024	-.051010	-.055123	-.068594	-.092967	-.130015	.002612	-.153576	-.122202	-.102742	-.094086	1.042594	-.100141	.017325	.021259	.020006	.000316	-.010074	-.040199	.121124	-.009020	.001234	.001132	-.000846	-.018422	-.050037
34	.172796	.171484	.114032	.070614	.040301	.018279	.000310	-.004604	-.005484	-.007525	-.009925	-.011426	-.010364	-.011745	-.013206	-.011107	-.009030	-.006907	-.001257	.001094	-.020129	.000059	.001465	.000065	.000375	-.000523	.000886	-.023741	.000499	.001264	.000925	.000457	-.000191
35	.198185	.203911	.201320	.140926	.092569	.056604	.020291	-.008279	-.001197	-.010008	-.010939	-.000261	-.008400	-.069887	-.009977	-.012815	-.012057	-.009347	.004120	.007243	-.003211	-.016721	.002099	.002441	.002260	.001445	.006015	-.004449	-.020422	.002221	.002499	.002621	.002046
36	.186410	.213214	.242054	.212516	.204015	.152149	.114047	-.005405	-.007255	-.007596	-.002985	-.001554	-.003010	-.005722	-.001536	-.003265	-.009159	-.009354	.014520	.008421	.005280	-.002659	-.016158	.004726	.001121	.010161	.010027	.008729	-.002598	-.020711	.005199	.008193	.012090
37	.770048	.199372	.172467	.208549	.254048	.749827	.136913	-.002592	-.002016	.002102	.002161	.002291	-.000286	.001719	.004140	.005349	.003351	-.002324	.015224	.005451	.006061	.005889	.000148	-.013051	.007499	.012710	.007206	.007736	.001114	.000115	-.035633	.008471	.014507
38	.059082	.095750	.133153	.177430	.231705	.294600	.245127	.009076	.009427	.009645	.007932	.005595	.002652	.005152	.008519	.071241	.013088	.012660	.014816	.003501	.004110	.001941	.007443	.000720	-.012176	.077954	.005172	.007342	.004609	.009432	.000956	-.014912	.019598
39	1.644585	1.264612	.671240	.582507	.381745	.236291	.125521	-.141220	-.751111	-.777171	-.199479	-.251205	-.260713	-.008753	.033124	.055507	.069305	.079416	.044121	-.170024	-.714159	-.050911	-.026692	-.075200	.065596	.032350	.465625	-.002466	.098825	.087010	.041238	.014854	-.051667
40	1.480464	3.384765	1.202484	.944005	.747257	.601572	.493213	-.150072	-.767491	-.178896	-.193547	-.200204	-.270420	.039474	.061792	.092792	.170169	.121407	.174199	-.022760	-.704325	-.021661	-.050214	-.004616	.022507	.055537	.260760	.496039	.008922	.106442	.060421	.053477	.060540
41	1.368118	1.465911	1.505092	1.497732	1.264461	1.159516	1.002490	-.171166	-.723432	-.153184	-.722821	-.124659	-.155814	.044464	.056910	.074613	.173917	.739625	.160114	-.019967	-.044177	-.045846	-.049666	.003071	.030747	.075104	.176523	.293046	.905074	.016235	.760412	.123032	.028074
42	1.022489	3.301120	1.506522	1.660514	1.708590	1.765125	1.797464	.009007	-.002437	-.004421	-.001146	-.006749	-.021063	.008615	.026028	.038630	.080041	.110785	.176404	.029191	.020244	.007616	-.076742	-.011324	.032504	.052937	.096074	.129267	.290696	.560154	.050313	.237420	.247421
43	.808426	1.080157	1.400672	1.738631	2.090781	2.178270	2.523415	.265948	.250014	.231063	.211259	.108326	.142729	-.123225	-.100559	-.084460	-.073752	-.057241	-.010704	.103253	.103351	.103620	.074460	.074022	-.036449	-.078706	-.001017	.040542	.711420	.249015	.550605	.127930	.518617
44	1.121070	.729457	.446256	.252407	.721074	.050245	-.042269	.078456	.078953	.073651	.088511	.060115	.045273	-.248048	-.209963	-.176791	-.150049	-.132945	-.251102	-.066403	.015320	.049400	.036921	.079946	-.081528	-.038762	-.204602	-.058795	-.040780	-.029450	-.025159	-.084028	.021790
45	1.626127	1.243054	.848700	.558752	.357326	.213201	.100924	.115600	.177924	.105344	.099719	.076237	.036740	-.303207	-.273521	-.240559	-.206585	-.165000	-.254117	.494094	.014204	.100039	.071493	.043601	.011790	-.047027	-.200056	-.155028	-.058534	-.019098	-.020400	.004442	.041077
46	7.459944	1.381413	1.216088	.971915	.787990	.655197	.561643	.183540	.170958	.166108	.151901	.111292	.093546	-.255299	-.247520	-.241994	-.224403	-.400176	-.344348	.205636	.044400	.039719	.744054	.095449	.054004	-.003212	-.107531	-.725420	-.112525	-.041545	-.009409	.030399	.029794
47	1.450185	1.533505	1.552515	1.490290	1.298150	1.752449	1.056201	.182521	.168870	.141253	.091077	.075474	.040448	-.162000	-.455743	-.159320	-.144604	-.161329	-.043492	.178104	.265412	.529823	.039122	.164774	.117555	.096740	-.021262	-.033703	-.063940	-.073264	-.001444	.041002	.014440
48	1.096564	1.317166	1.423554	1.707448	1.606169	1.785980	1.811700	.156812	.109290	.044314	.020539	.066492	-.011313	-.063563	.072020	.076612	.009192	.006043	.117392	.061773	.127795	.244829	.504043	.036780	.238447	.243261	.044306	.032055	.072159	-.010167	-.010977	.036509	.052627
49	.789096	1.075757	1.405162	7.252429	2.116384	2.418536	2.576154	-.071465	-.718046	-.743478	-.153777	-.168378	-.190604	.233455	.260125	.284009	.565425	.373935	.344443	-.036960	.000308	.044433	.249526	.525957	.143074	.555505	.118445	.133644	.130900	.100677	.038492	-.043489	-.101679

TABLE X
Matrix $\{AT\}$

1	-92.32476370	26	-1100.86489153
2	1592.32476383	27	-939.50998485
3	-60.24970900	28	-859.54667804
4	-222.63401679	29	-3524.82157683
5	-253.07605061	30	-3361.35473430
6	-94.44139715	31	-3227.87656528
7	442.23779340	32	-2977.44333845
8	-2286.41063917	33	-2714.08887357
9	-3785.32614148	34	767.79220127
10	-4119.10557437	35	904.95734172
11	-4764.02371061	36	592.93390626
12	-4985.30832517	37	-17.28751687
13	-4969.72981596	38	-720.49754617
14	-4492.37862730	39	8592.00505352
15	-4354.58987951	40	8725.85882282
16	-4887.04344642	41	7870.68588331C
17	-5013.05519950	42	4969.65661299
18	-4765.98693502	43	1010.45895720
19	-4219.25686240	44	5460.77078927
20	-3867.37383425	45	8681.69078517
21	5143.74844420	46	8356.94250321
22	200.58214441	47	7980.72271180
23	-379.38246968	48	4504.14537561
24	-1720.33535162	49	769.32658458
25	-1354.25763476		

TABLE XI

RESULTS AT STATION $y_w = 34.5$

Comparison of Maximum Normal Stress, Maximum Shear Stress
And Principal Axis Deviation From Y-Axis. Left Wing,
Forward Of Y-Axis Is Positive. Theoretical Loading
Corresponds To Experimental Loading Of
336000 in. lb Torque

Lower Skin

Panel No.	Maximum Normal Stress		Maximum Shear Stress		Principal	
	Experi-mental	Theo-retical	Experi-mental	Theo-retical	Experi-mental	Theo-retical
15	+894	+2234	+759	1757	+ 3°36'	-5°15'
17		+2025		1328		-9°18'
19		+1420	525	1025	5°28'	-1°50'
21	+780	+1009	690	844	+ 7°8'	+6°49'
23		-827		723		+10°29'
25	-576	-994	562	706	+10°56'	+4°55'

Rear Beam

Upper Skin

Panel No.	Exp.	Theo.	Exp.	Theo.	Exp.	Theo.
28	+868	+813	800	593	+10°37'	+6°9'
30		+714		596		+0°11'
32		-835		670		+2°24'
34	-525*	-1068	525	773	+ 5°18'	+1°16'
36		-1575		1075	·	+0°08'
38	-800	-1974	535	1493	-15°19'	+7°41'

* Max. compressive stress in panel 34

TABLE XII

COMPARISON OF LINEARITY OF STRAIN READINGS

AT VARIOUS LOCATIONS FOR THE 7000 LB AND 8000 LB TESTS

General Location in Wing	Gage Number	Strain (μ in/in)			
		Measured 7000 lb Test	8000 lb Load		
			Measured 8000 lb test	Extra-polated from 7000 lb test	Differ-ence Between Measured And Extrap
Upper Skin					
Outboard Near	131	− 52	− 52	− 59	7
Leading Edge	132	+123	+147	+141	6
	133	+ 31	+ 44	+ 35	9
Outboard Near	43	− 21	− 22	− 23	1
Trailing Edge	44	+ 46	+ 53	+ 53	0
	45	+ 2	+ 4	+ 2	2
Inboard Near	16	− 11	− 12	− 13	1
Leading Edge	17	+ 72	+ 83	+ 82	1
	18	+ 28	+ 30	+ 32	2
Inboard Near	89	+ 8	+ 8	+ 9	1
Trailing Edge	90	+ 50	+ 53	+ 57	4
	91	− 11	− 17	+ 13	4
Lower Skin					
Outboard Near	169	+ 55	+ 66	+ 63	3
Leading Edge	170	+141	+162	+161	1
	171	− 36	− 41	− 41	0
Outboard Near	394	− 26	− 30	− 30	0
Training Edge	395	+150	+170	+171	1
	396	+ 40	+ 49	+ 46	3
Inboard Near	161	+ 12	+ 17	+ 14	3
Leading Edge	162	+ 10	+ 15	+ 11	4
Inboard Near	367	+ 13	+ 14	+ 15	1
Trailing Edge	368	− 42	− 50	+ 48	2
	369	+ 21	+ 24	+ 24	0
FB Web	152	− 7	− 10	− 8	2
	153	+157	+176	+179	3
	154	+ 25	+ 25	+ 29	4
CIB Web	273	+ 2	+ 3	+ 2	1
	274	− 25	− 28	− 29	1
	275	− 2	− 1	− 2	1
RB Web	409	− 20	− 22	− 23	1
	410	+134	+155	+153	2
	111	+ 7	+ 5	+ 8	3
Average Difference Between Measured and Extrapolated					= 2.3

TABLE XIII

EXPERIMENTAL AND THEORETICAL SHEAR FLOWS AND TOTAL

TORQUE REACTED AT THE SECTION PERPENDICULAR TO

CIB AT $y_w = 98.7$

Cell No.	Rosette No.	Twice Cell Area (2A) in^2	Shear Flow, q, (lb/in.)				Torque = 2Aq (in. lb)		
			Experimental		Theoretical		Exp.	Theoretical	
			Initial 8000 lb test	Average 8000 lb test	323,785 in. lb load	336,000 in. lb load	8000 lb test	323,785. in. lb load	336,000 in. lb load
Web	152		222*	211	206.2	213.95			
a	131 169	86.2	211 211	211	206.2	213.95	18188.2	17774.4	18442.1
Web	181 196		224 175	200	232.5	241.35			
b	46 216	105.8	415 415	415	438.7	455.30	43907.0	46239.0	48170.3
Web	225 237		48.8 53.8	51.3	49.9	51.78			
c	49 252	127.6	495 481	488	488.6	507.08	62268.8	62345.4	64703.9
Web	273 261		10.9 Bad Gage	10.9	4.7	4.83			
d	52 291	140.0	512 505	509	493.3	511.91	71260.0	69062.0	71667.4
Web	300 312		5.8 7.8	7	17.8	18.52			
e	55 333	143.4	543* 478	478	475.5	493.39	68545.2	68186.7	70752.4
Web	342 355		35.5 41.3	38.4	40.7	42.20			
f	58 394	138.0	414 450	432	434.8	451.19	59616.0	60002.4	62263.9
Web	409		405*	432	434.8	451.19			
Total Reacted Torque = $\sum 2Aq$ =							323785.2	323609.9	336000.0

* Considered Stray Values

83

TABLE XIV

EXPERIMENTAL RESULTS AT $y_w = 34.5$

Panel No	Gage No.		Strain Readings		Average Strains	σ_{max}	τ_{max}	ϕ_p **
	Interior	Exterior	Interior	Exterior				
			μ-in/in.	μ-in/in.	μ-in/in	psi	psi	
15	161*	486	+12.	−43.5	−15.8	+894	759	+37°34'
		485		+103.	+103.			
	162	484	+14.5	+52.5	+33.5			
21	279	459	+14.	+22.	+18.	+780	690	+41°06'
	280	458	+92.	+95.	+93.5			
	281	457	+2.	−14.	−6.			
25	367	468	+14.	−46.	−16	−576	572	−44°54'
	368	467	−49.	−95.	−72			
	369	466	+24.	+7.	+15.5			
28	28	474	−22.	+28.	+3			
	29	473	+136.	+78.	+107	+868	800	−44035'
	30	472	+25.	−13.	+6			
34	19	480	−6.	−16.	+11	+555	525	−39°26'
	20	479	+72.	+64.	+68			
	21	478	+26.	+4.	+5			
38	13	483	−78.	−66.	−72	−800	535	+18039'
	14	482	+59.5	+59.	+59			
	15	481	+35.	+39.	+37			

* Two gage rosette.

** Angle measured from sweep angle of CIB. Plus angles are measured in the direction of the diagonal gage of the interior rosette.
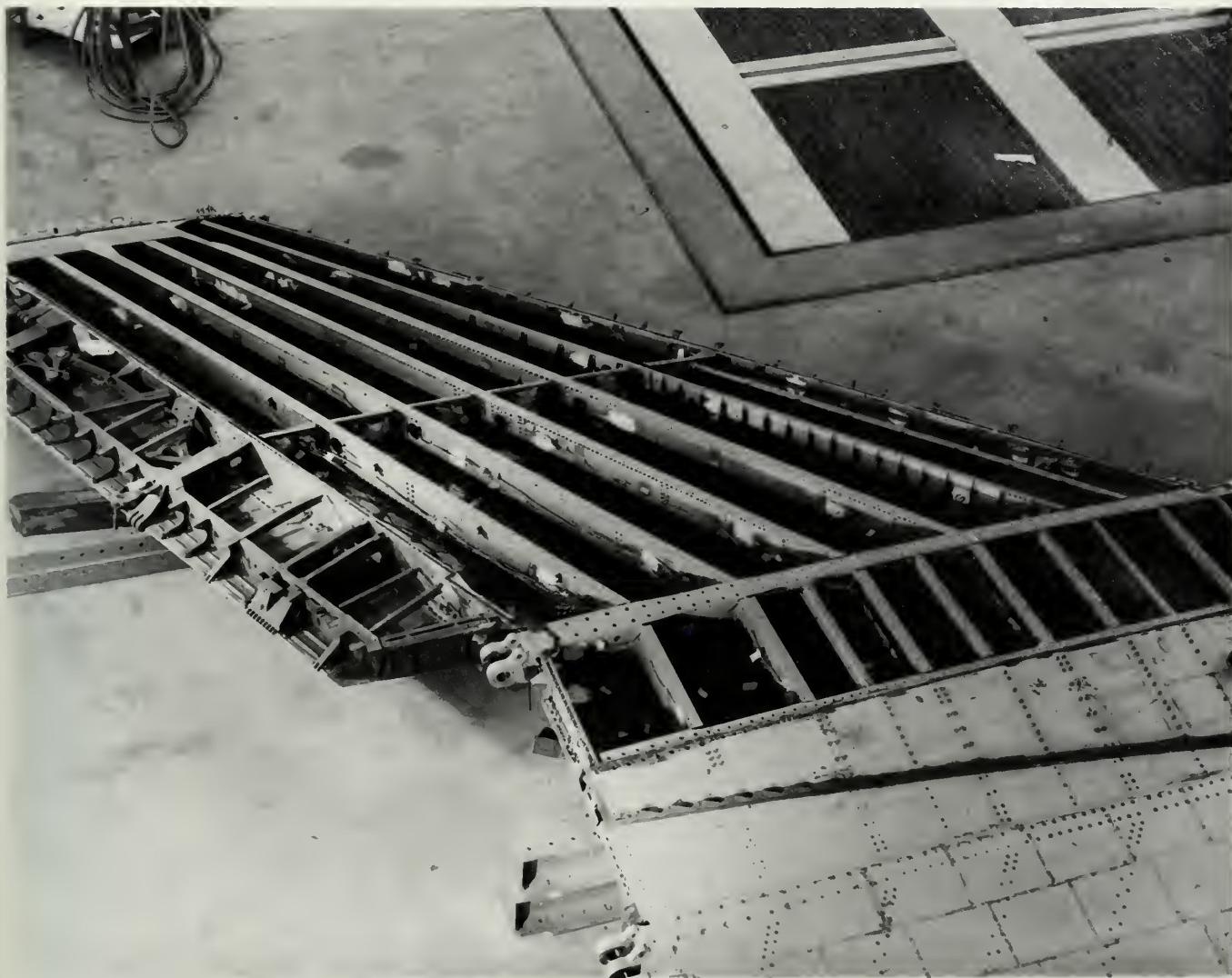
Fig. 19

F8U-3 Wing With Upper Skin Removed

Fig. 20

F8U-3 Wing Mounted Inverted
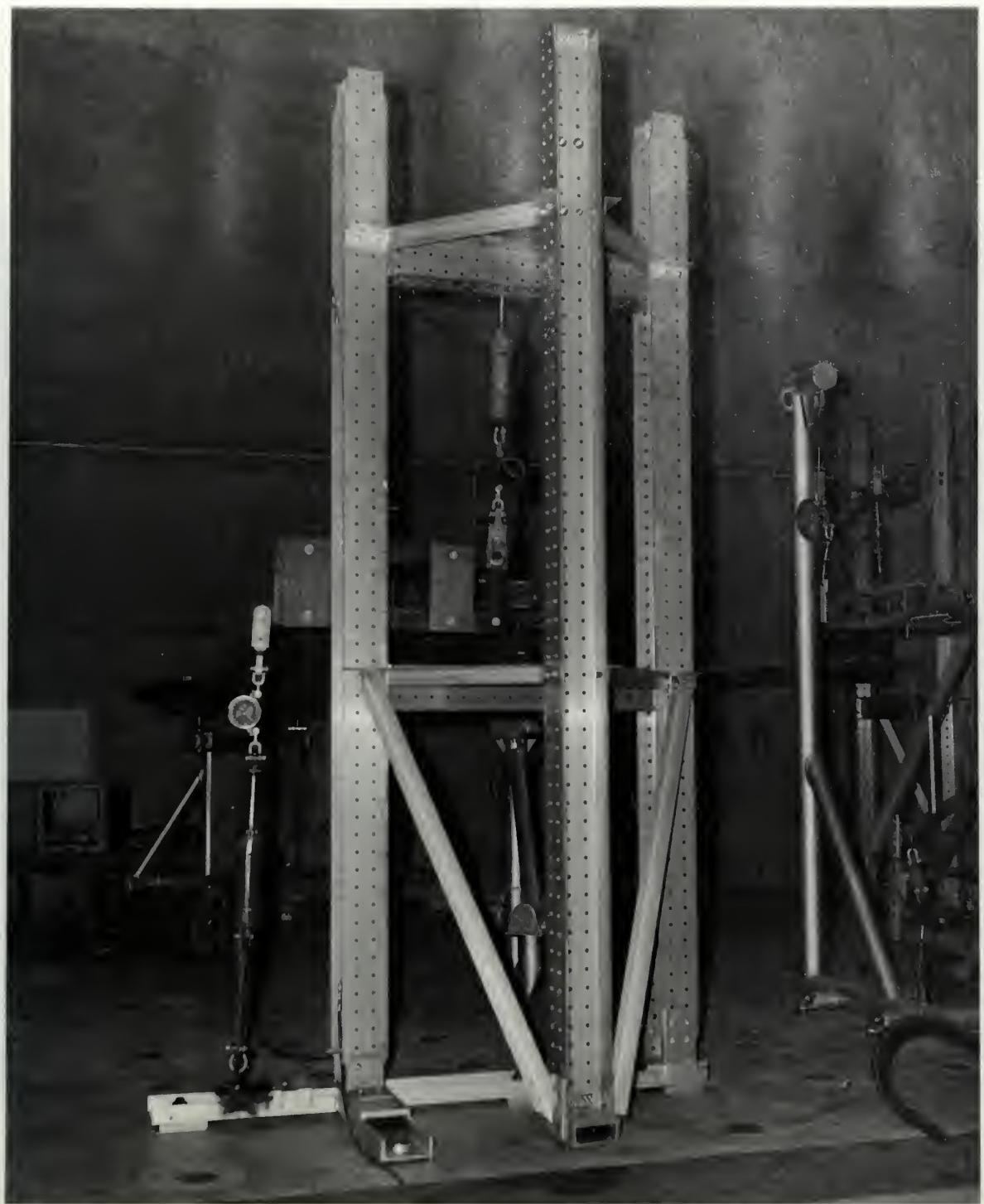
Fig. 21

Loading Frame and Linkage

87
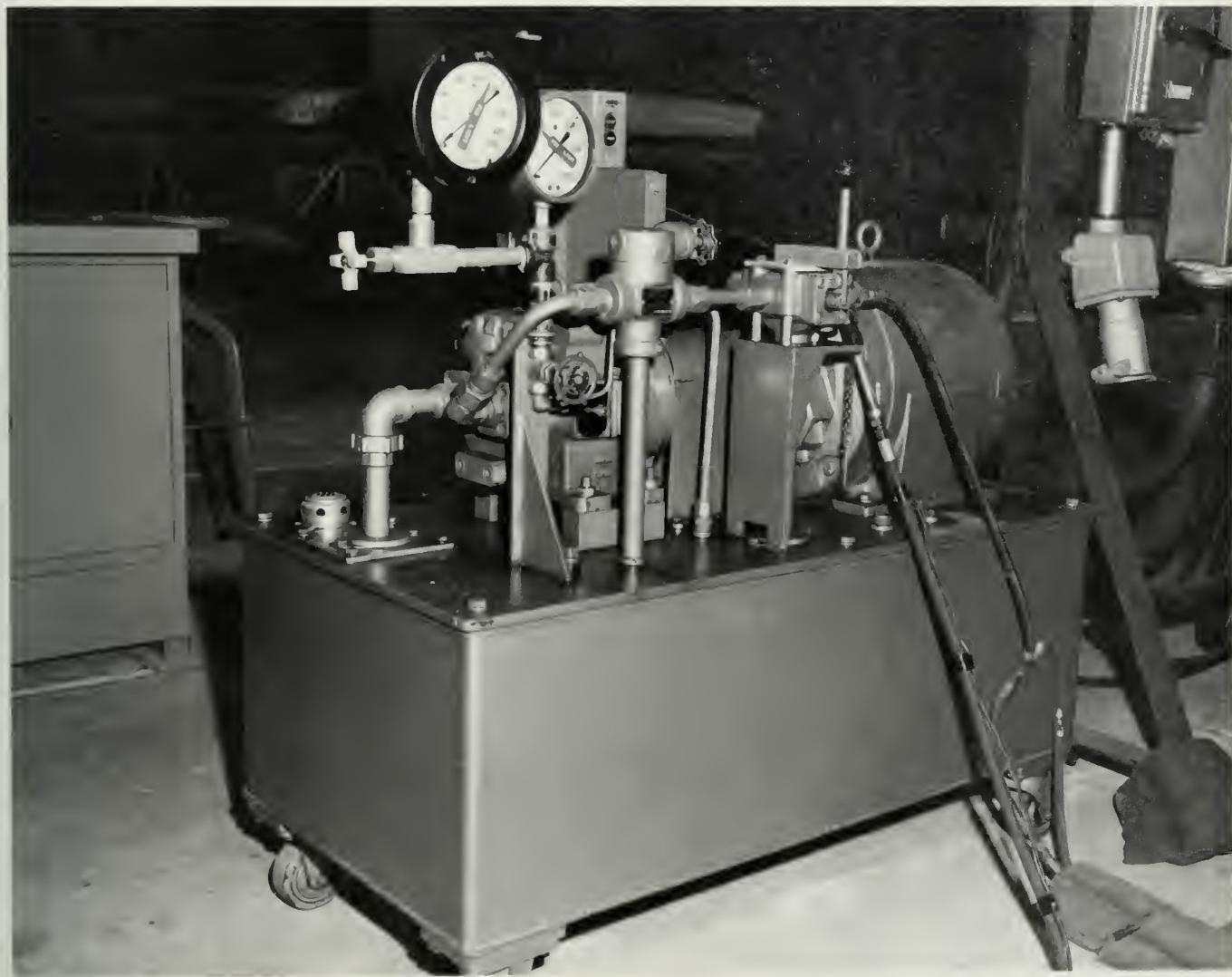
Fig. 22

Vickers V-Line Piston Type Pump Assembly

Fig. 23

SKETCH OF PERTINENT STRAIN GAGE LOCATIONS

F8U-3 PORT WING

Top View
Lower Skin And Beams

Top View
Upper Skin
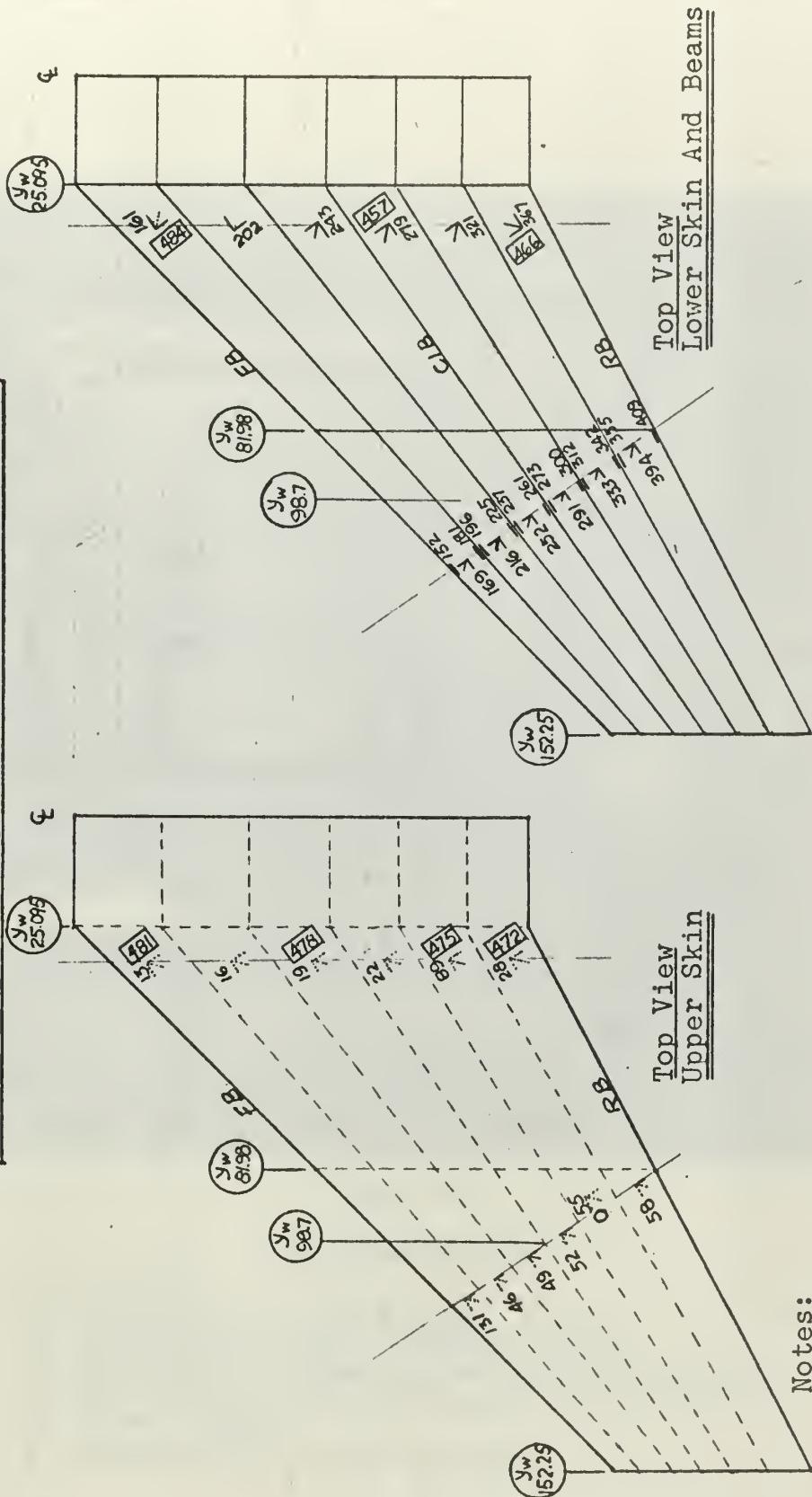
Notes:
1. All numbers are rosette numbers.
2. Except for web rosettes, number
   orientation is that of the gage.
3. Dotted gages indicate opposite surface.
4. Boxed numbers indicate back-up
   rosette number.
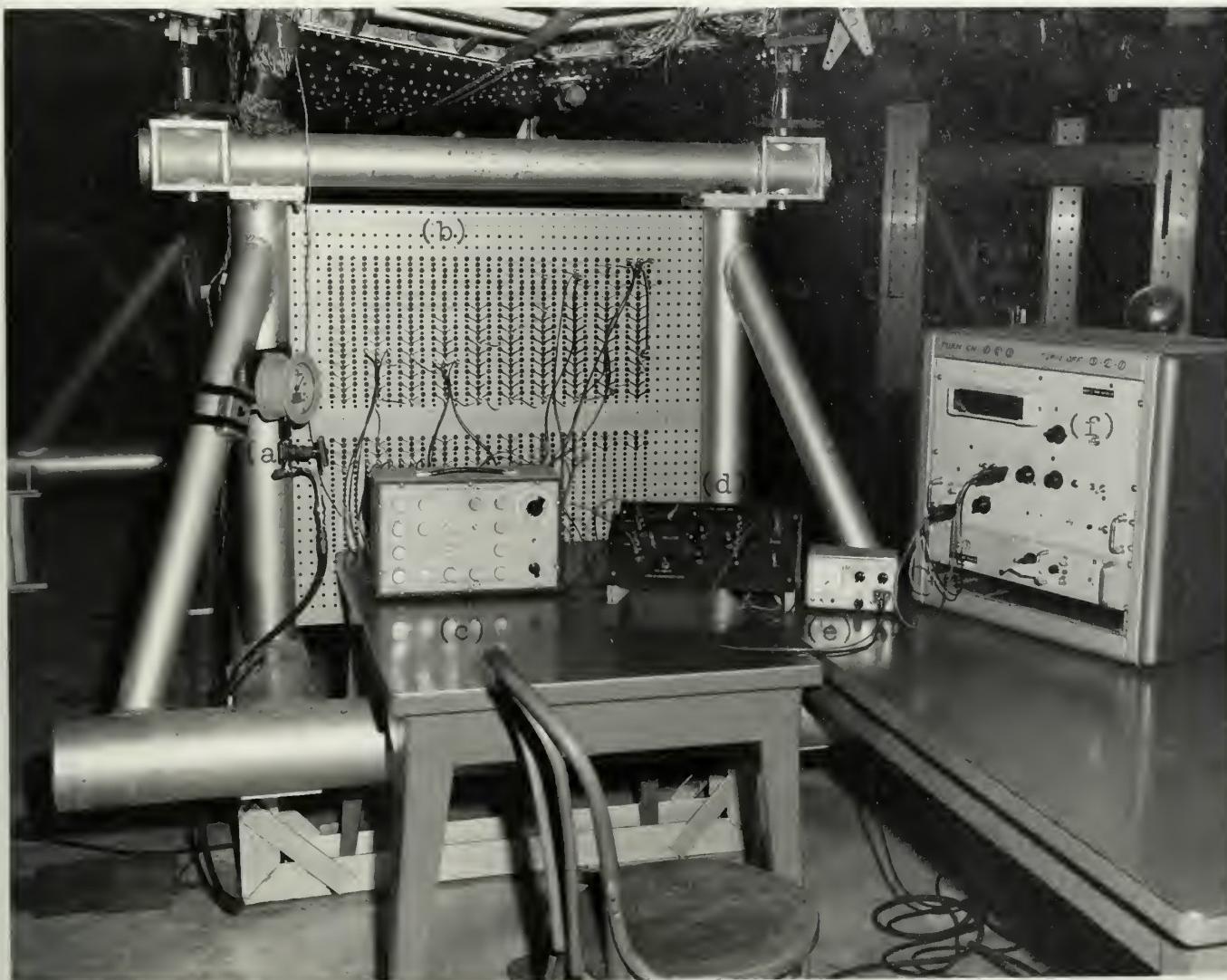
Fig. 24

Instrumentation

a. Hydraulic Pressure Gage
b. Strain Gage Lead Junction Panel
c. 20 Channel Switching and Balancing Unit
d. Wheatstone Bridge Circuit
e. Power Supply
f. Electronic Counter Assembly

90

Fig. 25

EXPERIMENTAL AND THEORETICAL SHEAR FLOWS
AT CUT SECTION PERPENDICULAR TO C.I.B. AT $y_w = 98.7$

EXPERIMENTAL RESULTS.
8000 lb Test (T = 323785 in. lb)
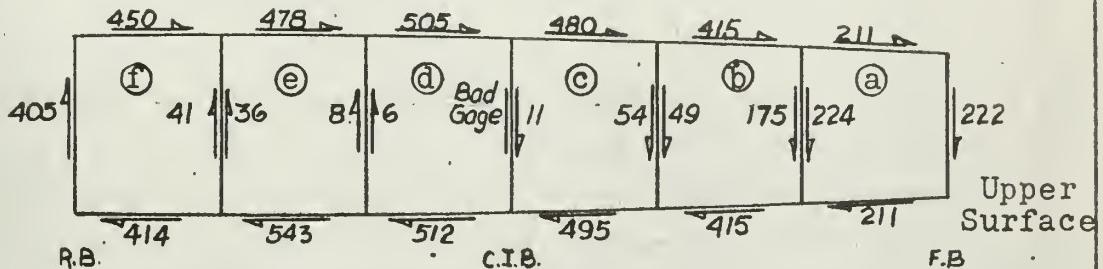
Direct Results From Rosette Readings.
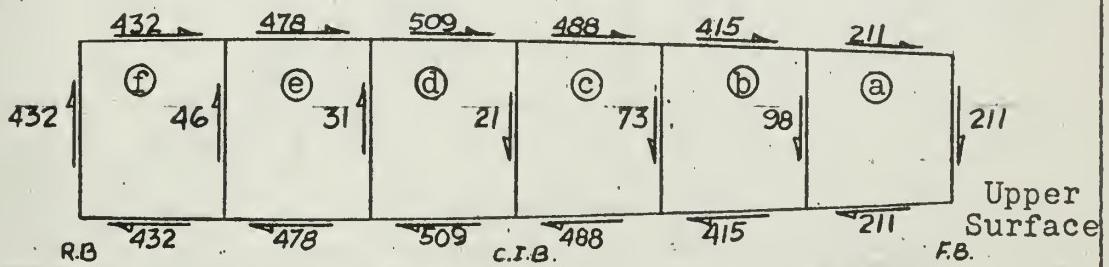
Final Results After Averaging Skin Values.

THEORETICAL RESULTS
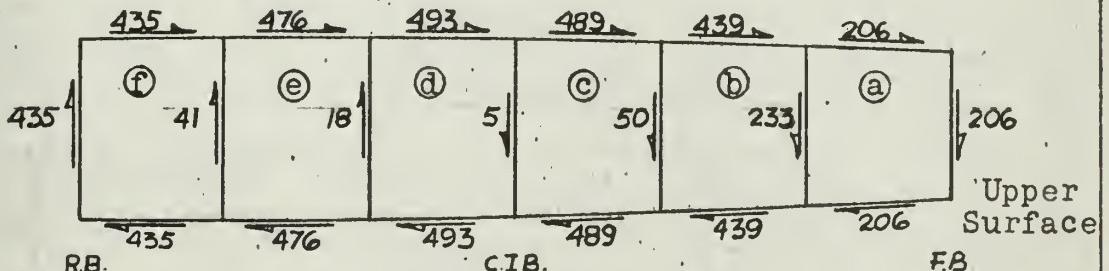
T = 323785 in. lb
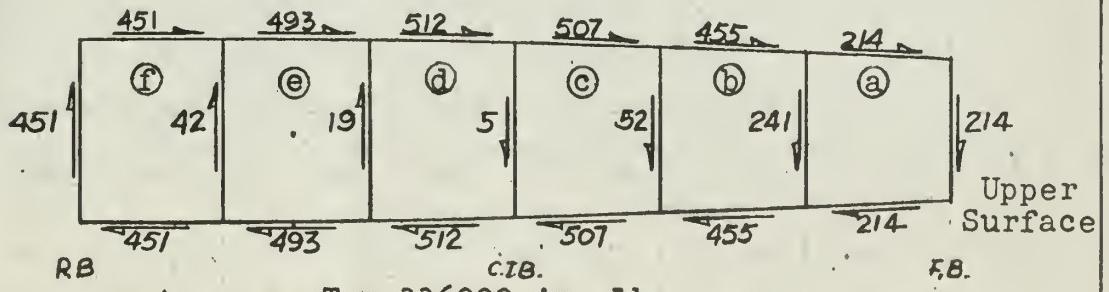
T = 336000 in. lb

Fig. 26

FRONT AND REAR BEAM DEFLECTIONS

Left Wing, Mounted Inverted
8000 lb Test (T = 323785 in. lb)

92
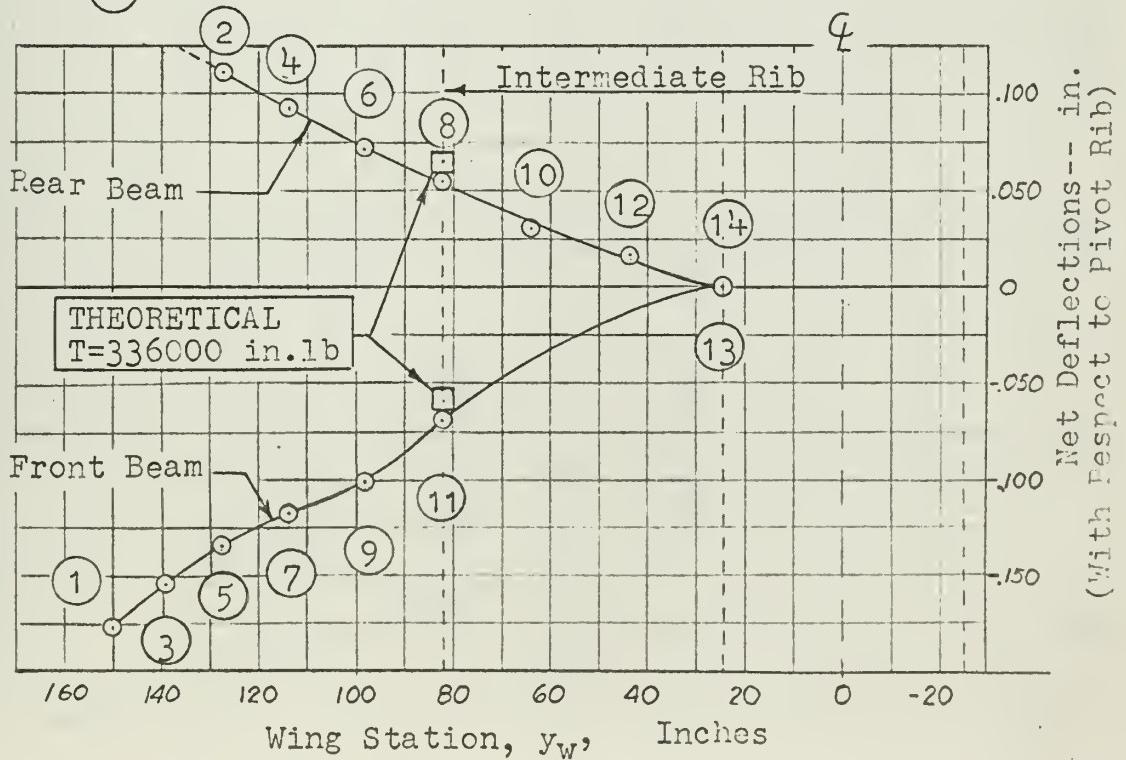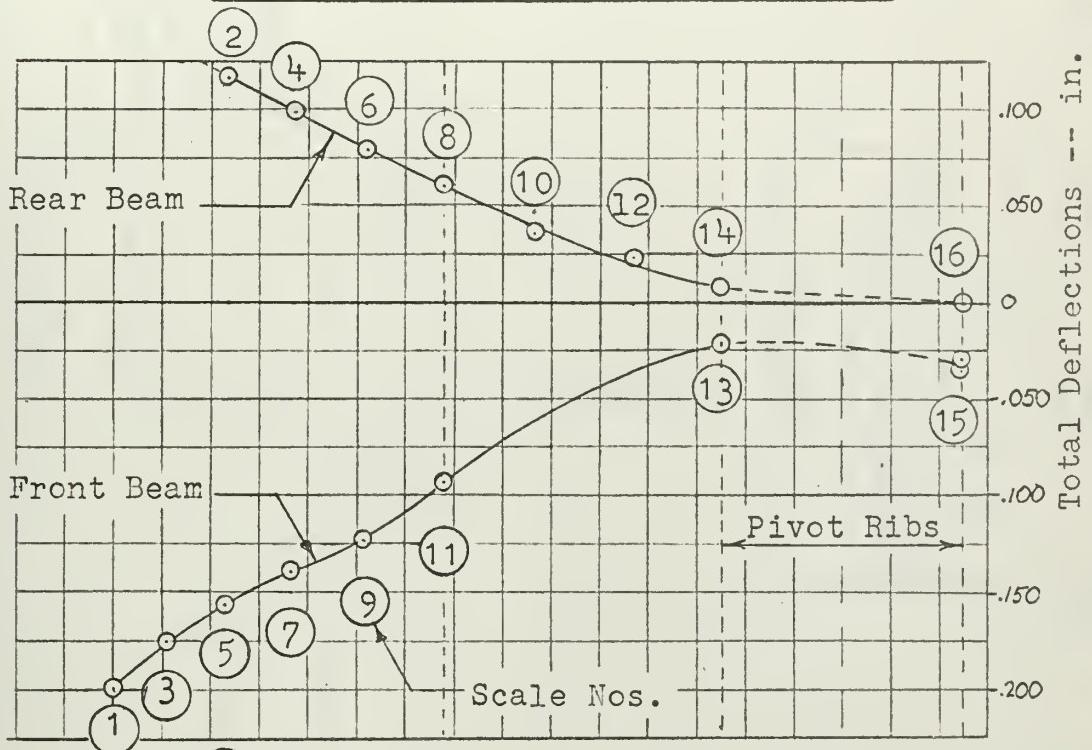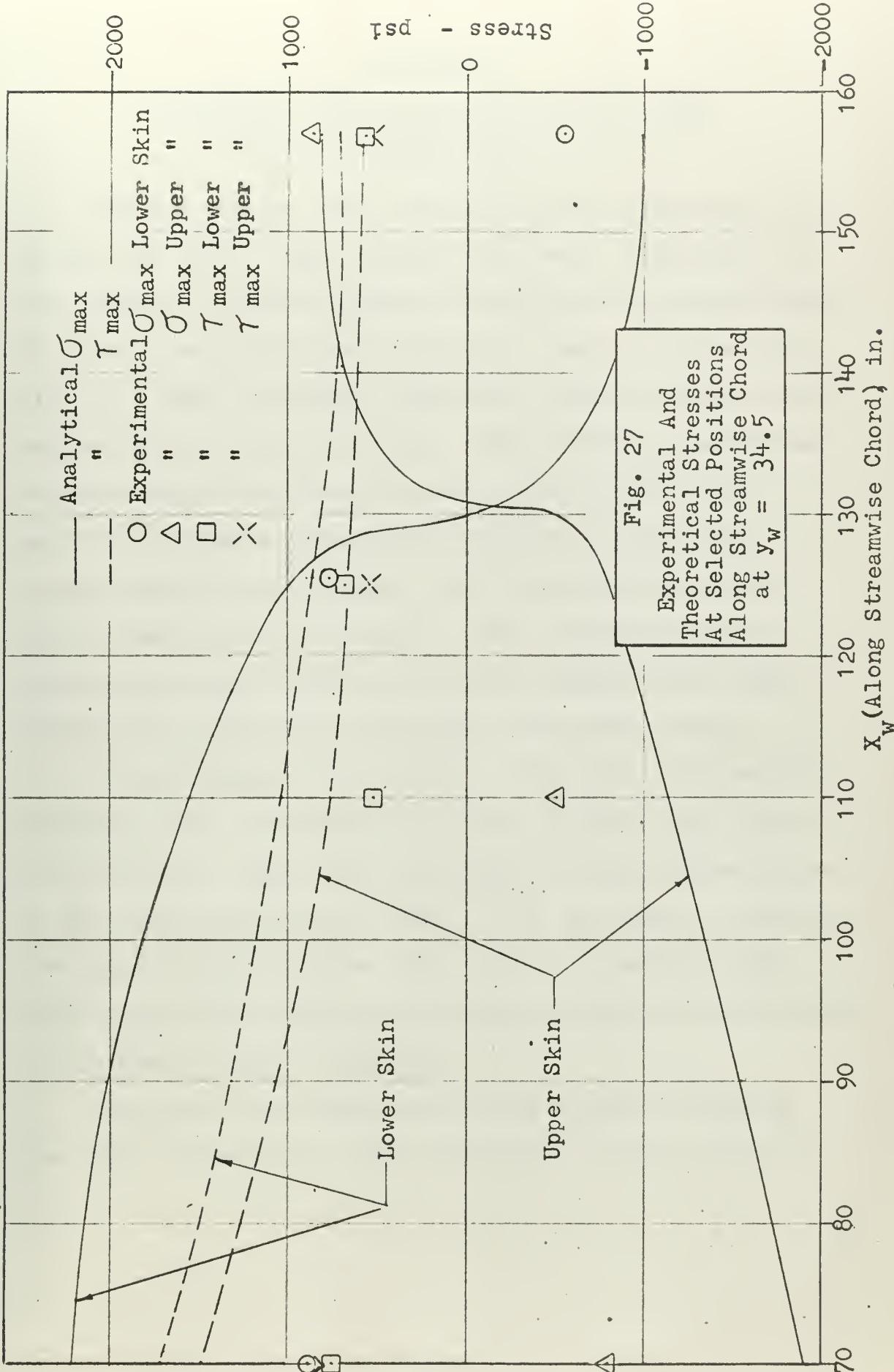
Fig. 27
Experimental And
Theoretical Stresses
At Selected Positions
Along Streamwise Chord
at $y_w = 34.5$

Legend:

	Analytical	σ_{max}
	"	τ_{max}
○	Experimental	σ_{max} Lower Skin
△	"	σ_{max} Upper "
□	"	τ_{max} Lower "
✕	"	τ_{max} Upper "

Stress - psi

2000
1000
0
-1000
-2000

X_w (Along Streamwise Chord) in.

160 150 140 130 120 110 100 90 80 70

Lower Skin

Upper Skin

APPENDIX A

THEORETICAL DETERMINATION OF SHEAR FLOWS AT SECTIONS PERPENDICULAR TO CIB AT $y_w = 98.7$ AND $y_w = 74.3$

The theoretical shear flows at sections perpendicular to the CIB at $y_w = 98.7$ and $y_w = 74.3$ were calculated for two reasons. First the shear flows at both sections would be used to establish the theoretical loads at streamwise rib, $y_w = 81.98$. Secondly, the shear flows at the section perpendicular to the CIB at $y_w = 98.7$ would be determined experimentally and comparison with theoretical values would facilitate a check of the degree to which pure torque loading was achieved. Both cross-sections are shown schematically in Fig. A1. The thicknesses were average mid-panel values and the web heights were taken between the mid-panel of the upper and lower skins.

A box structure with several cells will have one less redundant than the number of cells. In this case there is five redundant webs. It is desired to write six equations in the six unknown shear flows. This was done by equating the angle of twist of one cell with the remaining five, which gives five equations, and then writing an equilibrium of torsional moments equation.

The first five equations were obtained by equating the angle of twist per unit length, θ, of one cell with

the other five using the well known expression for a
box beam,

$$Q = \sum \frac{q \, \Delta s \, L}{2 \, A \, t \, G} \tag{A1}$$

The equilibrium of torsional moments may be written
as

$$T = \sum 2 \, A_n \, q_n \tag{A2}$$

In using equation (A2) the summation is carried out
around the entire perimeter of each cell. The unit length
L and the constant factor 2G drop out leaving, for cells
a and b,

$$\sum_a \frac{q \, \Delta s}{A_a \, t} = \sum_b \frac{q \, \Delta s}{A_b \, t} \tag{A3}$$

The value of q for any exterior web of cell a is q_{at} and
for the interior web is $(q_{at} - q_{bt})$. Using the
abbreviations,

$$\delta_{aa} = \sum_a \frac{\Delta s}{t}$$

$$\delta_{bb} = \sum_b \frac{\Delta s}{t}$$

$$\delta_{ab} = \left[\frac{\Delta s}{t} \right]_{a--b}$$

95

equation A3 is rewritten.

$$\frac{q_{at}}{A_a} \delta_{aa} - \frac{q_{bt}}{A_a} \delta_{ab} = \frac{q_{bt}}{A_b} \delta_{bb} - \frac{q_{at}}{A_b} \delta_{ab} \qquad (A4)$$

The terms δ_{aa} and δ_{bb} represent summation around the entire perimeter of their respective cells and δ_{ab} the value for the interior web.

For each cell the values of δ were easily calculated and are shown in Table A1. The enclosed areas were taken as the average web height times the distance between webs.

Equating the angle of twist per unit length of cell a to the remaining cells gives the following equations:

$$\frac{1}{A_a} \left(q_{at} \delta_{aa} - q_{bt} \delta_{ab} \right)$$

$$= \frac{1}{A_b} \left(q_{bt} \delta_{bb} - q_{at} \delta_{ab} - q_{ct} \delta_{bc} \right)$$

$$= \frac{1}{A_c} \left(q_{ct} \delta_{cc} - q_{bc} \delta_{bc} - q_{dt} \delta_{cd} \right)$$

$$= \frac{1}{A_d} \left(q_{dt} \delta_{dd} - q_{ct} \delta_{cd} - q_{et} \delta_{de} \right) \qquad (A5)$$

$$= \frac{1}{A_e} \left(q_{et} \delta_{ee} - q_{dt} \delta_{de} - q_{ft} \delta_{ef} \right)$$

$$= \frac{1}{A_f} \left(q_{ft} \delta_{ff} - q_{et} \delta_{ef} \right)$$

Substituting values of δ from Table A1, performing the indicated arithmetic and rearranging, one gets five equations in terms of the six shear flows with constant coefficients.

These are shown in Table A2 for both sections. The sixth equation is also shown in Table A2, in which case the coefficients are simply two times the cell areas.

The solution to these six simultaneous equations was obtained on the CDC 1604 Digital Computer using a FORTRAN program with a CO-OP identification of F2 UTEX LINE QN which is included herein as pages 102 through 110. It utilizes Gauss's method of elimination with row pivoting and back substitution and is designed to give solutions for one or more column vectors forming the right side of the set of equations. This means it would give solutions for one or more values of applied torque in this case. Three torque values were used as shown in Table A3. The values of 294000 in. lb and 336000 in. lb were used in the analysis. The value of 177825 in. lb was used to check the computer results. The check values of q were hand calculated using a iterative procedure suggested by Bruhn (Ref. 11) and within slide rule accuracy agree well with the computer solutions.

Fig. A1

SCHEMATIC DRAWING OF SECTIÔNS
PERPENDICULAR TO THE C.I.B.
AT y_w = 98.7 AND 74.3

y_w = 98.7

98
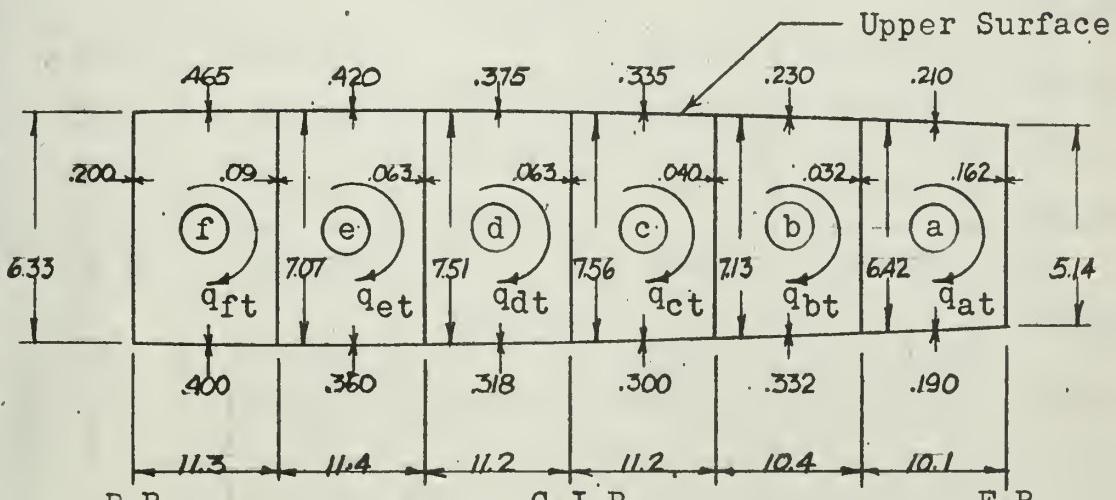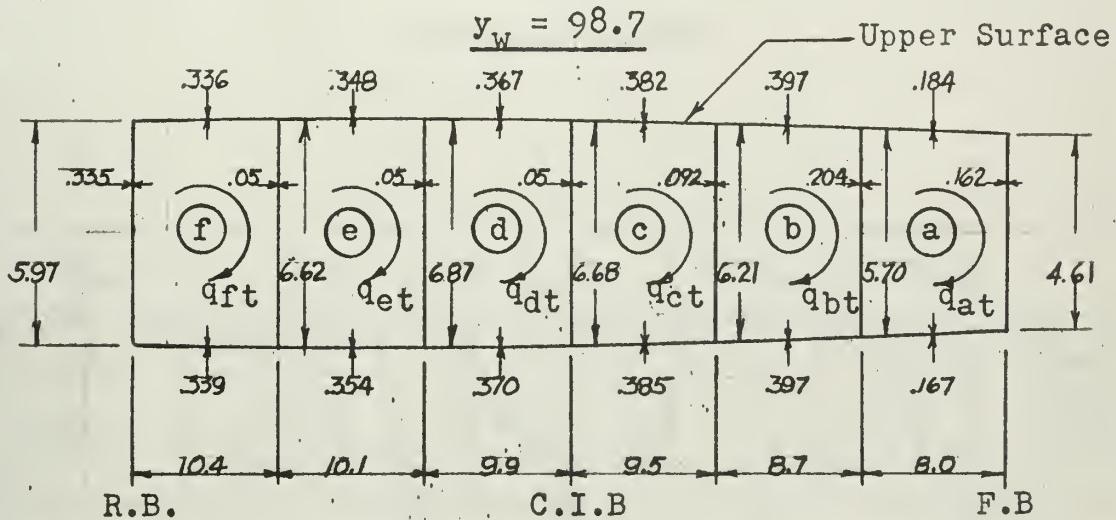
TABLE AI

SECTION PROPERTIES

	Section $y_w = 98.7$			Section $y_w = 74.3$		
Cell No.	Area in^2	$\delta_{nn}= \sum\limits_{j=1}^{4}\dfrac{\Delta s_j}{t_j}$	$\delta_{mn}= \left(\dfrac{\Delta s_j}{t_j}\right)$	Area in^2	$\delta_{nn}= \sum\limits_{j=1}^{4}\dfrac{\Delta s_j}{t_j}$	$\delta_{mn}= \left(\dfrac{\Delta s_j}{t_j}\right)$
a	43.1	147.804		58.38	333.606	
			27.940			200.625
b	.52.9	139.371		70.46	455.417	
			67.600			178.250
c	63.8	250.743		82.26	369.016	
			133.60			120.000
d	70.0	324.737		84.39	304.293	
			137.40			119.206
e	71.70	327.360		83.11	256.572	
			132.40			78.556
f	69.0	211.850		75.11	162.757	

TABLE AII

COEFFICIENTS FOR SIMULTANEOUS EQUATIONS IN UNKNOWN SHEAR FLOWS.

FOR SECTIONS PERPENDICULAR TO CIB AT $y_w = 98.7$ AND $y_w = 74.3$

Source of Equation	q_{at} +	q_{bt} +	q_{ct} +	q_{dt} +	q_{et} +	q_{ft}	= column vector
$y_w = 98.7$							
$\theta_a = \theta_b$	-3.957493	+3.282872	-1.277883	0.0	0.0	0.0	0.0
$\theta_a = \theta_c$	-3.429327	- .411301	+3.930141	-2.094044	0.0	0.0	0.0
$\theta_a = \theta_d$	-3.429327	+ .648260	-1.908571	+4.639100	-1.962857	0.0	0.0
$\theta_a = \theta_e$	-3.429327	.648260	0.0	-1.916318	+4.565690	-1.846583	0.0
$\theta_a = \theta_f$	-3.429327	.648260	0.0	0.0	-1.918841	+3.070290	0.0
$T = \sum 2Aq$	86.2	105.8	127.6	140.0	143.40	138.0	T
$y_w = 74.3$							
$\theta_a = \theta_b$	-8.561748	+9.900019	-2.529804	0.0	0.0	0.0	0.0
$\theta_a = \theta_c$	-5.714388	1.269626	+4.485971	-1.458789	0.0	0.0	0.0
$\theta_a = \theta_d$	-5.714388	3.436536	-1.421969	+3.605795	-1.412561	0.0	0.0
$\theta_a = \theta_e$	-5.714388	3.436536	0.0	-1.434316	3.087138	- .945205	0.0
$\theta_a = \theta_f$	-5.714388	3.436536	0.0	0.0	-1.045879	+2.166915	0.0
$T = \sum 2Aq$	116.76	140.92	164.52	168.78	166.22	150.22	T

TABLE AIII

SHEAR FLOW RESULTS FOR VARIOUS TORQUES

AT SECTIONS PERPENDICULAR TO CIB AT

$$y_w = 98.7 \text{ AND } y_w = 74.3$$

Cell	Shear Flows (lb/in.)			
	Hand Calculated	Computer Results		
	T=177,825 in. lb	T=177,825 in. lb	T=294,000 in. lb	T=336,000 in. lb
$y_w = 74.3$				
a	134.28	135.289	223.675	255.628
b	166.09	167.416	276.790	316.332
c	196.21	197.292	326.185	372.782
d	222.05	222.450	367.779	420.319
e	229.65	229.231	378.990	433.132
f	203.48	201.905	333.811	381.500
$y_w = 98.7$				
a			187.202	213.945
b			398.384	455.296
c			443.699	507.084
d			447.921	511.910
e			431.719	493.392
f			394.789	451.188

A. IDENTIFICATION

   TITLE: Solution of Simultaneous Linear Algebraic Equations

   CO-OP ID: F2 UTEX LINEQN

   CATEGORY: Simultaneous Linear Equations

   PROGRAMMER: C. B. Bailey

   DATE: August 14, 1961

B. PURPOSE

   Solve one or more sets of linear algebraic equations using Gaussian elimination with row pivoting and back substitution.

C. USAGE

   1. Calling sequence:

       The program is called by the program execute card, i.e. LINEQN., in the normal sequence of Fortran control cards.

   2. Arguments:

       The following parameters and data are read in on cards. (See 9a).

       a. N - the order of the matrix in the equations $Ax = b$, that is, the number of linear equations.

       b. M - the number of vectors b for which solution vectors x are to be obtained, that is, the number of sets of linear equations.

       c. EP - Matrix condition parameter. (See Mathematical Method.)

       d. A - the elements of the matrix of coefficients of the equations.

       e. B - the elements of the column vectors b_1, b_2, ..., b_m.

   3. Space required: Undetermined.

   4. Temporary storage required: Space is reserved for solving 50 equations in 50 unknowns for 60 vectors b. This amounts to 8500 locations.

   5. Alarms or print-outs: If the equations are inconsistent or dependent, MATRIX SINGULAR is printed.

   6. Error returns: None.

   7. Error stops: None.

   8. Input and output tape mounting: Not applicable.

   9. Input and output formats: For a more complete description of the I, E, and F formats, see 15.

a. Input (data cards)

(1) First card

Columns 1-5   contain the value of N in I5 format. Thus N is
                is punched a right-justified fixed-point integer.
                Leading zeros need not be punched.

Columns 6-10   contain the value of M in I5 format.

Columns 11-20 contain the value of EP in E10.4 format.
                To enter the value of 10^{-8} one can punch
                .1E-07 right-justified in the field.

(2) The coefficients of the matrix are read a row at a time. Each
     row is begun on a new card. Five coefficients per card are in
     16 column fields (1-16, 17-32, 33-48, 49-54, 55-80) using F16.8
     format.

          The matrix of coefficients has the following form:

$$a_{11} \quad a_{12} \quad \cdots \quad a_{1N}$$

$$a_{21} \quad a_{22} \quad \cdots \quad a_{2N}$$

$$\vdots$$

$$a_{N1} \quad a_{N2} \quad \cdots \quad a_{NN}$$

     Thus, for N = 6, the input cards would contain the following
     information.

Columns

Card No.	1-16	17-32	33-48	49-54	55-80
2	a_{11}	a_{12}	a_{13}	a_{14}	a_{15}
3	a_{16}				
4	a_{21}	a_{22}	a_{23}	a_{24}	a_{25}
5	a_{26}				
6	a_{31}	a_{32}	a_{33}	a_{34}	a_{35}
7	a_{36}				
$\vdots$					
12	a_{61}	a_{62}	a_{63}	a_{64}	a_{65}
13	a_{66}				

F2 UTEX LINEQN - 2

(3) The elements of the column vectors b_1, b_2, ..., b_m are also read row wise in F 16.8 format. For M = 6, the vectors b_1, b_2, ..., b_6 are assumed to be arranged in the following manner:

$$
\begin{matrix}
b_{11} & b_{21} & \cdots & b_{61} \\
b_{12} & b_{22} & \cdots & b_{62} \\
 & & \vdots & \\
b_{16} & b_{26} & \cdots & b_{66}
\end{matrix}
$$

where b_{ij} denotes the j-th component of the column vector b_i. Thus, for N = 6 and M = 6, the data cards would contain the following information:

			Columns		
Card No.	1-16	17-32	33-48	49-54	55-80
14	b_{11}	b_{21}	b_{31}	b_{41}	b_{51}
15	b_{61}				
16	b_{12}	b_{22}	b_{32}	b_{42}	b_{52}
17	b_{62}				
.					
.					
.					
24	b_{16}	b_{26}	b_{36}	b_{46}	b_{56}
25	b_{66}				

(4) Several sets of data may be processed at one run. To terminate the run, place one blank card after the last set of data.

b. Output

The components of the x vectors are printed row wise six per line in E20.11 format. For the above example of N = 6 and M = 6, the output values would be arranged in the following manner:

Line No.	Values					
1	x_{11}	x_{21}	x_{31}	x_{41}	x_{51}	x_{61}
2	x_{12}	x_{22}	x_{32}	x_{42}	x_{52}	x_{62}
.						
..						
.						
6	x_{16}	x_{26}	x_{36}	x_{46}	z_{56}	x_{66}

where x_{ij} denotes the j-th component of the column vector x_i.

10. Selective jump and stop settings: Not applicable.

11. Timing: Undetermined.

12. Accuracy: Not applicable.

13. Cautions to user: None.

14. Equipment configuration: Not applicable.

15. References:

(a) Fortran System for the Control Data 1604 Computer, Control Data Corporation, Computer Division Publication 087A, Minneapolis, Minnesota (1961).

(b) Fortran Automatic Coding System for the IBM Data Processing System, International Business Machines Corporation (1958).

(c) Fortran II for the IBM 704 Data Processing System, International Business Machines Corporation (1958).

(d) Kunz, K. S., Numerical Analysis, McGraw-Hill Book Co., Inc., New York, 1957.

(e) Fadeeva, V. N., Computational Methods of Linear Algebra, translated by Curtis D. Benster, Dover Publications, Inc., New York, 1959.

D. MATHEMATICAL METHOD

Gauss's method of elimination with row pivoting and back substitution is used.

Suppose we wish to solve

$$Ax = b \quad \text{and} \quad Ax = c$$

for the same matrix A. This routine is designed to give the solutions for one or more column vectors b, c, etc. simultaneously.

Consider a 3 by 3 matrix A augmented by two column vectors b
and c.

$$
\begin{array}{ccccc}
a_{11} & a_{12} & a_{13} & b_1 & c_1 \\
a_{21} & a_{22} & a_{23} & b_2 & c_2 \\
a_{31} & a_{32} & a_{33} & b_3 & c_3
\end{array}
$$

The A matrix is triangularized by adding multiples of one row to another
row. For column 1 find the row containing the largest element in column 1
on or below the principal diagonal. Interchange this row with the first row.
Subtract from row i (i = 2, 3) $\dfrac{a_{i1}}{a_{11}}$ times row 1.

$$
a'_{ij} = a_{ij} - \frac{a_{i1}}{a_{11}} a_{1j} \qquad j = 1, \ldots, 5.
$$

This eliminates the elements in column 1 below the principal diagonal.
This process of pivoting and then eliminating elements below the diagonal
may be repeated now on the second and third rows. The method is ex-
tendible to any number of equations.

Although only the A matrix is triangularized, the process of row
interchange and addition of multiples of rows is applied to the n by n+m
matrix consisting of the n by n coefficient matrix augmented by m
column vectors.

Thus we have

$$
\begin{array}{ccccc}
d_{11} & d_{12} & d_{13} & e_{11} & e_{12} \\
0 & d_{22} & d_{23} & e_{21} & e_{22} \\
0 & 0 & d_{33} & e_{31} & e_{32}
\end{array}
$$

Back substitution is used.

$$
x_{i,j} = \frac{e_{ij} - S}{d_{ii}} \qquad \begin{array}{l} j = 1, \ldots, M \\ i = N, \ldots, 1 \end{array}
$$

where

$$
S = 0 \quad \text{for } i = N
$$

and

$$
S = \sum_{k=i+1}^{N} d_{ik} x_{kj} \qquad \text{for } i = N-1, \ldots, 1.
$$

The back substitution is also extendible to any order matrix.

If the equations are either inconsistent or dependent (or nearly so), then some diagonal element of the triangularized matrix will be zero or nearly zero. In this case exponential overflow or even division by zero may occur in the back substitution phase. The alarm print-out (see C.5) is set off when a diagonal element of the triangularized matrix is less than or equal to argument EP (see C.2.c). Thus, EP is that value which the user is willing to call zero. It should be larger than the round-off error which can occur.

SIMULTANEOUS LINEAR ALGEBRAIC EQUATIONS

START

L = 1

Is L < N ? — Yes → α — Find KP such that $|A(KP, L)|$ is greatest for $L \leq KP \leq N$ → β

No → δ

PIVOTING

β → Is KP > L ? — Yes → Interchange rows KP and L of A for columns L to N+M

No

CHECK FOR SINGULAR MATRIX

Is $|A(L, L)| < EP$? — Yes → ζ

No → γ

ELIMINATE ONE ELEMENT

γ → Is L < N ? → δ

K = L + l → Is A(K, L) = 0? → K

No: Replace A(K, J) with
$A(K, J) - \dfrac{A(K, L)}{A(L, L)} A(L, J)$
J = L+l, ---, N+M

ε

K → Is K < N ? — Yes → K+1 → K → ε

No → Is L < N ? — Yes → L+l → L → α

No → δ

F2 UTEX LINEQN - 7

BACK SUBSTITUTION

SOLVE FOR
ONE UNKNOWN

$$X(K, J) = \frac{A(K, J+N) - S}{A(I, I)}$$

$$S = \sum_{K=I+1}^{N} A(I, K) \, X(K, J)$$

Is I = N ?

No / Yes

Is J < M ? No / Yes

J+1 → J

Is K > 1 ? No / Yes

I-1 → I

Clear error flag

Set error flag

END

F2 UTEX LINEQN - 8

```
       PROGRAM LINEQN
       DIMENSION A(50,110),X(50,60)
   1   READ 101,N,M,EP
 101   FORMAT(2I5,E10.4)
       IF(N)99,99,10
  10   PRINT 105
 105   FORMAT(15H1PROGRAM LINEQN5X20HGAUSSIAN ELIMINATION//)
       NPM = N+M
       NPO = N+1
       DO 2 K=1,N
   2   READ 102,(A(K,J),J=1,N)
       DO 3 K=1,N
   3   READ 102,(A(K,J),J=NPO,NPM)
 102   FORMAT(5F16.8)
       CALL GAUSS2(N,M,EP,A,X,K1)
       GO TO (60,50),K1
  60   DO 61 K=1,N
  61   PRINT 104,(X(K,J),J=1,M)
       GO TO 1
 104   FORMAT(/(6E20.11))
  50   PRINT 103
 103   FORMAT(16H MATRIX SINGULAR)
       GO TO 1
  99   STOP
       END
       SUBROUTINE   GAUSS2(N,M,EP,A,X,KER)
       DIMENSION A(50,110),X(50,60)
       NPM=N+M
  10   DO 34 L=1,N
       KP=0
       Z=0.0
       DO 12 K=L,N
       IF(Z-ABSF(A(K,L)))11,12,12
  11   Z=ABSF(A(K,L))
       KP=K
  12   CONTINUE
       IF(L-KP)13,20,20
  13   DO 14 J=L,NPM
       Z=A(L,J)
       A(L,J)=A(KP,J)
  14   A(KP,J)=Z
  20   IF(ABSF(A(L,L))-EP)50,50,30
  30   IF(L-N)31,40,40
  31   LP1=L+1
       DO 34 K=LP1,N
       IF(A(K,L))32,34,32
  32   RATIO=A(K,L)/A(L,L)
       DO 33 J=LP1,NPM
  33   A(K,J)=A(K,J)-RATIO*A(L,J)
  34   CONTINUE
  40   DO 43 I=1,N
       II=N+1-I
       DO 43 J=1,M
       JPN=J+N
       S=0.0
       IF(II-N)41,43,43
  41   IIP1=II+1
       DO 42 K=IIP1,N
  42   S=S+A(II,K)*X(K,J)
  43   X(II,J)=(A(II,JPN)-S)/A(II,II)
       KER=1
       RETURN
  50   KER = 2
       END
       END
```

110

APPENDIX B

DETERMINATION OF INDIVIDUAL MEMBER FLEXIBILITIES REQUIRED FOR MATRIX $[F]$

I.   Development of Equations

The symmetric matrix $[F]$ of equation (2) is obtained by formulating the strain energy in terms of internal forces.   For example, the un-tapered bar ($A_1 = A_2$) of Fig. B1 is attached to a web, and acted upon by an external axial load, P, and an internal axial load, a_3.
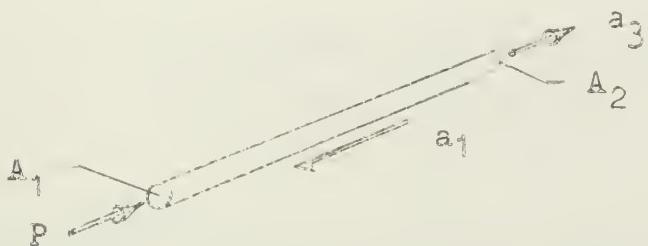
Fig. B1

The strain energy of such a bar may be expressed (Ref. 8) in terms of the end loads as

$$U = \int_{0}^{\ell} \frac{p(y)^2}{2AE} \, dy \qquad (B1a)$$

For a load equal to

$$p(y) \;=\; u \;+\; (v - u)\,\frac{y}{\ell}$$

the strain energy becomes

$$U \;=\; \frac{\ell}{3AE}\,(\,u^2 + uv + v^2\,) \qquad \text{(B1b)}$$

Upon placing the bar of Fig. B1 in equilibrium the end loads may be expressed in terms of the internal forces as

$$u \;=\; -2\,a_1 \;+\; a_3 \qquad\qquad \text{(B2a)}$$

$$v \;=\; 0\,a_1 \;+\; a_3 \qquad\qquad \text{(B2b)}$$

By substituting equations (B2) into (B1) the internal strain energy can be written as

$$2\,EU \;=\; \frac{\ell}{3A}\,(\,4\ell^2 a_1{}^2 \;-\; 6\,\ell a_1 a_3 \;+\; 3a_3{}^2\,) \qquad \text{(B3)}$$

Now referring again to equation (2),

$$2\,EU \;=\; \left| a_1 \ldots a_3 \right| \begin{bmatrix} F_{11} & F_{13} \\ F_{31} & F_{33} \end{bmatrix} \{ a_1 \ldots a_3 \} \qquad \text{(2)}$$

112

it can be shown by taking partial derivative of the energy that the $[F]$ matrix terms are merely coefficients of squared and cross terms such as:

$$2 \ EU \ = \ a_1^2 \ F_{11} + F_{13} \ a_1 a_3 + F_{31} a_1 a_3 + a_3^2 F_{33} \qquad (2a)$$

Due to the symmetry required of $[F]$, F_{13} is exactly one-half the coefficient of the cross-term, $a_1 a_3$.

Three factors, f_{11}, f_{12}, and f_{22} are now introduced,

$$\left. \begin{aligned} f_{11} &= \frac{\ell}{3A_1} = f_{22} \\ f_{12} &= \frac{\ell}{6A_1} \end{aligned} \right\} \qquad (B4)$$

where f_{11} and f_{22} will refer to the squared terms, and f_{12} refers to the cross-terms.

The coefficients of a_1 and a_3 in equations (B2) are now identified by

$$\begin{aligned} u &= \alpha_1 a_1 + \alpha_3 a_3 \\ v &= \beta_1 a_1 + \beta_3 a_3 \end{aligned} \qquad (B5)$$

so that the member flexibilities can be found from

$$F_{11} = f_{11}\alpha_1^2 + 2f_{12}\alpha_1\beta_1 + f_{22}\beta_1^2$$

$$F_{33} = f_{11}\alpha_3^2 + 2f_{12}\alpha_3\beta_3 + f_{22}\beta_3^2 \qquad\qquad (B6)$$

$$F_{13} = f_{11}\alpha_1\alpha_3 + f_{22}\beta_1\beta_3 + f_{12}(\beta_1\alpha_3 + \alpha_1\beta_3)$$

Using the values of   and   from equations (B2)

$$F_{11} = \frac{4\ell^3}{3A}$$

$$F_{13} = -\frac{\ell^2}{A} = F_{31}$$

$$F_{33} = \frac{\ell}{3A}$$

II. Application to Tapered Bars

For linearly tapered bars the coefficients f_{11}, f_{12}, and f_{22} were modified by the functions of A_1/A_2, $\emptyset_{11}$, $\emptyset_{12}$, and $\emptyset_{22}$, according to the method shown in Ref. 4, giving:

$$f'_{11} = f_{11}\,\emptyset_{11}$$

$$f'_{12} = f_{12}\,\emptyset_{12} \qquad\qquad (B7)$$

$$f'_{22} = f_{22}\,\emptyset_{22}$$

Equations (B7) are then used directly in equations (B6).

Consider the tapered bar shown as element number 29 in Fig. 13, and re-drawn below in Fig. B2. The bar

$\ell = 64.9038$

q_2

$A_2 = 8.36$ in.^{2}

q_1

$A_1 = 3.87$ in.^{2}

$$\frac{A_1}{A_2} = .463$$
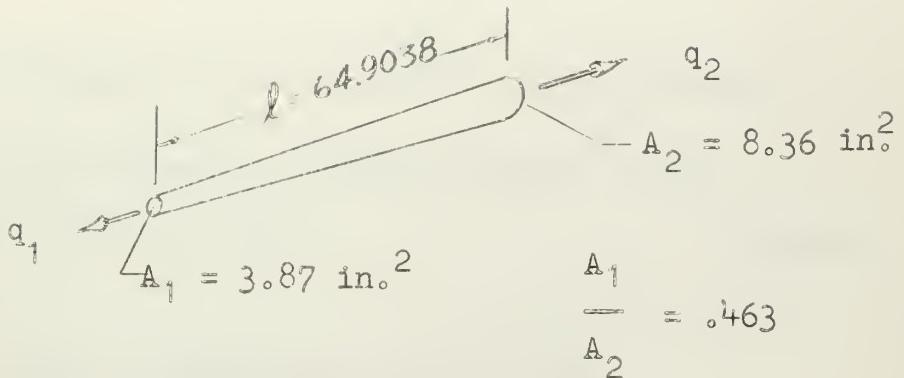
Fig. B2

geometry is obtained from Table I. Using the ratio A_1/A_2, the ϕ functions are obtained from Fig. 4 of Ref. 4, giving

$$f_{11} = \frac{\ell\phi_{11}}{3A_1} = 4.4387$$

$$f_{12} = \frac{\ell\phi_{12}}{6A_1} = 1.8001$$

$$f_{22} = \frac{\ell\phi_{22}}{3A_1} = 3.0188$$

From the loading system upon the bar, as shown in Fig. 13, the alpha (α) and beta (β) equations are respectively:

$$q_1 = -4.7055\, a_{13} + 4.1502\, a_{14} + 7.8009\, a_{38} - a_{49}$$

$$q_2 = - .4483 \ a_{13} - .4286 \ a_{14} + 0 - a_{49}$$

Substituting into equation (B6), $F_{13,13}$ becomes

$$F_{13,13} = 4.4387(-4.7055)^2 + 1.8001(-4.7055)(-.4483)$$
$$+ (3.0188)(-.4483)^2 = \underline{102.6485}$$

III. Application to Symmetrical Shear Panel

For the case of the symmetrical shear panel, shown in Fig. B3, the strain energy can be written as in equation (B8):
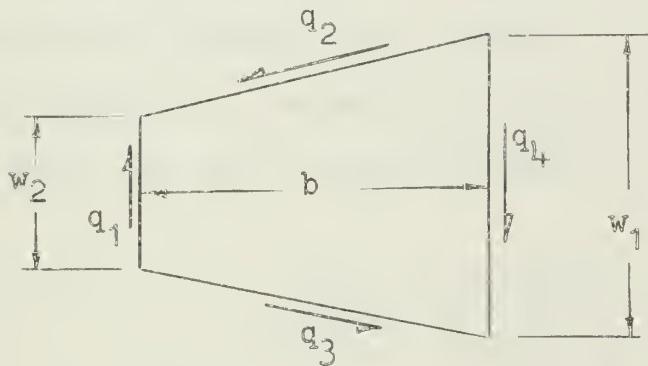
Fig. B3

Symmetrical Shear Panel

116

$$2EU = \left[\frac{b(w_1 + w_2)}{w_1^2 t} \left(1/6(\frac{w_1 - w_2}{b^2})^2 + (1 + \mu) \right) \right] q_1^2 \quad (B8)$$

and
$$F_{11} = \frac{\partial^2 U}{\partial q_1^2} \qquad \qquad 9$$

giving for element number 13, Fig. 13:

$$F_{8,8} = 1/tE \left[\frac{63.8339(13.50)}{51.84} \left(1/6(\frac{.900}{63.8339})^2 + 1.32 \right) \right] 1.0^2$$

or:
$$E \left[F_{8,8} \right] = E(109.7173)$$

IV. Application to Skewed Shear Panels

Skewed panels are treated according to the method of Garvey (Ref. 10), and as used in Ref. 6.
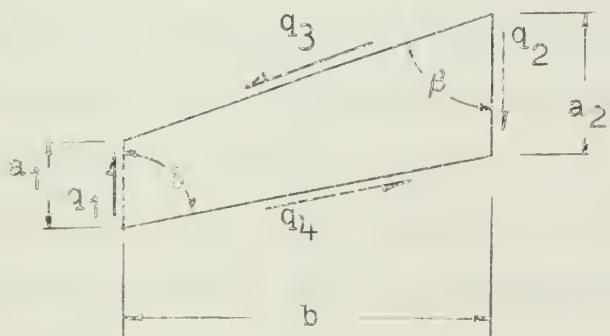
Fig. B4

The energy of the swept panel shown in Fig. B4 may be written as

$$2\ EU = \left[\frac{(1+\ )(a_1 + a_2)}{\ell\ t}\sin^2\delta\left(1 + \frac{2}{3(1+\ )}\delta\right)\right]q_4^2 \qquad (B9)$$

where gamma is written as

$$\delta = \cot^2\beta + \cot\delta\cot\beta + \cot^2\beta$$

Take for example element number 38. There is

$$F_{9,9} = \frac{\partial^2 U}{\partial q_4^2} \qquad \text{giving}$$

$$F_{9,9} = \left[\frac{1.32(35.2288)(.5764)(1 + .50505 \times 2.5108)}{9.9549}\right](3.5868)^2$$

$$F_{9,9} = \frac{1}{E}(78.5635)$$

It should be noted that for both the bars and the panels, the terms of the $[F]$ matrix are usually made up from flexibilities of several elements. In addition, all main diagonal terms (F_{ii}) are positive. All non-zero terms of the flexibility matrix $[F]$ are given in the computer program data input, Appendix C.

118

APPENDIX C

FORTRAN PROGRAM FOR CDC 1604
DIGITAL COMPUTER

1. FORTRAN NAMES, SYMBOLS, AND DEFINITIONS

A   Matrix of coefficients of determinate
loads, basic input data, size 33x33

AI   Inverse of Matrix A, obtained by Gauss
3 single-precision subroutine

AR   Matrix of redundant loads, output,
size 33x1

AT   Matrix of all loads, output, size 49x1

B   Matrix of coefficients of applied and
redundant loads, basic input, size 49x33

C   Matrix of deflection influence coefficients,
output, size 33x33

CJ   Matrix product of (AI)(B), size 33x49

EN   Negative of matrix product (H22I)(H21),
size 16x33

ENP   Matrix product of (H22I)(H21), size 16x33

G   (CJ) matrix augmented by trivial relations,
size 49x49

GT   Transpose of (G) matrix

H   Matrix triple product of (GT)(UC)(G), size
49x49

H11   Matrix of first 33 columns and rows of (H),
            obtained during partitioning, size 33x33

H12   Matrix of last 16 columns (through first
            33 rows) of (H) matrix, size 33x16

H21   Matrix of last 16 rows (through first 33
            columns) of (H) matrix, size 16x33

H22   Remainder of (H) matrix, size 16x16

H22I   Inverse of (H22) matrix

H12N   Matrix product of (H12)(EN), size 33x33

KER   Gauss 3 subroutine error flag, where
            assigned value of 2 indicates singular matrix

LIST   Numbering index

P   Column matrix of applied loads, size 33x1

S   Matrix of stress coefficients, size 49x33

UC   Matrix of flexibilities, referred to in
            text as (F) matrix, basic input data,
            size 49x49

UNITN   Matrix formed by placing unit diagonal
            matrix on top of matrix (EN), giving
            matrix size of 49x33

PROGRAM ENERGY

```
              ┌─────────┐
              │  Start  │
              └─────────┘
                   │
          ┌─────────────────┐
          │  Clear Arrays   │
          └─────────────────┘
                   │
      ┌───────────────────────────┐
      │ Form A, B, UC Matrices    │
      └───────────────────────────┘
                   │
          ┌─────────────────┐              ┌──────────┐
          │  Call Gauss 3   │              │  Return  │
          └─────────────────┘              └──────────┘
                   │                             │
              ╱────────╲                   ╭──────────────────╮
             ╱    ?     ╲─── Yes ──────────│      Print       │
             ╲ Ker = 2  ╱                  │ Matrix Singular  │
              ╲────────╱                   ╰──────────────────╯
                   │
                  No
                   │
          ┌───────────────────┐
          │ Invert A Matrix   │
          └───────────────────┘
                   │
  ╭──────────────╮ ┌───────────────────┐
  │  Write Out   │─│  Form AI Matrix   │
  │The AI Matrix │ └───────────────────┘
  ╰──────────────╯        │
          ┌───────────────────┐
          │   Call MATMPY     │
          └───────────────────┘
                   │
          ┌───────────────────┐
          │       Form        │
          │ CJ Matrix = A⁻¹B  │
          └───────────────────┘
                   │
  ┌─────────────────────────────────┐      ┌───┐
  │ Form G Matrix From CJ By        │─────▶│ 1 │
  │ Adding Trivial Relations        │      └───┘
  └─────────────────────────────────┘
                   │
  ╭──────────────╮ ○
  │  Write Out   │─│
  │ The G Matrix │
  ╰──────────────╯
                   │
          ┌───────────────────┐
          │   Transpose G     │
          └───────────────────┘
                   │
                   ○──────────┐ ┌──────────┐    ┌───┐
                   │          │ │  Form P  │───▶│ 2 │
                   │          │ └──────────┘    └───┘
          ┌──────────┐
          │  Form H  │
          └──────────┘
                   │
  ╭──────────────╮ ○               ╭──────────────────╮
  │  Write Out   │─│               │    Write Out     │
  │ The H Matrix │                 │ The H22 Matrix   │
  ╰──────────────╯                 ╰──────────────────╯
                   │                        │
  ┌──────────┐ ┌───────────────┐  ┌──────────┐
  │ Form H21 │─│ Partition H   │──│ Form H22 │
  └──────────┘ └───────────────┘  └──────────┘
       │        │           │           │
     ┌───┐  ┌─────────┐ ┌─────────┐   ┌───┐
     │ 3 │  │Form H11 │ │Form H12 │   │ 6 │
     └───┘  └─────────┘ └─────────┘   └───┘
                │           │
              ┌───┐       ┌───┐
              │ 4 │       │ 5 │
              └───┘       └───┘
```

```
   ( 3 )                                              ( 6 )
     │                                                  │
     │              ┌──────────┐           ┌─────────────────┐
     │              │  Return  │           │  Call Gauss 3   │
     │              └──────────┘           └─────────────────┘
     │                   ▲                          │
     │         ╭─────────────────────╮         ╱─────────╲
     │         │       Print         │ ◄─Yes──╱   Ker = 2? ╲
     │         │  Matrix Singular    │        ╲            ╱
     │         ╰─────────────────────╯         ╲─────────╱
     │                                              │
     │                                             No
     │                                              ▼
     │                                     ┌──────────────┐
     │                                     │  Invert H22  │
     │                                     └──────────────┘
     │                                              │
     │         ┌──────────────────┐        ┌──────────────┐
     └────────►│    Form ENP      │◄───────│  Form H22I   │
               │ ENP = H22I x H21 │        └──────────────┘
               └──────────────────┘                │
                        │                  ╭──────────────────╮
   ( 7 )◄───── ┌──────────────┐            │     Write        │
               │  EN = -ENP   │            │ The H22I Matrix  │
               └──────────────┘            ╰──────────────────╯
                        │
               ┌──────────────┐
               │ UNITN = I/EN │
               └──────────────┘
   ( 1 )───────────────○
               ┌──────────────┐            ╭──────────────────╮
   ( 8 )◄──────│   Form S     │───────────►│   Write Out      │
               │ S = G x UNITN│            │  The S Matrix    │
               └──────────────┘            ╰──────────────────╯
   ( 2 )───────────────○
               ┌──────────────┐            ╭──────────────────╮
               │   Form  AR   │───────────►│   Write Out      │
               │ AR = EN x  P │            │  The AR Matrix   │
               └──────────────┘            ╰──────────────────╯
   ( 8 )╲
         ├──────────────○
   ( 2 )╱
               ┌──────────────┐            ╭──────────────────╮
               │   Form  AT   │───────────►│   Write Out      │
               │  AT = S x P  │            │  The AT Matrix   │
               └──────────────┘            ╰──────────────────╯
   ( 4 )╲
         ├─────────────○◄──────────────────( 7 )
   ( 5 )╱
           ┌────────────────────────┐      ╭──────────────────╮
           │        Form C          │─────►│   Write Out      │
           │ C = 1/E(H11 + H12 x EN)│      │  The C Matrix    │
           └────────────────────────┘      ╰──────────────────╯
                        │
                  ┌──────────┐
                  │   END    │
                  └──────────┘
```

```
      PROGRAM ENERGY
C     COEFFICIENT MATRICES A, B, AND UC ARE BASIC STRUCTURAL DATA
      ODIMENSION A(5C,50),AI(50,5C),B(50,50),CJ(50,50),UC(5C,50),
      1G(50,5C),H(50,50),GT(50,5C),H22(50,50),H12(50,50),UCG(50,5C),
      2H21(50,50),H22I(5C,50),EN(16,33),AR(16),UNITN(50,50),S(50,50),
      3AT(50),H12N(50,50),C(50,50),LIST(50),P(35),ENP(16,33)
      OEQUIVALENCE(A,CJ,UCG,H22,H21,S),(B,G,H12,C),(UC,H),
      1(AI,GT,H22I,UNITN,H12N)
C     CLEAR ARRAYS TO RECEIVE INPUT
      DO 10 I=1,5C
      DO 1C J=1,5C
      A(I,J) = 0.C
      B(I,J) = C.C
      UC(I,J) = 0.0
   10 AI(I,J) = 0.0
C     READ NCN-REDUNDANT MATRIX A
  310READ 21,I,J,(A(I,J)),I1,J1,(A(I1,J1)),I2,J2,(A(I2,J2)),
      1I3,J3,(A(I3,J3)),NEXT
   21 FORMAT (4(2I2,F12.6),I1)
      GC TO (31,32),NEXT
C     READ LOAD AND REDUNDANT MATRIX B
  320READ 22,I,J,(B(I,J)),I2,J2,(B(I2,J2)),I2,J2,(B(I2,J2)),
      1I3,J3,(B(I3,J3)),NEXT
   22 FCRMAT(4(2I2,F12.6),I1)
      GO TO (32,33),NEXT
C     FORM ENERGY COEFFICIENT MATRIX UC
  330READ34,I,J,(UC(I,J)),I1,J1,(UC(I1,J1)),I2,J2,(UC(I2,J2)),
      1I3,J3,(UC(I3,J3)),NEXT
   34 FORMAT (4(2I2,F12.6),I1)
      GO TO (33,35),NEXT
   35 DO 36 I =1,49
      DO 36 J =1,49
   36 UC(J,I) = UC(I,J)
C     INVERT THE A MATRIX
      CALL GAUSS3(33,1.E-10,A,AI,KER)
      GO TO(365,364),KER
  364 PRINT 151
  151 FORMAT(24H      MATRIX A IS SINGULAR)
  365 PRINT 200
   37 PRINT 38
  380FORMAT(64H A MATRIX INVERSE BY GAUSS3, 9 COLUMNS, IE 1-9, 10-18
      1PER PAGE//)
      PRINT 100,((AI(I,J),J=1,9),I=1,33)
      PRINT 200
      PRINT 100,((AI(I,J),J=10,18),I=1,33)
      PRINT 200
      PRINT 100,((AI(I,J),J=19,27),I=1,33)
      PRINT 200
      PRINT 300,((AI(I,J),J=28,33),I=1,33)
  100 FORMAT(/9F13.7)
  150 FORMAT(/11F1C.6)
  200 FCRMAT(1H1)
C     POST MULTIPLY AI WITH B MATRIX
      CALL MATMPY(33,33,49,AI,B,CJ)
C     FORM G MATRIX BY ADDITION OF TRIVIAL RELATIONS TO CJ
      DO 4C I=34,49
   40 CJ(I,I)= 1.C
      DO 41 I=1,45
      DO 41 J=1,45
   41 G(I,J) = CJ(I,J)
      PRINT 200
   42 PRINT 43
   43 FORMAT(50H  G MATRIX ,FORMED FROM CJ WITH TRIVIAL RELATIONS//)
      PRINT 100,((G(I,J),J=1,9),I=1,49)
      PRINT 200
      PRINT 100,((G(I,J),J=10,18),I=1,49)
      PRINT 200
      PRINT 100,((G(I,J),J=19,27),I=1,49)
      PRINT 200
      PRINT 100,((G(I,J),J=28,36),I=1,49)
      PRINT 200
      PRINT100,((G(I,J),J=37,45),I=1,49  )
      PRINT 200
```

123

```
          PRINT 400,((G(I,J),J=46,49),I=1,49)
   300 FORMAT (/ 6F13.7)
   400 FORMAT (/ 4F13.7)
C      TRANSPOSE G
       DO 44  I=1,49
       DO 44  J=1,49
    44 GT(I,J) = G(J,I)
C      FORM H MATRIX BY TRIPLE PRODUCT (GT)(UC)(G)
       CALL MATMPY(49,49,49,UC,G,UCG)
       CALL MATMPY(49,49,49,GT,UCG,H)
       PRINT 200
       PRINT 45
    45 FORMAT(44H MATRIX H FORMED BY TRIPLE   PRODUCT, GTXUCXG//)
       PRINT 500,((H(I,J),J=1,9),I=1,49)
       PRINT 200
       PRINT 500,((H(I,J),J=10,18),I=1,49)
       PRINT 200
       PRINT 500,((H(I,J),J=19,27),I=1,49)
       PRINT 200
       PRINT 500,((H(I,J),J=28,36),I=1,49)
       PRINT 200
       PRINT 500,((H(I,J),J=37,45),I=1,49)
       PRINT 200
       PRINT 600,((H(I,J),J=46,49),I=1,49)
   500 FORMAT (/9F13.4)
   600 FORMAT (/ 4F13.4)
C      READ LOAD MATRIX   P
       DO 510 I = 1,35
   510 P(I) = 0.0
    57 READ 58, I,      (P(I)),NEXT
    58 FORMAT ( I2  , F12.4, I1 )
       GO TO (57,581),NEXT
C      PARTITION  H MATRIX
   581 DO 54  I=34,49
       DO 54  J=34,49
       II = I-33
       JJ = J-33
    54 H22(II,JJ) = H(I,J)
       PRINT 200
   521 PRINT 522,((H22(I,J),J =1,8),I =1,16)
   522 FORMAT(/8F12.4)
       PRINT 200
       PRINT 522,((H22(I,J),J =9,16),I =1,16)
C      INVERT  H22 MATRIX
       CALL GAUSS 3 (16,1.E-10, H22, H22I,KER)
       GO TO(525,524),KER
   524 PRINT 150
       PRINT 200
   525 PRINT 522,((H22I(I,J),J=1,8),I=1,16)
       PRINT 522,((H22I(I,J),J=9,16),I=1,16)
       DO 53 I =34,49
       DO 53  J=1,33
       KK = I-33
    53 H21(KK,J) = H(I,J)
C      FORM REDUNDANT LOAD COEFFICIENT MATRIX, EN.
       DO 540 I=1,16
       DO 540 K=1,33
       SUM =0.0
       DO 541 J=1,16
   541 SUM = SUM + H22I(I,J)*H21(J,K)
   540 ENP(I,K) = SUM
       DO 56  I=1,16
       DO 56  J=1,33
    56 EN(I,J) = -1.0 * ENP(I,J)
C      FORM MATRIX  UNITN BY PLACING EN  BELOW  UNIT MATRIX
       DO 99 I = 1,33
       DO 99 J = 1,33
    99 UNITN(I,J) = 0.0
       DO 62  I = 1,33
    62 UNITN(I,I) = 1.0
       DO 63  I=34,49
       DO 63  J=1,33
       KK = I-33
    63 UNITN(I,J) = EN(KK,J)
```

124

```
C       FORM S MATRIX .   S = (G)(UNITN)
        CALL MATMPY (49,49,33, G, UNITN, S )
        PRINT 200
        PRINT 800
  800 FORMAT (43H STRESS COEFFICIENT MATRIX.  S = (G)(UNITN) //)
        PRINT 150,((S(I,J),J=1,11),I =1,49)
        PRINT 200
        PRINT150,((S(I,J),J=12,22),I =1,49)
        PRINT 200
        PRINT150,((S(I,J),J=23,33),I=1,49)
C       RECUNDANT LOAD MATRIX, AR
        DO 80 I = 1,16
        SUM = 0.0
        DO 81 J= 1,33
   81 SUM = SUM + EN(I,J)*P(J)
   80 AR(I  ) = SUM
        DO 59  I=1,49
   59 LIST(I) = 1*I
        PRINT 200
        PRINT 60
  600FORMAT (50H RECUNDANT LCAD MATRIX.   AR = -  H22I      H21      P
     1  16H AR(1-16)= A(  ))
        PRINT 700,(LIST(J),AR(J),J=1,16)
  700 FORMAT (/13X,I2,F2C.8)
C       TOTAL UNKNOWN INTERNAL LCADS.   AT = (S)(P)
        DO 640 I=1,49
        SUM =0.0
        DO 641 J=1,33
  641 SUM = SUM + S(I,J)*P(J)
  640 AT(I) = SUM
        PRINT 200
        PRINT 900
 9000FORMAT ( 45H  MATRIX OF ALL INTERNAL LOADS.   AT = (S)(P)   //
     1  16H AT(I)   = A(  ))
        PRINT 1000, (LIST(I),AT(I ), I=1,49)
 1000 FORMAT (/13X,I2,F20.8)
        DO 52  I=1,33
        DO 52  J=34,49
   52 H12(I,J-33) = H(I,J)
        E = 1030000C.C
C       INFLUENCE CCEFFICIENT MATRIX.   C = ( H11 + (H12) (EN)) / E
        DO 90  I = 1,33
        DO 90  K =1,33
        SUM = 0.0
        DO 95  J = 1,16
   95 SUM = SUM + H12(I,J)*EN(J,K)
   90 H12N(I,K) = SUM
        SCALE = 100C0.
        DO 70  I=1,33
        DO 70  J=1,33
   70 C(I,J) = ((F(I,J)  + H12N(I,J))/E)*SCALE
        PRINT 200
        PRINT 73
  730FORMAT (45 H MATRIX OF DEFLECTION INFLUENCE COEFFICIENTS  /
     1 35H  C  =(( H11 +(H12)(N))/ E)*(SCALE))
        PRINT 150,((C(I,J),J= 1,11),I=1,33)
        PRINT 200
        PRINT 150,((C(I,J),J=12,22),I=1,33)
        PRINT 200
        PRINT 150,((C(I,J),J=23,33),I=1,33)
        END
```

```
      SUBROUTINE    GAUSS3(N,EP,A,X,KER)
      DIMENSION A(50,50),X(50,50)
      DO 1 I=1,N
      DO 1 J=1,N
  1   X(I,J)=0.0
      DO 2 K=1,N
  2   X(K,K)=1.0
 10   DO 34 L=1,N
      KP=C
      Z=C.C
      DO 12 K=L,N
      IF(Z-ABSF(A(K,L)))11,12,12
 11   Z=ABSF(A(K,L))
      KP=K
 12   CONTINUE
      IF(L-KP)13,20,20
 13   DO 14 J=L,N
      Z=A(L,J)
      A(L,J)=A(KP,J)
 14   A(KP,J)=Z
      CO 15 J=1,N
      Z=X(L,J)
      X(L,J)=X(KP,J)
 15   X(KP,J)=Z
 20   IF(ABSF(A(L,L))-EP)50,50,30
 30   IF(L-N)31,34,34
 31   LP1=L+1
      CC 36 K=LP1,N
      IF(A(K,L))32,36,32
 32   RATIO=A(K,L)/A(L,L)
      DO 33 J=LP1,N
 33   A(K,J)=A(K,J)-RATIO*A(L,J)
      CO 35 J=1,N
 35   X(K,J)=X(K,J)-RATIO*X(L,J)
 36   CCNTINUE
 34   CONTINUE
 40   DO 43 I=1,N
      II=N+1-I
      CO 43 J=1,N
      S=0.0
      IF(II-N)41,43,43
 41   IIP1=II+1
      DO 42 K=IIP1,N
 42   S=S+A(II,K)*X(K,J)
 43   X(II,J)=(X(II,J)-S)/A(II,II)
      KER=1
      RETURN
 50   KER=2
      END
      SUBROUTINE MATMPY (L, M, N, A, B, C)
      DIMENSION A(50,50), B(50,50), C(50,50)
      CC 10 I=1,L
      CO 10 K=1,N
      SUM = 0.0
      CO 20   J=1,M
 20   SUM = SUM + A(I,J) * B(J,K)
 10   C(I,K) = SUM
      END
      END
```

[F] Matrix

Input Form

```
 1  1    40.5860    2  2  4712.54     2  9   568.242    220    656.335   1
221   -334.075     244  -289.5395    3  3    36.7518    4  4    35.4129   1
 5  5    36.0195    6  6    37.5382    7  7    41.9716    8  8  1554.5632   1
814   -395.2744    815  -438.193     822  -109.0759    823  -121.1411   1
 9  9   415.0763   910  -123.270     934  -335.6280    944   -70.3038   1
945     63.0954   1010   271.1617   1011   -90.9668   1034   236.8452   1
1035  -207.059    1045   -38.5243   1046    42.6268   1111   208.6649   1
1112   -79.0163   1135   150.650    1136  -162.1008   1146   -27.5895   1
1147    34.1926   1212   194.3713   1213   -80.2663   1236   123.1598   1
1237  -156.6048   1247   -23.5277   1248    31.7581   1313   199.0123   1
1314   -85.8209   1337   124.342    1338  -169.2272   1348   -23.198    1
1349    31.517    1414   327.3802   1422    64.8044   1438   137.6857   1
1449   -23.8269   1515   371.9172   1516  -102.9527   1523    72.1931   1
1538   165.0686   1543   -28.6228   1616   239.0326   1617   -97.174    1
1637   150.4141   1638  -202.5909   1642   -28.2054   1643    37.8843   1
1717   235.8671   1718   -96.6455   1736   150.466    1737  -189.7857   1
1741   -28.9633   1742    38.8136   1818   257.8147   1819  -113.6383   1
1835   188.001    1836  -198.8093   1840   -34.6218   1841    42.5174   1
1919   330.3452   1920  -146.3721   1934   280.9922   1935  -259.2942   1
1939   -45.7466   1940    53.9308   2020   485.5535   2021   -81.2121   1
2034  -398.6962   2039    75.1214   2121    60.9998   2222    21.9326   1
2323    24.5350   2424     2.4861   2425     0.5188   2525     1.9818   1
2526     0.4721   2626     1.7829   2627     0.4193   2727     1.6776   1
2728     0.4194   2828     1.6758   2929     1.9267   2930     0.4860   1
3030     2.0048   3031     0.5164   3131     2.062    3132     0.5146   1
3232     2.0661   3233     0.5184   3333     2.7071   3434  1997.6131   1
3439  -133.6859   3445  -112.4532   3535  1194.6992   3540   -83.7719   1
3546   -66.4386   3636   822.3501   3641   -62.6632   3647   -50.6107   1
3737   808.2336   3742   -57.4131   3748   -47.0957   3838   804.7401   1
3843   -58.4006   3849   -48.6683   3939    31.4094   4040    21.5756   1
4141    16.5636   4242    14.3990   4343    13.3832   4444    52.8680   1
4545    26.3247   4646    16.8506   4747    13.0860   4848    11.6485   1
4949    11.0577.                                                        2
```

MATRIX $[P]$

Input Form

1	1500.00	1
2	252.80	1
3	714.00	1
4	528.00	1
5	109.00	1
6	-210.50	1
7	-2782.00	1
8	-4523.56	1
9	-5212.17	1
10	-5568.74	1
11	-5395.86	1
12	-4593.58	1
13	-4654.94	1
14	-4654.94	1
15	-4593.58	1
16	-5395.86	1
17	-5568.74	1
18	-5212.17	1
19	-4523.56	1
20	2390.73	1
21	4825.58	1
22	5395.02	1
23	6125.17	1
24	6229.25	1
25	5802.52	1
26	2738.27	1
27	2390.73	1
28	4825.58	1
29	5395.02	1
30	6125.17	1
31	6229.25	1
32	5802.52	1
33	2738.27	2

SUBPROGRAM
CHECK

Start

Clear Arrays

Set
BA = A ← Form A → Write A

Call Gauss 3

Ker $\overset{?}{=}$ 2 →yes→ Print
A is Singular

No

Invert A

Form Product
CHECK = BA x AI

Write CHECK

END
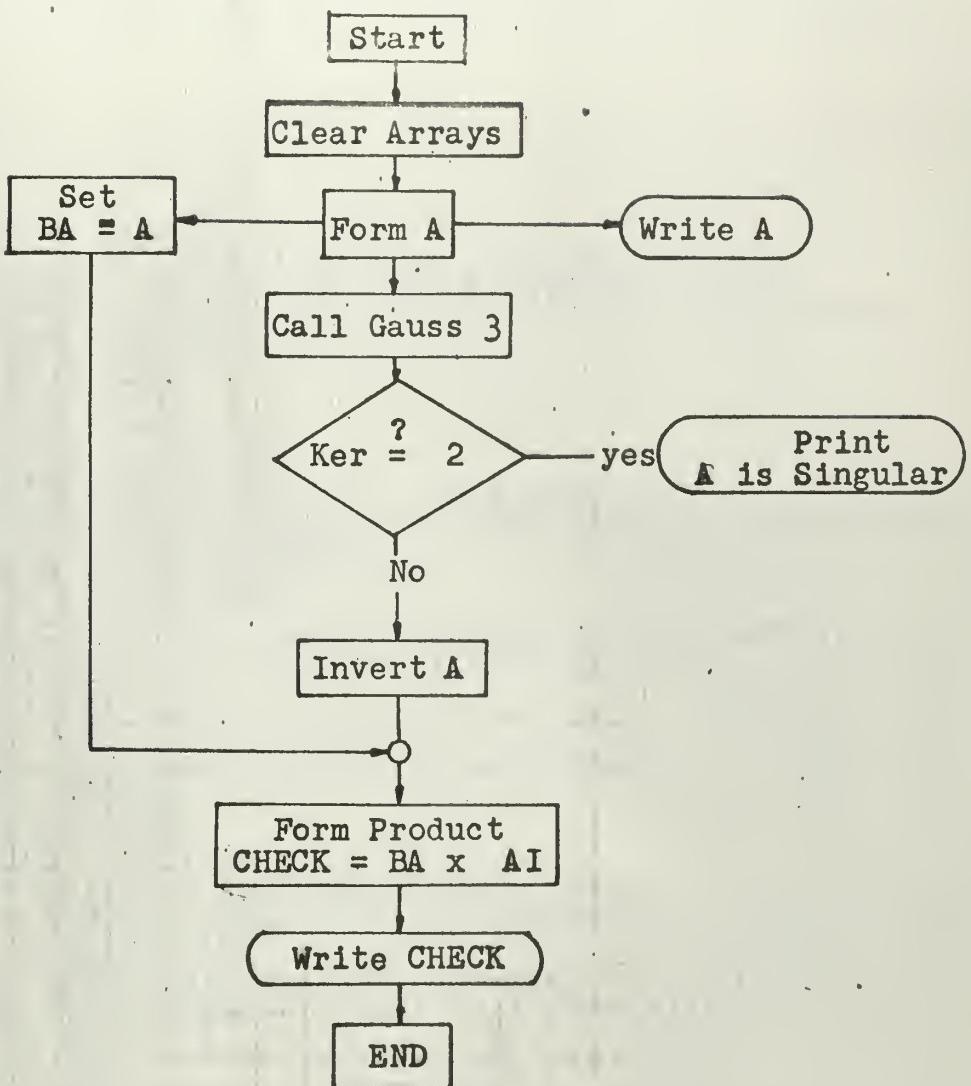
```
      PROGRAM  ECHECK
C INVERSE  CHECK FOR (A) MATRIX.  VARIABLE CHECK
C IS PRODUCT OF (A)(AI) AND SHOULD GIVE UNIT MATRIX
      DIMENSION A(50,50),AI(50,50),CHECK(50,50),BA(50,50)
C CLEAR ARRAYS FOR INPUT
      DO 10 I =1,50
      DO 10 J=1,5C
      A(I,J) = 0.C
      AI(I,J) = 0.0
      CHECK(I,J) = 0.0
   10 BA(I,J) = 0.0
C READ NON-REDUNDANT MATRIX A, THEN PRINT IT.
  310READ 21,I,J,(A(I,J)),I1,J1,(A(I1,J1)),I2,J2,(A(I2,J2)),
     1I3,J3,(A(I3,J3)),NEXT
   21 FORMAT (4(2I2,F12.6),I1)
      GO TO (31,32),NEXT
   32 PRINT 33
   33 FORMAT(42H   (A) MATRIX, ELEVEN COLUMNS PER PAGE////)
      PRINT 150,((A(I,J),J= 1,11),I=1,33)
      PRINT 200
      PRINT 150,((A(I,J),J=12,22),I=1,33)
      PRINT 200
      PRINT 150,((A(I,J),J=23,33),I=1,33)
      PRINT 200
      DO 40 I=1,33
      DO 40 J=1,33
   40 BA(I,J) = A(I,J)
C INVERT MATRIX (A) AND FORM PRODUCT (A)(AI)
      CALL GAUSS 3 (33,1.E-10,A,AI,KER)
      GO TO (42,41),KER
   41 PRINT 201
   42 CALL MATMPY(33,33,33,BA,AI,CHECK)
      PRINT 150,((CHECK(I,J),J= 1,11),I=1,33)
      PRINT 200
      PRINT 150,((CHECK(I,J),J=12,22),I=1,33)
      PRINT 200
      PRINT 150,((CHECK(I,J),J=23,33),I=1,33)
  150 FORMAT(11F10.6)
  200 FORMAT(1H1)
  201 FORMAT(23H   MATRIX A IS SINGULAR)
      END
      SUBROUTINE MATMPY (L, M, N, A, B, C)
      DIMENSION A(50,50), B(50,50), C(50,50)
      DO 10 I=1,L
      DO 10 K=1,N
      SUM = 0.0
      DO 20  J=1,M
   20 SUM = SUM + A(I,J) * B(J,K)
   10 C(I,K) = SUM
      END
```

MATRIX [CHECK]_{33x33}

Sample Showing First 10 Columns Correct to Sixth Decimal

CALIBRATION CURVES FOR DILLON DYNAMOMETERS
AND HYDRAULIC PRESSURE SYSTEM
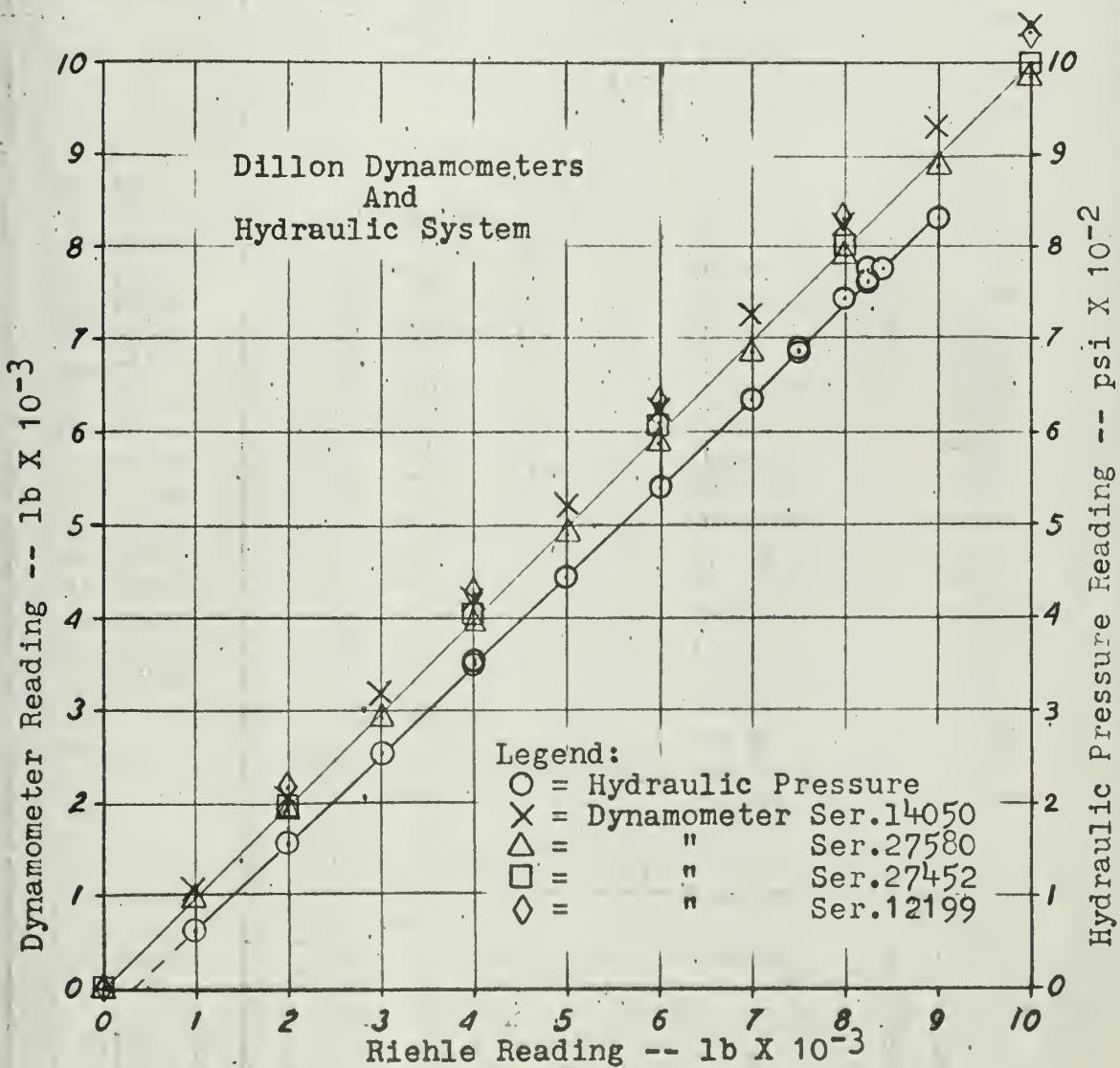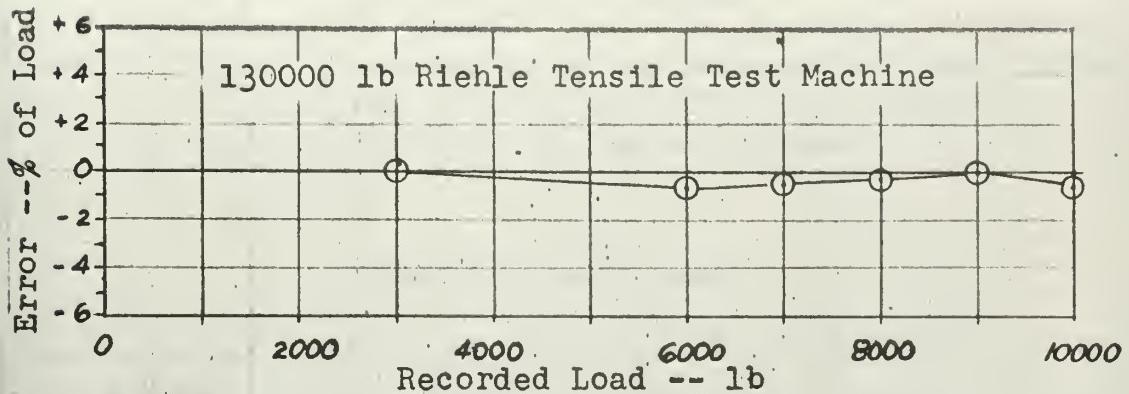
APPENDIX E

Coordinate Location of Strain Gages
F8U-3 Wing Center Section

Note: 1. $X_w = 0 =$ Intersection of the center section droop leading
edge and the center line of the airplane.

2. $Y_w = 0 -$ The center line of the airplane.

Upper Skin Inside Gages

Gage Number	Gage Type	X_w	Y_w
1-2	AX-5	63.15	5.82
3-4	"	83.00	5.94
5-6	"	101.95	5.91
7-8	"	119.25	5.88
9-10	"	138.38	5.94
*11-12	"	153.78	5.94
13-14-15	AR 7-2	70.66	33.03
16-17-18	"	94.83	33.27
19-20-21	"	112.88	33.06
22-23-24	"	129.34	33.09
*25-26-27	AR 1 or 2	153.54	33.15
28-29-30	"	161.02	33.33
31-32-33	AR 7-2	127.60	75.04
34-35-36	"	142.40	75.13
37-38-39	"	155.64	75.07
40-41-42	"	168.56	75.10
43-44-45	"	180.00	75.25
46-47-48	"	153.48	106.54
49-50-51	"	161.20	101.26
52-53-54	"	169.22	95.79
55-56-57	"	176.49	88.92
58-59-60	"	185.31	84.92
61	A-7	144.86	66.10
62	"	146.09	65.22
63	"	150.48	62.22
64	"	151.74	61.44
65	"	146.67	68.68
66-67-68	AR 7-2	147.90	67.87
69-70-71	"	149.34	66.94
72-73-74	"	150.78	65.92
75-76-77	"	152.22	64.92

Gage Number	Gage Type	X_w	Y_w
78	A-7	153.48	64.05
79	"	151.20	72.70
80	"	152.61	71.74
81	"	154.05	70.72
82	"	155.52	69.76
83-84-85	AR 7-2	137.72	28.53
86-87-88	"	140.00	32.25
89-90-91	"	142.55	30.48
92-93-94	"	145.25	28.74
95-96-97	"	147.99	45.40
*98-99-100	"	150.30	43.84
101-102-103	"	152.73	42.25
104-105-106	"	155.95	58.68
107-108-109	"	158.11	57.21
110-111-112	"	160.24	55.74
113-114-115	"	163.84	71.68
116-117-118	"	165.77	70.51
119-120-121	"	167.72	69.19
122-123-124	"	169.23	78.83
125-126-127	"	170.60	78.83
128-129-130	"	173.00	78.83
131-132-133	"	147.30	110.81

Notes

1. a) Gages 1-2, 3-4, 5-6, 7-8, 9-10, 11-12 mounted by Chance-Vought and oriented with one leg parallel to Y_w and the other leg perpendicular to Y_w.

    b) No gage factor or other information available.

2. a) All AR 7-2 gages mounted at USNPS and oriented with one leg perpendicular to C.I.B., 45° gage pointing outboard and toward trailing edge, other leg parallel to C.I.B.

    b) All gages from lot B-31, 120.5 ± .5 ohms, 1.97 ± 2%, b factor = -200.

3. a) All A-7 gages mounted at USNPS and oriented parallel to C.I.B.

    b) All gages from lot B-31, 120.0 ± .3 ohms, 1.99 ± 2%.

4. a) Gages 25-26-27, 28-29-30 mounted by Chance-Vought and oriented approximately the same as USNPS mounted AR 7-2 gages.

    b) No gage factor or other information available.

Bottom Skin and Beam Assembly

Gage Number	Gage Type	X_w	Y_w
134-135-136	AR 1	72.82	41.26
137-138-139	"	78.08	46.75
140-141-142	"	92.18	61.29
143-144-145	"	104.02	73.54
146-147-148	"	114.54	84.50
149-150-151	"	131.50	102.19
152-153-154	AR 7-2	142.46	113.48
155-156-157	AR 1	148.86	120.06
158-159-160	AR 1	155.01	126.39
161-162	AX 5	70.60	33.33
163-164-165	AR 1	120.00	82.28
166-167-168	AR 1	back-up gage to 163-165	
169-170-171	AR 7-2	146.64	110.90
172-173-174	AR 1	91.38	40.18
175-176-177	AR 1	118.29	71.86
178-179-180	AR 7-2	134.35	90.78
181-182-183	AR 7-2	149.67	108.86
184-185-186	AR 1	164.74	126.64
187-188-189	"	back-up gage to 172-174	
190-191-192	"	back-up gage to 175-177	
193-194-195	"	back-up gage to 178-180	
196-197-198	AR 7-2	back-up gage to 181-183	
199-200-201	AR 1	back-up gage to 184-186	
202-203	AX 5	95.13	33.60
204-205-206	AR 7-2	127.63	75.43
207-208-209	AR 1	133.09	82.22
210-211-212	AR 1	back-up gage to 207-209	
*213-214-215	AR 7-2	141.50	92.64
216-217-218	AR 7-2	152.91	106.70
219-220-221	AR 1	110.60	42.61
222-223-224	AR 1	133.24	72.67
225-226-227	AR 7-2	156.76	104.11
228-229-230	AR 1	174.23	127.33
*231-232-233	AR 1	back-up gage to 219-221	
234-235-236	AR 1	back-up gage to 222-224	
237-238-239	AR 7-2	back-up gage to 225-227	
240-241-242	AR 1	back-up gage to 228-230	
243-244-245	AR 7-2	113.15	33.18
246-247-248	AR 1	146.31	82.07
249-250-251	AR 1	back-up gage to 246-248	

Bottom Skin and Beam Assembly (continued)

Gage Number	Gage Type	X_w	Y_w
252-253-254	AR 7-2	160.63	101.50
255-256-257	AR 1	126.07	41.11
258-259-260	AR 1	146.67	72.07
*261-262-263	AR 7-2	164.53	98.86
264-265-266	AR 1	174.23	127.57
267-268-269	AR 1	back-up gage to 255-257	
270-271-272	AR 1	back-up gage to 258-260	
273-274-275	AR 7-2	back-up gage to 261-263	
276-277-278	AR 1	back-up gage to 264-266	
279-280-281	AR 7-2	129.19	33.78
282-283-284	AR 7-2	154.98	74.65
285-286-287	AR 1	159.04	82.16
288-289-290	AR 1	back-up gage to 285-287	
291-292-293	AR 7-2	168.71	96.19
294-295-296	AR 1	140.63	39.40
297-298-299	AR 1	160.60	72.55
300-301-302	AR 7-2	172.61	93.42
303-304-305	AR 1	192.55	126.85
306-307-308	AR 1	back-up gage to 294-296	
309-310-311	AR 1	back-up gage to 297-299	
312-313-314	AR 7-2	back-up gage to 300-302	
315-316-317	AR 1	back-up gage to 303-305	
*318-319-320	AR 7-2	142.55	34.41
321-322-323	AR 7-2	147.42	34.62
324-325-326	AR 7-2	167.90	74.74
327-328-329	AR 1	170.00	82.16
*330-331-332	AR 1	back-up gage to 327-329	
333-334-335	AR 7-2	177.00	90.60
336-337-338	AR 1	155.64	41.08
339-340-341	AR 1	173.60	73.93
342-343-344	AR 7-2	180.99	87.84
345-346-347	AR 1	201.95	126.43
348	omitted by numbering error		
349-350-351	AR 1	back-up gage to 336-338	
352-353-354	AR 1	back-up gage to 339-341	
355-356-357	AR 7-2	back-up gage to 342-344	
358-359-360	AR 1	back-up gage to 345-347	
361-362-363	"	153.81	33.27
364-365-366	"	157.59	33.15
367-368-369	"	159.78	33.45

Bottom Skin and Beam Assembly (continued)

Gage Number	Gage Type	X_w	Y_w
370-371-372	AR 1	162.58	33.06
373-374-375	AR 1	160.90	30.00
376-377-378	AR 7-2	165.88	40.81
379-380-381	"	171.08	50.93
382-383-384	"	176.64	69.04
385-386-387	"	179.49	74.20
388-389-390	AR 1	184.92	82.10
391-392-393	AR 1	back-up gage to 388-390	
394-395-396	AR 7-2	185.10	85.13
397-398-399	AR 1	166.57	36.18
400-401-402	"	170.21	43.45
403-404-405	"	179.67	62.64
406-407-408	"	184.65	72.70
409-410-411	AR 7-2	190.93	84.71
412-413-414	AR 1	208.77	120.12
415-416-417	" 1	214.08	130.93
418-419-420	"	141.17	25.34
421-422-423	"	156.06	25.09
424-425-426	"	back-up gage to 418-420	
427-428-429	"	back-up gage to 421-423	
430-431-432	"	147.39	8.56
433-434-435	"	back-up gage to 430-432	
436-437-438	"	97.51	10.12
439-440-441	"	back-up gage to 436-438	
442-443-444	"	61.05	25.68
* 445-446-447	"	back-up gage to 442-444	
448-449-450	AR 7-2	back-up gage to 152-154	
451-452-453	"	back-up gage to 409-411	

The following listed gages are mounted externally on
the upper and lower skins, and are back-up gages as
indicated, or mounted over an internal beam member:

454-455-456	AR 7-2	121.45	33.61
457-458-459	"	back-up gage to 279-281	
460-461-462	"	136.59	33.61
463-464-465	"	151.86	33.61
466-467-468	"	back-up gage to 367-369	
469-470-471	"	165.64	33.61
472-473-474	"	back-up gage to 28-30	
475-476-477	"	back-up gage to 89-91	
478-479-480	"	back-up gage to 19-21	
481-482-483	"	back-up gage to 13-15	
484-485-486	"	back-up gage to 161-162	

Bottom Skin and Beam Assembly (continued)

Notes

I. BEAM GAGES

1. a) All AR 1 gages mounted on vertical webs of beams,
   outboard of pivot rib, were mounted by Chance-Vought
   and are oriented with center leg of strain gage
   pointing inboard and on the center line of the web.
   Other legs 45° each side. (Note: Gage 178-179-180
   is an AR 7-2 mounted at USNPS, but oriented same as
   above gages.)

   b) All AR 1 gages mounted on vertical web of pivot rib
   were mounted by Chance-Vought and are oriented with
   center leg of strain gage pointing aft and on the center
   line of the web. Other legs 45° each side.

   c) All AR 1 gages mounted on vertical webs of center
   section beams were mounted by Chance-Vought with center
   leg of strain gage pointing inboard and on the center
   line of the web. Other legs 45° each side.

   d) All AR 7-2 gages mounted on vertical webs of beams,
   outboard of pivot rib, were mounted at the USNPS and are
   oriented with one leg perpendicular to CIB, and other
   legs pointing outboard and up or down depending on
   whether it is a "walk-around" gage or a "back-up" gage.

   e) All AR 1 gages mounted on vertical web of Intermediate
   Rib were mounted by Chance-Vought and are oriented
   with the center leg of the strain gage pointing forward
   and on the center line of the web. Other legs 45°
   each side.

II. LOWER SKIN

1. a) AX 5 gages were mounted by Chance-Vought and are
   oriented with one leg parallel to the center line of
   the skin between the beams and other leg rotated
   90° away.

138

Bottom Skin and Beam Assembly (continued)

b) All AR 1 gages (361 thru 375) were mounted by Chance-Vought and are oriented with one leg (the first number on each rosette) parallel to the center line of the skin between the beams; the second leg (second number of sequence) rotated 45° counter-clockwise; and the third leg (third number of sequence) rotated another 45° counter-clockwise, making it perpendicular to first leg. The entire rosette points inboard.

c) All AR 7-2 gages were mounted at USNPS and oriented with one leg perpendicular to CIB and the entire rosette pointing outboard and forward.

2. No gage factor or other information available on gages mounted by Chance-Vought on either the beams or the lower skin.

3. All AR 7-2 gages mounted at USNPS are from lot B-31, 120.5 $\pm$ 0.5 ohms, 1.97 $\pm$ 2% gage factor, b factor ≠ -200.

*The following gage elements are inoperable or give questionable results:

                    11
                    25-26-27
                    98-99-100
                    213
                    233
                    261
                    318-319-320
                    332
                    445-446-447
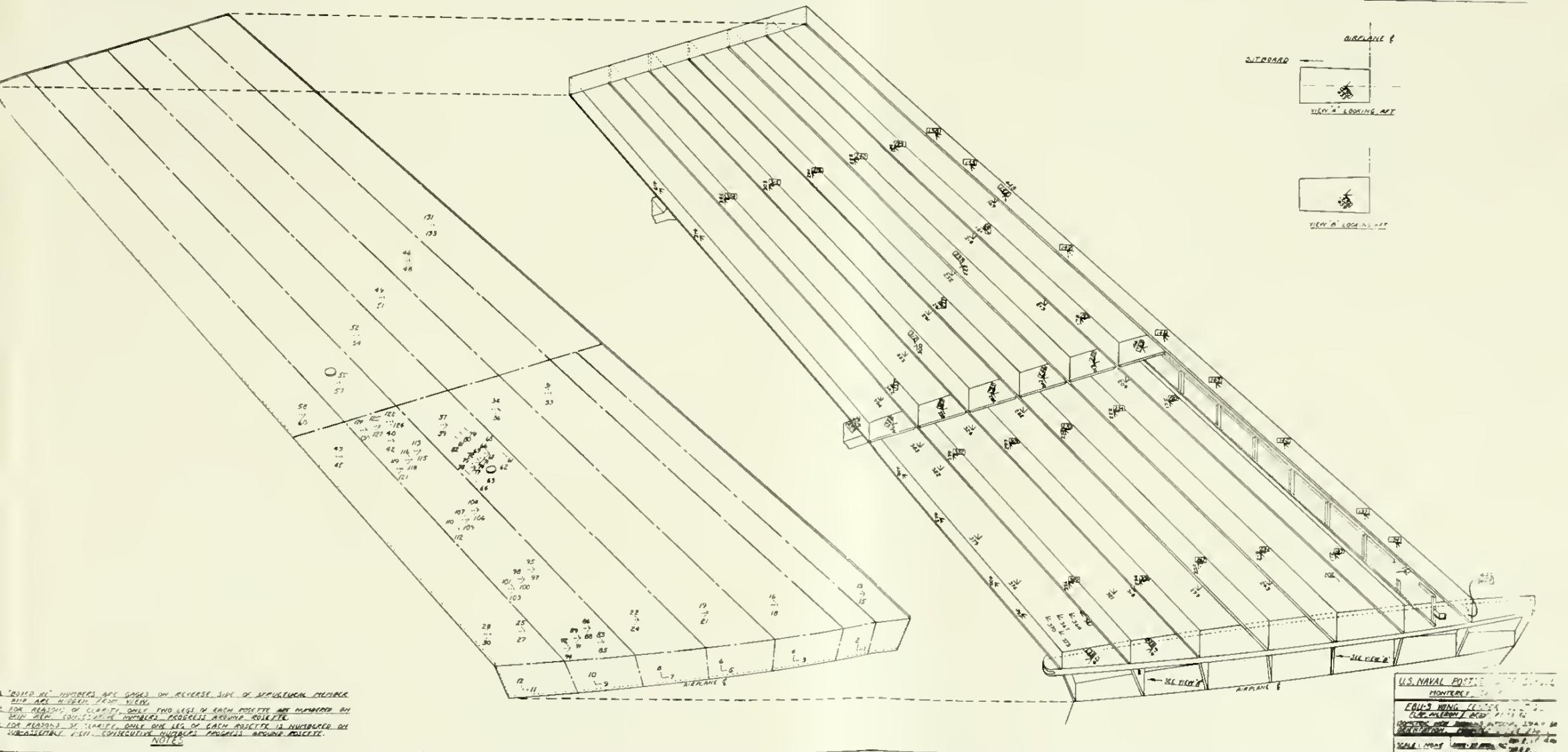
The method of taking strain readings employed common Wheatstone bridge circuitry shown in Fig F1. The unique part of the method was the use of a digital counter to indicate bridge unbalance and give a visual display of the strain directly in units of micro-inches per inch.

For the special case considered here where all four legs of the bridge have the same known resistances R, and for a small change of resistance in one leg $\triangle R$, it can be shown that the standard Wheatstone bridge equation for output voltage V_O reduces to

$$V_O = \frac{V\ R_O\ \triangle R}{4\ R\ (R + R_O)} \quad , \qquad (F1)$$

where R_O is a constant resistance across terminals AC and V is the constant voltage source. Further, the expression for the gage factor (GF) that relates strain and change of resistance is

$$(GF)\,\epsilon\ = \frac{\triangle R}{R} \quad . \qquad (F2)$$

By substituting equation (F2) into (F1) it is immediately apparent that the output voltage is a linear function of strain,

$$V_O = \left[\frac{V\ (GF)\ R_O}{4\ (R + R_O)}\right]\epsilon\ = (\text{Constant})\ \epsilon\ \quad . \qquad (F3)$$

141

Utilizing this fact it was then easy to calibrate the electronic counter in units of strain.

Considering again the basic bridge circuit, a shunt resistance R_c across one of the legs effectively unbalances the bridge. Its effect on the basic balanced bridge equations is developed below.

$$(GF)\epsilon \ = \ \frac{\triangle R}{R}$$

$$\triangle R = R \ (GF)\epsilon \qquad\qquad (F4)$$

$$R - \triangle R = \frac{1}{\frac{1}{R} + \frac{1}{R_c}} \ = \ \frac{R \ R_c}{R + R_c}$$

$$\triangle R = R - \frac{R \ R_c}{R + R_c} \ = \ \frac{R^2}{R + R_c} \qquad\qquad (F5)$$

Substituting equation (F5) into (F4) and solving for R_c gives,

$$R_c = R \ \left[\frac{1}{\epsilon(GF)} - 1 \right] \qquad\qquad (F6)$$

From equation (F6) the shunt resistance necessary to produce an equivalent strain of 0.001 in. per in. when R is 120 ohms and (GF) equals 2.0 is then,

$$R_c = 120 \left[\frac{1}{(0.001)(2.0)} - 1 \right] = 59780 \text{ ohms.}$$

If on the other hand a more standard 60000 ohm resistor were used for R_c, the equivalent strain would be 998 micro inches per inch. This feature was used to calibrate the electronic counter.

A Wheatstone bridge circuit was permanently constructed into which precision 120 ohm ($\pm$ .25%) resistors were readily connected to form the four legs. A precision 60000 ohm ($\pm$ .05%) shunt resistor was connected with a switch as shown in Fig. F1. In addition a precision 50000 ohm potentiometer was provided through connection CE as a variable resistance for any delicate balancing.

With the switching and balancing unit and the switch F disconnected, the amplifier connected across terminals AC and the variable resistance connected across CE, we have the special bridge circuit described previously. The variable resistance was then adjusted to exactly balance the bridge and consequently give a zero indication on the electronic counter. Switch F was then closed and the amplifier gain adjusted to give a 998 reading on the counter. The counter had been previously set to repeatably indicate the integrative result of a one second sampling of V_o which greatly enhanced smooth readings.

Repeating this procedure and noting the consistancy
of returning to zero with switch F open and to 998 with
the switch closed insured the establishment of a linear
calibration of the counter to read in units of micro-inches
per inch.

After calibrating the counter, switches E and F were
opened and resistances R_1 and R_2 were replaced by the
switching and balancing unit leads for the active and
compensating gages respectively as shown in Fig. F1. The
active and compensating gages also had 120 ohm resistances.
Each of the 20 gages connected through the switching and
balancing unit was then zeroed on the switching and balancing
unit in the conventional manner prior to subjecting them to
load. At any time during the test run switch F could be
closed and a change of 998 observed on the counter. This
gave a continual check on the calibration of the counter.

Fig. F1

SCHEMATIC DIAGRAM

STRAIN GAGE INSTRUMENTATION

20 Channel
Switch. &
Bal. Unit
Baldwin -
Lima-Hamilton

DC Pwr Supply
Model 721A
Hewlett-
Packard

Active Gage

Comp. Gage
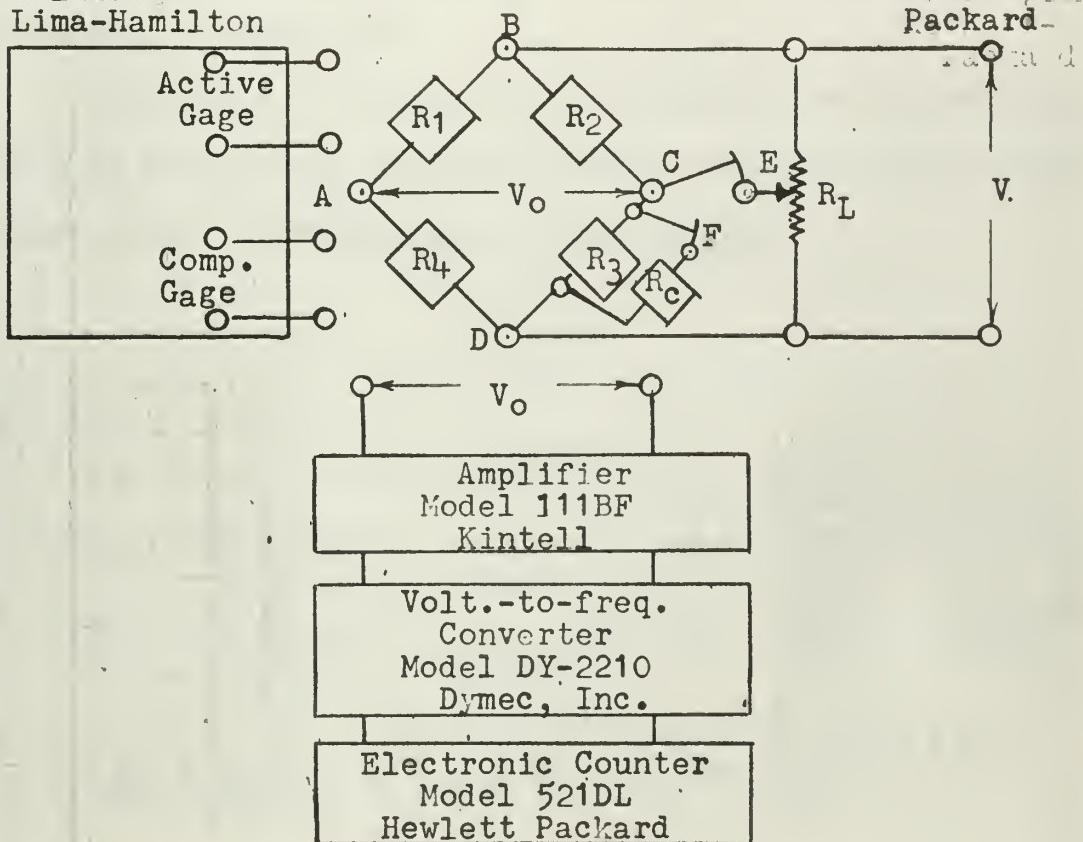
R_1 = R_2 = R_3 = R_4 = CRCA 120 ohm (.25%) 215-RL

R_c = CRCA 60000 ohm (.05%) 215-RL

R_L = 50000 ohm Helipot TP Precision Potentiometer
      Resistance Tolerance: 5%
      Linearity Tolerance: .5%

EXPERIMENTAL PRINCIPAL STRESSES AND
AXIS ORIENTATION

The magnitudes of principal stresses and the orientation of the principal axes were calculated for all rosette locations of interest. Experimental strain readings are listed in Table G1. Calculations were performed on the C.D.C. 1604 Digital Computer utilizing a FORTRAN program named ROSRED shown in Tables G2 and G3. The computer output is listed in Table G4.

The equations solved by the program were the relations between rectangular rosette readings and principal stresses found in any standard text on the subject.

Fig. G1

$$\sigma_{max} = \frac{E}{2}\left[\frac{\epsilon_1+\epsilon_3}{(1-\mu)} + \frac{1}{(1+\mu)}\sqrt{(\epsilon_1-\epsilon_3)^2 + \left[2\epsilon_2-(\epsilon_1+\epsilon_3)\right]^2}\right]$$

$$\sigma_{min} = \frac{E}{2}\left[\frac{\epsilon_1+\epsilon_3}{(1-\mu)} - \frac{1}{(1+\mu)}\sqrt{(\epsilon_1-\epsilon_3)^2 + \left[2\epsilon_2-(\epsilon_1+\epsilon_3)\right]^2}\right]$$

$$\tau_{max} = \frac{E}{2(1+\mu)}\sqrt{(\epsilon_1-\epsilon_3)^2 + \left[2\epsilon_2-(\epsilon_1+\epsilon_3)\right]^2}$$

$$\phi_p = \tfrac{1}{2}\arctan\left[\frac{2\epsilon_2-(\epsilon_1+\epsilon_3)}{\epsilon_1+\epsilon_3}\right]$$

ϕ_p is the angle from the axis of ϵ_1 to the maximum normal stress axis and ϵ_1, ϵ_2 and ϵ_3 are strain readings in the respectively numbered gages shown in Fig. G1. Rosettes used in this experiment were numbered with three con-secutive numbers and the lowest number identified the rosette. Logically then ϕ_p is the angle from the axis of the lowest numbered gage in each rosette to the maximum normal stress axis. A positive value indicates an angle in the direction of ϵ_2.

The input to program ROSRED (Table G1) was designed to accommodate this notation. Only the rosette identifying number is listed which is also the gage number for which the first column of strains are listed. The second and third columns are then the values of strain on the next two consecutive numbered gages comprizing the rosette.

The results listed in Table G4 are identified by the rosette numbers which quickly orients the axis reference for ϕ_p.

It should be pointed out that the program was designed for specific values of E and μ, namely 10.3×10^6 psi and 0.32 respectively.

Fig. G2

FLOW CHART FOR PROGRAM ROSRED

Start

READ Rosette Number, ϵ_{1i}, ϵ_{2i}, ϵ_{3i}.

$A_i = \epsilon_{1i} + \epsilon_{3i}$

$B_i = \epsilon_{1i} - \epsilon_{3i}$

$R_i = \sqrt{B_i^2 + (2\epsilon_{2i} - A_i)^2}$

$\sigma_{max} = \frac{10.3}{2}\left[\frac{A_i}{0.68} + \frac{1}{1.32}R_i\right]$

$\sigma_{min} = \frac{10.3}{2}\left[\frac{A_i}{0.68} - \frac{1}{1.32}R_i\right]$

$\tau_{max} = \frac{10.3\ R_i}{2.64}$

$\phi_p = \frac{1}{2}\arctan\left[\frac{2\epsilon_{2i} - A_i}{B_i}\right]$

Return ← no — i=n ? — yes

PRINT Rosette Number, σ_{max}, σ_{min}, τ_{max}, ϕ_p

STOP
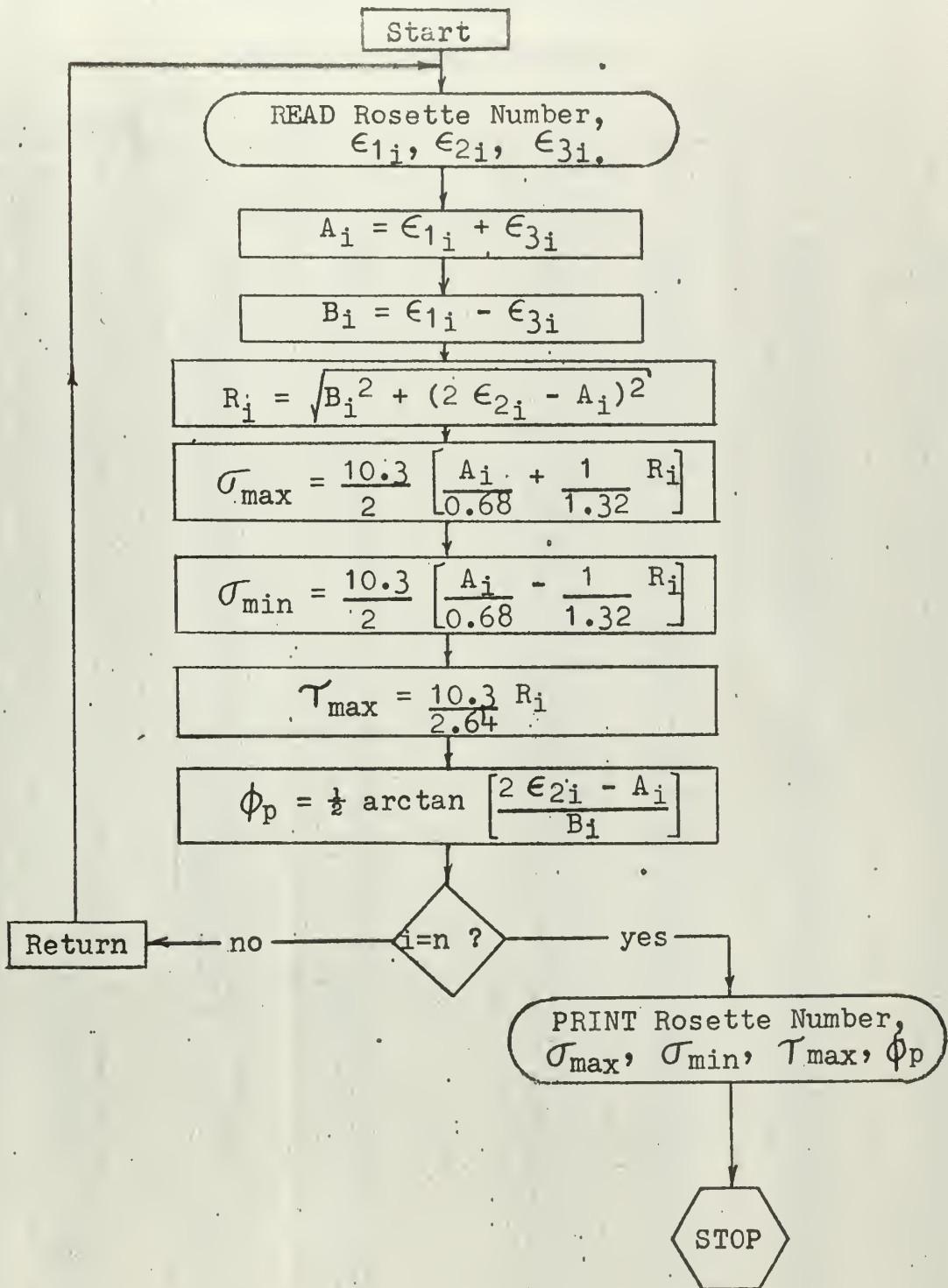
Table G1

EXPERIMENTAL STRAIN READINGS

(Input To ROSRED Program)

8000 lb Test

Rosette Number	ϵ_1	ϵ_2	ϵ_3	Rosette Number	ϵ_1	ϵ_2	ϵ_3
13	-76.	60.	34.	193	131.	8.	-130.
16	-12.	83.	30.	196	18.	-110.	-20.
19	-5.	76.	27.	199	140.	32.	-124.
22	-1.	68.	6.	204	33.	135.	0.
28	-22.	136.	25.	207	-19.	0.	34.
31	-10.	124.	42.	210	46.	-13.	-53.
34	-12.	124.	9.	216	32.	134.	-26.
37	1.	136.	1.	219	-141.	-11.	130.
40	23.	143.	-17.	222	-179.	-10.	191.
43	-22.	53.	4.	225	5.	68.	-5.
46	-29.	134.	31.	228	-117.	15.	111.
49	-23.	166.	29.	234	166.	46.	-188.
52	16.	179.	18.	237	1.	75.	2.
55	16.	200.	-16.	240	90.	2.	-101.
58	42.	158.	-21.	243	24.	94.	-10.
66	5.	98.	3.	246	-17.	1.	26.
69	20.	141.	-18.	249	40.	-10.	-46.
72	-26.	132.	22.	252	23.	160.	-18.
75	-9.	93.	6.	255	-1.	-104.	101.
83	5.	51.	-7.	258	-97.	-19.	-6.
86	7.	60.	-11.	264	-51.	5.	49.
89	8.	53.	-17.	267	110.	20.	-99.
92	7.	46.	-21.	270	94.	20.	-74.
95	5.	83.	-4.	273	3.	-28.	-1.
101	14.	83.	-6.	276	29.	0.	-61.
104	11.	106.	-6.	279	14.	93.	3.
107	10.	105.	-11.	282	11.	162.	14.
110	16.	103.	-13.	285	2.	1.	3.
113	9.	132.	-6.	288	0.	-6.	-5.
116	15.	130.	-17.	291	3.	175.	7.
119	18.	130.	-14.	294	-48.	2.	50.
122	18.	148.	-15.	297	-40.	2.	35.
125	12.	146.	-17.	300	1.	-15.	-6.
128	15.	144.	-23.	303	73.	-8.	-71.
131	-52.	147.	44.	306	-36.	11.	-45.
134	164.	-14.	-194.	309	34.	6.	-34.
137	200.	-32.	-192.	312	4.	-20.	2.
140	213.	0.	-207.	318	-7.	73.	13.
143	215.	-11.	-219.	333	-23.	173.	23.
146	135.	-2.	-134.	342	-2.	91.	-12.
149	163.	-13.	-162.	355	-9.	106.	31.
152	-10.	176.	25.	367	14.	-49.	24.
155	189.	-4.	-182.	394	-30.	170.	49.
158	214.	75.	-176.	409	-22.	155.	5.
163	12.	2.	-3.	454	-15.	89.	31.
166	15.	-9.	-20.	457	-14.	95.	22.
169	66.	162.	-41.	466	11.	-95.	-46.
172	-221.	-47.	153.	469	18.	42.	-21.
175	-241.	-4.	240.	472	-11.	83.	35.
178	-134.	3.	135.	475	-23.	59.	14.
181	-7.	-141.	-2.	478	4.	64.	-16.
184	-164.	-11.	158.	481	39.	59.	-66.
187	159.	33.	-120.	484	53.	103.	-44.
190	223.	1.	-132.				

7000 lb Test

Rosette Number	ϵ_1	ϵ_2	ϵ_3	Rosette Number	ϵ_1	ϵ_2	ϵ_3
13	-64.	53.	28.	237	+ 2.	+ 69.	+ 2.
16	-11.	72.	28.	243	19.	183.	- 10.
19	-7.	64.	22.	246	- 19.	0.	22.
22	-2.	58.	2.	249	35.	- 10.	- 43.
28	-20.	18.	25.	252	18.	138.	- 18.
31	-8.	106.	35.	255	- 3.	-100.	90.
34	-13.	107.	6.	258	- 85.	- 15.	70.
37	1.	119.	1.	264	- 45.	3.	44.
40	18.	125.	-15.	267	98.	18.	- 87.
43	-21.	46.	2.	270	80.	18.	- 65.
46	-29.	117.	26.	273	2.	- 25.	- 2.
49	-21.	143.	24.	276	25.	- 2.	- 50.
52	12.	157.	14.	279	12.	86.	5.
55	14.	174.	-15.	282	13.	144.	14.
58	35.	138.	-20.	285	1.	2.	3.
66	- 2.	+ 84.	- 4.	288	1.	- 4.	- 4.
69	+15.	+126.	- 17.	291	4.	156.	8.
72	-27.	+117.	+ 16.	294	- 40.	3.	43.
75	-12.	+ 84.	+ 4.	297	64.	2.	29.
83	+ 6.	+ 48.	- 5.	300	1.	- 17.	- 7.
86	+ 7.	+ 56.	- 4.	303	70.	- 7.	- 66.
89	+ 8.	+ 50.	- 11.	306	41.	8.	- 40.
92	+ 8.	+ 45.	- 15.	309	28.	3.	29.
95	+ 5.	+76.	-2.	312	3.	- 20.	4.
98	+12.	+ 77.	- 3.	315	- 76.	- 20.	70.
101	+14.	+ 77.	- 4.	321	- 6.	71.	19.
104	+ 8.	+ 95.	- 4.	324	- 8.	144.	32.
107	+ 8.	+ 94.	- 7.	327	10.	3.	- 10.
110	+14.	+ 94.	- 10.	333	20.	151.	22.
113	+ 7.	+116.	- 3.	336	46.	4.	- 43.
116	+ 4.	+105.	- 21.	339	68.	10.	- 66.
119	+ 6.	+105.	-19.	342	- 4.	85.	- 7.
122	+ 22.	+120.	- 21.	345	115.	2.	-104.
125	0.	+121.	- 23.	349	- 47.	- 1.	44.
128	+ 2.	+116.	- 23.	352	- 74.	1.	75.
131	- 52.	+123.	+ 31.	355	- 9.	96.	27.
134	+151.	+ 91.	-166.	358	110.	- 18.	-128.
137	+181.	- 28.	-166.	361	- 13.	- 60.	15.
140	+194.	0.	-181.	364	- 6.	- 44.	23.
143	+198.	- 7.	-187.	367	13.	- 42.	21.
146	+128.	0.	-117.	370	- 2.	- 58.	18.
149	+153.	- 11.	-141.	373	9.	- 20.	21.
152	- 7.	+157.	+ 25.	376	- 41.	50.	7.
155	+169.	- 5.	-161.	379	- 31.	77.	26.
158	+191.	69.	-156.	382	- 20.	105.	21.
163	+ 10.	0.	- 6.	385	- 21.	124.	36.
166	+ 16.	- 7.	- 20.	388	- 13.	1.	11.
169	+ 55.	+141.	- 36.	391	43.	- 4.	- 46.
172	-187.	- 41.	+137.	394	- 26.	150.	40.
175	-216.	- 3.	+213.	397	182.	14.	-190.
178	-121.	+ 7.	+121.	400	165.	0.	-167.
181	- 8.	-128.	- 2.	403	216.	30.	-209.
184	-147.	- 11.	+143.	406	224.	0.	-230.
187	+143.	+ 24.	-101.	409	- 20.	134.	7.
190	+197.	0.	-203.	412	229.	83.	-189.
193	+121.	+ 8.	-118.	415	240.	15.	222.
196	+ 16.	-100.	- 16.	418	- 9.	- 3.	6.
199	+126.	+ 30.	-112.	421	- 10.	- 5.	4.
204	+ 32.	+121.	- 3.	424	7.	- 1.	- 5.
207	- 15.	+ 1.	+ 33.	427	0.	- 1.	- 2.
210	+ 43.	- 11.	- 46.	430	- 18.	- 10.	11.
213	+ 26.	+109.	- 14.	433	- 15.	- 9.	9.
216	+ 30.	+121.	- 19.	436	- 4.	5.	5.
219	-124.	- 8.	+114.	439	- 4.	10.	15.
222	-157.	- 8.	+165.	442	77.	31.	- 73.
225	+ 3.	+ 69.	- 4.	448	10.	159.	0.
228	-108.	+ 13.	+ 98.	451	7.	162.	3.
234	+143.	+ 39.	-165.				

TABLE G2

LIST OF SYMBOLS USED IN
ROSRED PROGRAM

Computer Coded Name	Definition
EP1	ϵ_1, strain in lowest numbered gage of rosette
EP2	ϵ_2, strain in diagonal gage
EP3	ϵ_3, strain in perpendicular gage
SIGMAX	σ_{max}, maximum principal stress
SIGMIN	σ_{min}, minimum principal stress
TAUMAX	τ_{max}, maximum shearing stress
PHIP	ϕ , angle from the ϵ_1 axis to σ_{max} axis.
GAGE	Rosette number (lowest numbered gage in rosette)
N	Number of rosettes furnished as data input

Table G3

FORTRAN PROGRAM

"ROSRED"

```
      PROGRAM ROSRED
C     PROGRAM TO OBTAIN PRINCIPAL STRESSES AND AXIS ORIENTATION FROM
C     RECTANGULAR ROSETTE STRAIN DATA
     ODIMENSION EP1(400),EP2(400),EP3(400),SIGMAX(400),SIGMIN(400),
     1TAUMAX(400),PHIP(400),GAGE(400)
      READ 1,N
    1 FORMAT(I3)
      READ 2, (GAGE(I),EP1(I),EP2(I),EP3(I),    I=1,N)
C     FOR EACH ROSETTE, LOWEST NUMBER GAGE IDENTIFIES ROSETTE AND
C     GIVES REFERENCE POINT FOR ANGLE PHIPRINCIPAL,WHERE POSITIVE
C     ANGLE IS MEASURED TOWARDS GAGE 2 OF ROSETTE
C     STRAIN DATA IS MICRO-INCHES/INCH
    2 FORMAT (I3,3F8.0)
      DO 20 I = 1,N
      A(I)= EP1(I)+ EP3(I)
      B(I)= EP1(I)- EP3(I)
      R(I)= SQRTF(B(I)**2 + (EP2(I)*2.0 -A(I))**2)
      SIGMAX(I) = (10.3/2.0)*((A(I)/.68) +(1.0/1.32)*R(I))
      SIGMIN(I)= 5.15 *((A(I)/.68)-(1.0/1.32)*R(I))
      TAUMAX(I)= (10.3/2.64)*R(I)
   20 PHIP(I)= ((ATANF((2.0*EP2(I) -A(I))/B(I)))/2.0) * 57.3
      PRINT 30
   30 FORMAT (43H1           MAX           MIN         MAX           P)
      PRINT 31(GAGE(I),SIGMAX(I),SIGMIN(I),TAUMAX(I),PHIP(I) I =1,N)
   31 FORMAT (1X,I3,3F10.0,1F10.2)
      STOP
      END
      END
```

152

Table G4

EXPERIMENTAL RESULTS

(Output of "ROSRED" Program)

8000 lb Test

Rosette Number	σ_{max}, psi	σ_{min}, psi	τ_{max}, psi	ϕ_p, Deg.
13	446.	-1082.	764.	-27.91
16	737.	-464.	600.	-37.08
19	689.	-356.	522.	-38.09
22	550.	-474.	512.	-43.47
28	1088.	-1043.	1065.	-40.05
31	1109.	-624.	867.	-38.23
34	960.	-1005.	983.	-42.61
37	1069.	-1038.	1053.	.00
40	1149.	-1058.	1104.	40.94
43	358.	-631.	494.	-39.08
46	1079.	-1049.	1064.	-38.65
49	1333.	-1243.	1288.	-40.47
52	1522.	-1007.	1264.	-44.83
55	1566.	-1566.	1566.	42.72
58	1336.	-1018.	1177.	38.98
66	794.	-673.	734.	44.70
69	1118.	-1087.	1102.	41.14
72	1032.	-1093.	1062.	-39.93
75	717.	-762.	740.	-42.73
83	393.	-424.	408.	41.71
86	459.	-519.	489.	40.87
89	391.	-527.	459.	38.87
92	322.	-534.	428.	37.60
95	652.	-637.	645.	43.44
101	682.	-561.	621.	41.40
104	848.	-772.	810.	42.66
107	820.	-835.	827.	42.16
110	823.	-777.	800.	40.94
113	1043.	-997.	1020.	43.36
116	1015.	-1045.	1030.	41.52
119	1037.	-976.	1007.	41.44
122	1173.	-1128.	1150.	41.79
125	1126.	-1202.	1164.	42.21
128	1104.	-1225.	1164.	41.35
131	1176.	-1297.	1236.	-36.19
134	1170.	-1624.	1397.	.16
137	1616.	-1494.	1555.	-5.20
140	1684.	-1593.	1639.	-.41
143	1664.	-1725.	1695.	-1.19
146	1057.	-1042.	1050.	-.53
149	1280.	-1265.	1272.	-2.37
152	1435.	-1208.	1322.	-42.04
155	1502.	-1396.	1449.	-1.16
158	1871.	-1295.	1583.	8.01
163	130.	6.	62.	-9.22
166	108.	-184.	146.	-10.19
169	1428.	-1050.	1239.	35.16
172	948.	-1978.	1463.	1.99
175	1869.	-1884.	1877.	.42
178	1057.	-1042.	1050.	-.53
181	997.	-1133.	1065.	44.48
184	1212.	-1303.	1258.	1.42
187	1389.	-798.	1094.	2.76
190	2117.	-739.	1428.	-7.04

(Table G4 Continued)

8000 lb Test

Rossette Number	σ_{max}, psi	σ_{min}, psi	τ_{max}, psi	ϕ_p, Deg.
193	1028.	-1012.	1020.	1.64
196	848.	-879.	863.	-40.06
199	1168.	-926.	1047.	5.15
204	1184.	-684.	934.	41.04
207	329.	-101.	215.	7.90
210	340.	-446.	393.	-5.43
216	1092.	-1002.	1047.	38.76
219	975.	-1141.	1058.	1.16
222	1540.	-1358.	1449.	2.47
225	532.	-532.	532.	42.90
228	855.	-946.	901.	-4.49
234	1284.	-1618.	1451.	8.93
237	596.	-551.	574.	-44.81
240	664.	-831.	747.	2.25
243	798.	-586.	692.	39.47
246	238.	-102.	170.	4.62
249	295.	-385.	340.	-4.62
252	1277.	-1201.	1239.	41.30
255	2023.	-508.	1266.	35.84
258	-344.	-1216.	436.	-17.77
264	378.	-408.	393.	-3.42
267	907.	-740.	823.	3.95
270	812.	-509.	660.	3.39
273	242.	-212.	227.	-43.03
276	130.	-615.	373.	9.79
279	790.	-532.	661.	43.14
282	1356.	-977.	1167.	-44.72
285	50.	26.	12.	35.79
288	-4.	-71.	34.	-27.23
291	1402.	-1251.	1327.	-44.67
294	398.	-367.	382.	-.58
297	257.	-333.	295.	-3.42
300	63.	-139.	101.	-37.18
303	581.	-551.	566.	-3.56
306	-210.	-1017.	403.	42.51
309	269.	-269.	269.	5.00
312	225.	-134.	180.	-43.76
318	597.	-506.	552.	-40.94
333	1362.	-1362.	1362.	-41.22
342	660.	-872.	766.	43.54
355	924.	-591.	758.	-39.06
367	820.	-244.	532.	42.90
394	1434.	-1146.	1290.	-38.09
409	1151.	-1409.	1280.	-42.64
454	778.	-536.	657.	-37.08
457	784.	-663.	724.	-39.41
466	379.	-909.	644.	-34.91
469	349.	-395.	372.	32.93
472	764.	-401.	582.	-36.03
475	448.	-584.	516.	-36.88
478	461.	-643.	552.	40.94
481	494.	-903.	698.	27.05
484	925.	-789.	857.	31.89

7000 lb Test

Rossette Number	σ_{max}, psi	σ_{min}, psi	τ_{max}, psi	ϕ_p, Deg.
13	387.	-933.	660.	-28.53
16	647.	-390.	518.	-36.47
19	569.	-342.	455.	-37.81
22	453.	-453.	453.	-44.02
28	251.	-175.	213.	-17.28
31	946.	-537.	741.	-38.46
34	812.	-918.	865.	-42.55
37	936.	-906.	921.	.00
40	995.	-950.	972.	41.20
43	298.	-586.	442.	-39.15
46	927.	-972.	949.	-38.47
49	1141.	-1095.	1118.	-40.49
52	1321.	-927.	1124.	-44.80
55	1359.	-1374.	1366.	42.63
58	1154.	-927.	1041.	39.05
66	633.	-724.	679.	44.67
69	984.	-1014.	999.	41.41
72	887.	-1054.	970.	-40.03
75	629.	-750.	689.	-42.41
83	381.	-366.	373.	41.70
86	450.	-405.	427.	42.12
89	386.	-431.	409.	39.78
92	336.	-442.	389.	38.33
95	605.	-559.	582.	43.66
98	637.	-501.	569.	42.05
101	642.	-490.	566.	41.44
104	757.	-697.	727.	43.16
107	740.	-724.	732.	42.71
110	754.	-694.	724.	41.29
113	921.	-860.	890.	43.75
116	762.	-1020.	891.	41.86
119	777.	-974.	875.	41.80
122	955.	-940.	947.	39.90
125	864.	-1212.	1038.	42.52
128	833.	-1151.	992.	42.18
131	932.	-1250.	1091.	-36.37
134	1343.	-1570.	1456.	15.93
137	1495.	-1268.	1382.	-5.78
140	1562.	-1365.	1464.	-.99
143	1589.	-1422.	1505.	-1.86
146	1040.	-874.	957.	-1.29
149	1246.	-1064.	1155.	-3.30
152	1298.	-1025.	1162.	-41.92
155	1350.	-1229.	1289.	-1.56
158	1677.	-1147.	1412.	8.27
163	95.	-34.	64.	-7.02
166	115.	-176.	146.	-7.76
169	1230.	-942.	1086.	35.46
172	892.	-1649.	1270.	2.82
175	1651.	-1697.	1674.	.20
178	946.	-946.	946.	-1.66
181	884.	-1036.	960.	44.30
184	1103.	-1164.	1134.	1.78
187	1270.	-634.	952.	.70
190	1515.	-1606.	1561.	.43
193	957.	-911.	934.	1.56
196	790.	-790.	790.	-40.46
199	1052.	-840.	946.	5.47
204	1062.	-623.	842.	40.34
207	334.	-61.	197.	9.22
210	332.	-378.	355.	-6.03
213	910.	-728.	819.	39.51
216	1005.	-838.	921.	39.01
219	853.	-1005.	929.	.72
222	1320.	-1199.	1260.	2.13
225	535.	-551.	543.	43.56
228	740.	-892.	816.	-4.96
234	1097.	-1430.	1263.	8.99
237	553.	-493.	523.	.00

7000 lb Test

Rosette Number	σ_{max}, psi	σ_{min}, psi	τ_{max} psi	ϕ_p , Deg.
243	1466.	-1329.	1397.	42.68
246	183.	-138.	160.	2.09
249	247.	-368.	308.	-4.37
252	1086.	-1086.	1086.	41.29
255	1836.	-518.	1177.	36.03
258	494.	-721.	608.	2.76
264	341.	-356.	348.	-2.25
267	812.	-645.	728.	3.85
270	685.	-458.	572.	4.12
273	196.	-196.	196.	-42.72
276	115.	-493.	304.	7.82
279	734.	-477.	605.	43.71
282	1223.	-814.	1018.	-44.89
285	38.	22.	8.	.00
288	5.	-50.	28.	-22.50
291	1261.	-1080.	1171.	-44.62
294	347.	-301.	324.	-1.04
297	1077.	331.	373.	-34.27
300	68.	-159.	114.	-37.03
303	566.	-505.	535.	-3.77
306	329.	-314.	321.	5.25
309	631.	233.	199.	44.44
312	236.	-130.	183.	44.39
315	539.	-630.	585.	6.56
321	611.	-414.	513.	-39.52
324	1224.	-860.	1042.	-40.70
327	81.	-81.	81.	8.35
333	1333.	-696.	1014.	-44.78
336	371.	-325.	348.	1.61
339	543.	-512.	527.	3.83
342	623.	-790.	706.	44.53
345	938.	-772.	855.	-.92
349	332.	-378.	355.	-.31
352	589.	-574.	581.	-.19
355	830.	-557.	693.	-39.16
358	795.	-1068.	931.	-2.16
361	504.	-473.	488.	38.54
364	554.	-296.	425.	37.28
367	719.	-204.	461.	43.06
370	642.	-400.	521.	40.70
373	504.	-50.	277.	40.14
376	298.	-813.	555.	-35.15
379	621.	-697.	659.	-35.14
382	839.	-823.	831.	-39.45
385	1049.	-822.	936.	-38.13
388	80.	-110.	95.	-4.73
391	325.	-371.	348.	-1.61
394	1251.	-1039.	1145.	-38.51
397	1398.	-1519.	1458.	2.76
400	1280.	-1310.	1295.	.17
403	1724.	-1618.	1671.	3.55
406	1726.	-1817.	1771.	.38
409	1003.	-1200.	1101.	-42.26
412	2006.	-1400.	1703.	8.39
415	5.186.	1812.	1687.	-43.81
418	37.	-82.	60.	5.66
421	11.	-102.	57.	7.97
424	64.	-34.	49.	-9.22
427	-7.	-23.	8.	.00
430	71.	-177.	124.	12.07
433	59.	-150.	105.	13.28
436	57.	-42.	50.	-22.50
439	165.	1.	82.	-12.67
442	658.	-597.	627.	10.57
448	1278.	-1127.	1202.	44.07
451	1301.	-1149.	1225.	44.64